TECHNISCHE
UNIVERSITÄT
WIEN
Vienna University of Technology

DISSERTATION

Anthropomorphic Hand Optimization based on a Latent Space Analysis.

ausgeführt zum Zwecke der Erlangung des akademischen Grades eines Doktors der technischen Wissenschaften unter der Leitung von

Ao.Univ.Prof. Dipl.-Ing. Dr.techn. Heinz-Bodo Schmiedmayer
Institut für Mechanik und Mechatronik
Technische Universität Wien

und

Prof. Danica Kragic
Centre for Autonomous Systems, CSC
Königlich Technische Hochschule (KTH), Stockholm, Schweden

eingereicht an der Technischen Universität Wien
bei der Fakultät für Maschinenwesen und Betriebswissenschaften

von

Dipl.-Ing.(FH) Thomas Feix
Matrikelnummer: 0227312
Stadtplatz 9
3400 Klosterneuburg

Wien, im Oktober 2011

Erklärung zur Verfassung der Arbeit

Thomas Feix
Stadtplatz 9
3400 Klosterneuburg

Hiermit erkläre ich, dass ich diese Arbeit selbständig verfasst habe, dass ich die verwendeten Quellen und Hilfsmittel vollständig angegeben habe und dass ich die Stellen der Arbeit - einschließlich Tabellen, Karten und Abbildungen -, die anderen Werken oder dem Internet im Wortlaut oder dem Sinn nach entnommen sind, auf jeden Fall unter Angabe der Quelle als Entlehnung kenntlich gemacht habe.

(Ort, Datum) (Unterschrift Verfasser)

Acknowledgements

I would like to express my sincere gratitude to all who contributed to making this thesis possible. My supervisors Prof. Schmiedmayer and Prof. Kragic provided valuable guidance and continuous support. Their comments and assistance were of great help.

As the research work was done within the European EC-FP7 project GRASP, I would like to thank the concerned team members, too. It was highly inspiring to be part of such a project and get to know scientists from all over Europe. In particular, I would like to thank Javier Romero of KTH Stockholm for the continuous collaboration and discussions. He also deserves credit for creating the grasp images and for implementing the GMM/GMR code for grasp classification. Thanks are also due to Heiner Deubel and René Gilster of LMU Munich, where the human grasp data was recorded. Furthermore, I would like to thank the prosthetics company Otto Bock for providing me with the opportunity to work on this highly interesting topic.

Last but not least, I would like to thank my family and friends for supporting me throughout the past years.

Abstract

Humans use the hand as their primary manipulator, performing a wide range of movements with it. An important sub-set of those movements are one handed grasps, on which the thesis focus on. To this day there is no consensus on the grasp types humans use and how the hand kinematics influence the hand capabilities. As such knowledge is scarce, the design of artificial anthropomorphic hand is still depending to a large part on the intuition of its creators.

Within the thesis a comprehensive grasp taxonomy is developed, which incorporates all major grasp types found in literature. This allows for a detailed description of one handed static human grasping movements. Those movements are recorded, resulting in a dataset that consists of different grasp trajectories. That data is then projected onto a low dimensional space using a nonlinear dimensionality reduction algorithm. That allows to represent the human grasping movements in a more compact fashion.

In order to provide a design tool which evaluates the level of anthropomorphism of artificial hands, the data is processed further. The trajectories of artificial hands are projected to the human spanned low dimensional space. That allows for a straightforward and intuitive comparison between human and machine. An indication for a human-like hand is that its movements have a large overlap of the human space.

That method is applied to grade existing hands and to show how different design choices influence the level of anthropomorphism of artificial hands. Finally, new hand designs are developed. Starting from existing hands, the kinematic structure is altered and new actuators are added in order to increase the overlap with the human. Those improved hands need only a few control signals, but are able to mimic large proportions of the human hand capabilities.

Kurzfassung

Menschen verwenden ihre Hand als ihr primäres Werkzeug und setzen sie in einer Vielzahl von Bewegungen ein. Eine wichtige Untergruppe aller Bewegungen sind einhändige Griffe, die im Fokus dieser Arbeit stehen. Bis heute gibt es keinen Konsens welche Grifftypen verwendet werden und wie die Handkinematik die Fähigkeiten der Hand beeinflusst. Aufgrund des Mangels dieses Wissens, ist ein künstliches Handdesign hauptsächlich von der Intuition seines Erbauers abhängig.

Die Arbeit entwickelt eine vollständige Griffklassifizierung, die alle vorhergegangenen Arbeiten beinhaltet. Diese Taxonomie erlaubt es einhändige, statische Griffbewegungen genau zu beschreiben. Diese Bewegungen werden dann gemessen und erzeugen einen Datensatz der diese Greifbewegungen beherbergt. Diese Daten werden mit einem nichtlinearen Algorithmus zur Dimensionalitätsreduktion weiterverarbeitet und dadurch können sie in einem niederdimensionalen Raum dargestellt werden.

Um ein Werkzeug zur Bestimmung der Menschenähnlichkeit von künstlichen Händen zu kreieren, werden diese Daten herangezogen. Die Bewegungen einer künstlichen Hand werden in den Raum der menschlichen Bewegungen projiziert um einen direkten Vergleich zwischen Mensch und Maschine zu schaffen. Ein Indiz für ein anthropomorphes Design ist, dass die Bewegungen einen großen Teil des menschlichen Raumes abdecken. Die Methode wird verwendet um bestehende Hände zu bewerten und um zu zeigen wie verschiedene Designelemente die Menschenähnlichkeit beeinflussen können. Schlussendlich werden, ausgehend von existierenden Designs, neue, verbesserte Hände entwickelt. Diese benötigen nur wenige Steuersignale, aber können große Teile der menschlichen Fähigkeiten nachahmen.

Contents

1 Introduction **1**

1.1 Motivation . . . 1
1.2 Contributions . . . 2
1.3 Thesis Outline . . . 3

2 State of the Art **4**

2.1 Anatomy of the Hand . . . 4
2.1.1 Forearm . . . 4
2.1.2 Metacarpus . . . 5
2.1.3 Metacarpal Joints . . . 6
2.1.4 Interphalangeal Joints . . . 7
2.1.5 Thumb . . . 7
2.2 Theory of Grasping . . . 9
2.2.1 Opposition types . . . 10
2.2.2 Power, Precision, Intermediate Grasp . . . 10
2.2.3 Virtual Fingers . . . 11
2.2.4 Grasp Taxonomies . . . 12
2.3 Artificial Hands . . . 12
2.3.1 Prosthetic Hands . . . 12
2.3.2 Anthropomorphic Robotic Hands . . . 13
2.3.3 Hand Control . . . 15
2.3.4 Optimal Hand Designs . . . 16
2.4 Kinematic Chains . . . 17
2.4.1 Degrees of Freedom . . . 17
2.4.2 Denavit - Hartenberg Formalism . . . 19
2.4.3 Human Hand Models . . . 20
2.5 Unsupervised Machine Learning . . . 23

2.5.1 Principal Components Analysis . . . 23
2.5.2 Isomap . . . 27
2.5.3 Locally Linear Embedding . . . 27
2.5.4 Gaussian Process Latent Variable Models . . . 28

3 Comprehensive Grasp Taxonomy 31
3.1 Grasp Definition . . . 31
3.2 Compared Taxonomies . . . 32
3.2.1 Schlesinger . . . 32
3.2.2 Slocum and Pratt . . . 32
3.2.3 Cooney and Chao . . . 33
3.2.4 Kamakura et. al . . . 34
3.2.5 Lister . . . 34
3.2.6 Elliott and Connolly . . . 34
3.2.7 Lyons . . . 40
3.2.8 Kroemer . . . 40
3.2.9 Cutkosky . . . 40
3.2.10 Kang and Ikeuchi . . . 41
3.2.11 Light et al. . . . 44
3.2.12 Exner . . . 44
3.2.13 Edwards et al. . . . 46
3.2.14 Kapandji . . . 49
3.3 Comparison Sheet . . . 51
3.4 Grasp List . . . 51
3.5 Comprehensive Taxonomy . . . 53
3.6 Discussion . . . 57

4 Quantification of Anthropomorphic Hand Performance 58
4.1 System Description . . . 58
4.2 Overlap Measure . . . 61
4.3 The Latent Space . . . 63
4.3.1 Data Acquisition . . . 63
4.3.2 Data Set . . . 66
4.3.3 Rotation Representation . . . 67
4.3.4 Influence of the Kernel Width . . . 68
4.3.5 Metrics on Latent Space Quality . . . 69
4.3.6 Model Comparison . . . 74
4.3.7 The Selected Model . . . 75

4.4 Projection of Existing Hands . . . 79
4.4.1 SensorHand . . . 79
4.4.2 Michelangelo Hand . . . 81
4.4.3 FRH-4 Hand . . . 84
4.4.4 Human Hand Model . . . 85
4.4.5 Principal Components of the Space . . . 86
4.5 Discussion . . . 90

5 Optimizing Kinematic Hand Setups 92
5.1 Sensitivity Study . . . 92
5.1.1 SensorHand . . . 94
5.1.2 Michelangelo . . . 94
5.1.3 FR-H 4 Hand . . . 96
5.1.4 Discussion . . . 97
5.2 Optimization of Kinematic Parameters . . . 99
5.2.1 SensorHand Thumb . . . 100
5.2.2 Linear Human Hand Model . . . 103
5.2.3 Michelangelo Couplings . . . 107
5.2.4 Michelangelo with Human Thumb 3D . . . 108
5.3 Validation of Design Elements . . . 110
5.3.1 Michelangelo Couplings with Human Thumb 3D . . . 110
5.3.2 Michelangelo with Independent Index . . . 112
5.3.3 Michelangelo Underactuated Finger Joints . . . 113
5.3.4 Michelangelo with Human Thumb and Underactuation . . . 115
5.4 Discussion . . . 118

6 Conclusion 120
6.1 Outlook . . . 121

Glossary 123

List of Figures 125

List of Tables 128

Bibliography 129

A Curriculum Vitae 140

Chapter 1

Introduction

1.1 Motivation

The world around us determines how the human hand is used and how we manipulate objects. In human-built environments the relation is also reversed – we built objects in such a way as that they suit our dexterity. Commonly, objects that are supposed to be manipulated by humans have roughly the size of the human hand and have an intended way to be used. How would those objects look like if the kinematic structure of the human hand would be majorly different? Would we still use mugs, pens etc. the same way and create objects with the same shape? Those questions are not tackled in the thesis but are motivating ones.

Even though we use the hand everyday, its function is not well understood. A lot of work has been dedicated to structuring the human hand movements. Various grasp taxonomies have been proposed, but there is no real consensus on the existing grasp types. Additionally, it is not known which grasp types are frequently used in everyday tasks, and which are used only very seldom. Such knowledge could be of benefit for many applications like designing artificial hands, human-robot interaction and many more.

The human hand is still unmatched by any artificial design, therefore a lot of effort has been taken to mimic the human hand functionality. That is the case in prosthetics as well as robotics. In order to become more human-like, new motors and joints were added resulting in hands with a very complex structure. In the case of robotics, the number of motors can even exceed the human. The potential of such a hand is very large, but due to control problems the actual hand capabilities are much lower [1]. In the case of prosthetics such a large degree of complexity has not been reached due to the mechanical challenges such a hand design poses. The system has to be human-sized and self-contained, therefore only a few actuators can be placed within the hand. Still, only a few independent control signals pose a serious challenge to the user. Contemporary methods only allow the human

to control one Degree of Freedom (DoF) at a time, thus multiple movements have to be performed sequentially [2]. In that case a proper interface between the human and the prosthetic hand is the bottleneck [3].

The lessons learnt from this limitations are the same for robotic and prosthetic hands. The guideline on how such a hand should be built is that the control space of the hand should be low dimensional, thus diminishing the problems mentioned above. One should try to incorporate as much functionality as possible directly into the kinematic setup, without adding more control signals. Additionally, such a hand will be simpler to manufacture, as additional actuators and joints pose challenges in terms of the design. In the case of prosthetics that would have other benefits as well – hand weight, speed, strength and reliability are key factors for user acceptance [4, 5]. A simple design will leave enough margin, so those goals can be achieved as well.

For a few special cases it is possible to determine the quality of a hand model in simulation. Yet, at the moment there are no principled methods that allow to determine the functionality of an artificial hand prior to realization. The goal is to estimate the gap between the human and artificial hand prior to realization. Such a measure is important as it allows to iterative over new hand designs in a much faster and more efficient way compared to the classical approach of realizing hand prototypes.

1.2 Contributions

The contributions of the thesis can be divided into three main parts.

First, a human grasp taxonomy is created. It is based on a review of 14 literature sources which are merged to one comprehensive classification of one handed static grasps. The taxonomy consists of 33 grasp types, incorporating all major classifications presented in literature. Those grasp types define the human hand capabilities against which any artificial design will be contrasted against.

Second, a system to measure the gap between the human and artificial hand is created. Five subjects are recorded performing the grasps from the comprehensive grasp taxonomy. The dataset is further processed and projected to a two dimensional space, where the hand trajectories are easy to visualize. To determine the gap to an artificial hand, it is projected into that space as well. A large degree of overlap indicates that the hand is human-like. The human hand is used as the golden standard in grasping, thus assuming that mimicking the human hand is a way towards increased versatility of the artificial hand.

Third, the method is applied to grade existing artificial hands and create new, improved hand designs. In order to gain first experience with the measure, existing hands are graded. Two prosthetic and one robotic hand were analyzed. The results reveal that it

is important that the general kinematic setup has to be human-like, it is not sufficient to add many actuators in order to become anthropomorphic. To improve the hand designs, new actuators and joints are added, changing the kinematic structure. It is shown that by small adaptations of existing hands major improvements can be achieved.

1.3 Thesis Outline

The thesis starts with Chapter 2 by giving background information the thesis is based upon. That includes basic information on the human hand anatomy as well as means to analyze human grasping in a structured way. Also, a method to describe kinematic chains as well as state of the art prosthetic and robotic hands are presented. Finally, the mathematical basics of dimensionality reduction are given. That is needed as the measure to determine the level of anthropomorphism of artificial hands is heavily based on such a method.

Chapter 3 develops a comprehensive grasp taxonomy which is based on all major publications. The classification defines the movements of the human hand against which artificial hands are contrasted.

Chapter 4 presents a measure to determine the anthropomorphism of artificial hands. A large proportion of that Chapter is dedicated to finding an optimal low dimensional embedding that is a crucial element of the measure. Finally, it grades existing hand designs to gain first experience with the system.

Chapter 5 goes one step further, using the measure to create new, improved hands. That is achieved by two approaches. The first one optimizes kinematic parameters of artificial hands and the second adds new components to existing hands and determines their influence on the capabilities of the hand.

Finally, in Chapter 6 a conclusion is given. It sums up the results achieved in the thesis and proposes how the research can be continued.

Chapter 2

State of the Art

The approach presented in the thesis is multidisciplinary. It does not belong to one specific field, therefore knowledge of many different areas is needed. This Chapter presents only the relevant background, without going too much into detail.

The first two Sections are of high relevance for Chapter 3. It is important to know how the human hand works and to understand the "language" describing the movements. Therefore Section 2.1 presents the human hand anatomy and which joints confer the human hand. Additionally, Section 2.2 presents how the human hand movements can be analyzed in a structured way and describes concepts in grasping.

The next three Sections are important for Chapter 4. A human grasp dataset is projected onto a low dimensional space using an unsupervised machine learning algorithm presented in Section 2.5. Artificial hands are projected into that space as well, in order to compare human and machine. Such a hand is defined via five kinematic chains, where the mathematical background is presented in Section 2.4. The tested hands reproduce movements of existing prosthetic and robotic hands as presented in Section 2.3.

2.1 Anatomy of the Hand

This section gives a short overview over the anatomy of the human hand. The focus of this thesis is on the human hand, therefore most details will be given on the hand joints. The arm itself is out of scope, as its main purpose is to position the hand.

2.1.1 Forearm

On the forearm many of the muscles which articulate the fingers are located. Due to the high dexterity of the human hand a lot of different muscles are needed to achieve this high degree of independence between the joints of the hand. Figure 2.1(a) and Figure 2.1(b)

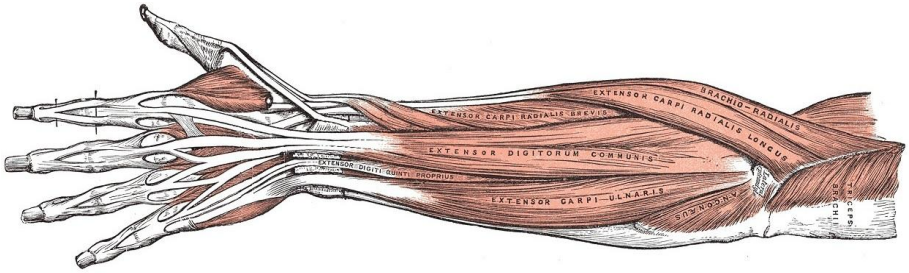

(a) Extensor muscles on the forearm.

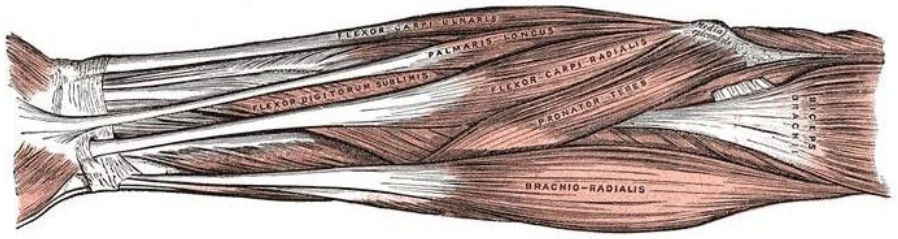

(b) Flexor muscles on the forearm.

Figure 2.1: The human forearm anatomy, muscles articulating the fingers [8]. The images show that a large number of muscles are used to drive the digits; the individual names of the muscles are not of interest for this thesis.

show the extensor, and the flexor muscles respectively of the arm. The muscles which drive the fingers are clearly visible. The structure of the forearm/hand articulation is very sophisticated. Many muscles are involved in the actuation of the fingers. For each joint movement at least a pair of muscles is needed. One muscle (the agonist) moves the joint into one direction, whereas the opposing muscle (the antagonist) hinders or reverses that movement [6]. The force produced by the muscles is transmitted via tendons to the joints of the hand. Commonly, one muscle is used to drive more than one joint and the tendons pass multiple other joints [7]. That makes it very difficult to define the joint a muscle is responsible for as the activation of one muscle induces a moment in many joints. Which joint finally moves depends on the contraction level of other muscles, in particular the antagonists. This interconnection from one muscle with multiple joints introduces a coupling between fingers. Overall, a large number of different muscles are present, resulting in a highly sophisticated anatomical structure.

2.1.2 Metacarpus

The palma manus or the palm of the hand, is formed by the five metacarpal bones (Figure 2.2). Due to its unique position the thumb is described in Section 2.1.5. The Carpo-Metacarpal (CMC) joints are of amphiarthrosis type allowing the palm to form an arch [9, p. 174]. The amount of movement in the CMC joints increases from index to

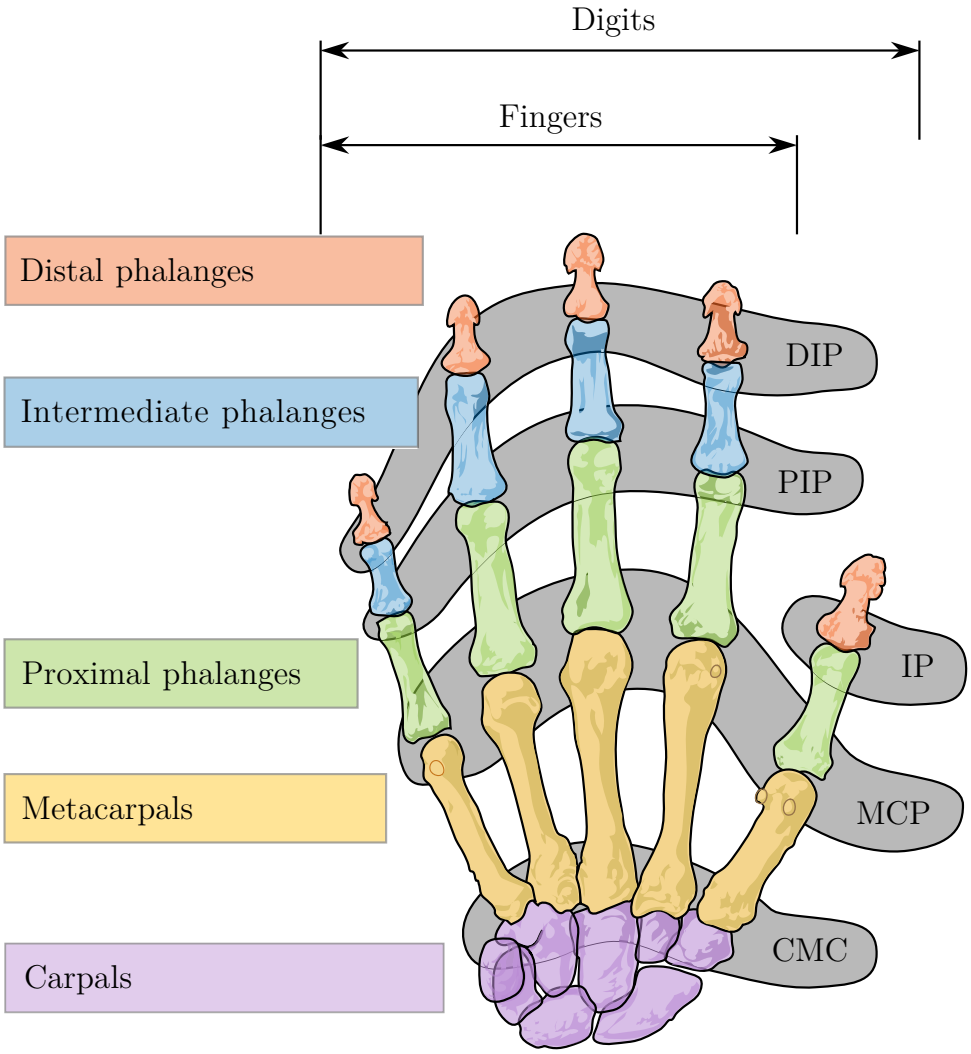

Figure 2.2: Bones of the human hand. Commonly, the index, middle, ring and little finger are regarded as the fingers, whereas digits also include the thumb. Figure modified from [10].

little finger and supports opposition of the little finger against the thumb. In conjunction with the flexion, the little finger is also moved in a suppinatory manner which rotates the little finger inwards, so that spherical grasps are facilitated. The angular movements in the CMC joints are small, therefore many hand models regard the palm as rigid. Nevertheless, as the distance to the fingertips is large, a small rotation in such a joint results in a large translation in the fingertips. For an average hand size, a five degree flexion of the CMC joint results in $10 - 15$ mm difference of the fingertip.

2.1.3 Metacarpal Joints

The Metacarpal (MCP) joints are spherical joints [9, p. 178], but along the longitudinal direction the movement is very limited. Therefore, most publications regard this joint as

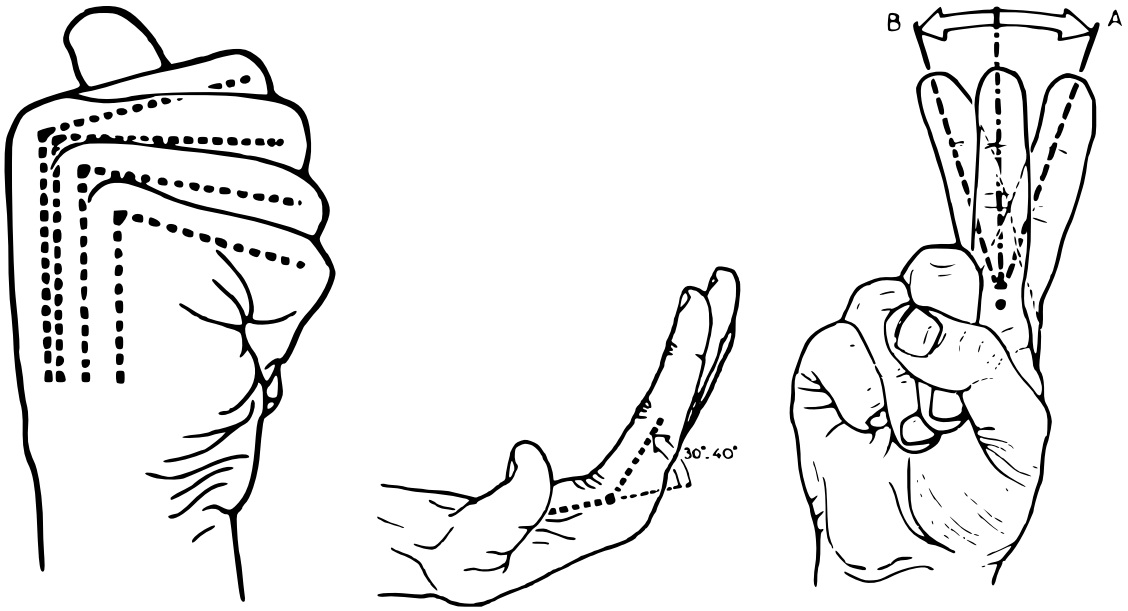

(a) Flexion of the MCP joints of the hand. The amount of flexion increases from index to little finger.

(b) Active extension of the fingers.

(c) Adduction (B) and Abduction (A) movement of the index finger.

Figure 2.3: Range of motion of the Metacarpal joint [9, p. 185].

having two axes, allowing flexion/extension and abduction/adduction. Maximal flexion of the MCP joint is about 90 degrees, and as shown in Figure 2.3(a) it increases towards the little finger. Active extension can be up to 30 - 40 degrees (Figure 2.3(b)). Adduction and Abduction of the fingers is possible, having a small movement amplitude. The index finger has the biggest range of motion with an amplitude of about 30 degrees (Figure 2.3(c)).

2.1.4 Interphalangeal Joints

Each of the fingers has two Interphalangeal (IP) joints; the Proximal Interphalangeal (PIP) and the Distal Interphalangeal (DIP) joint. They are hinge joints with one Degree of Freedom (DoF) – flexion and extension. The amount of flexion increases from index to little finger. The PIP joint can be flexed up to 135 degrees and the DIP joint flexion is slightly below 90 degrees [9, p. 186]. Active extension in both joints is limited to zero degrees, but the DIP joint allows for a passive extension of about 30 degrees. This is important when grasping objects in a precision grasp as the contact area is increased.

2.1.5 Thumb

The thumb has a unique position amongst the digits as it can be controlled very independently to the movements of the other fingers. Consequently, movements of thumb joints

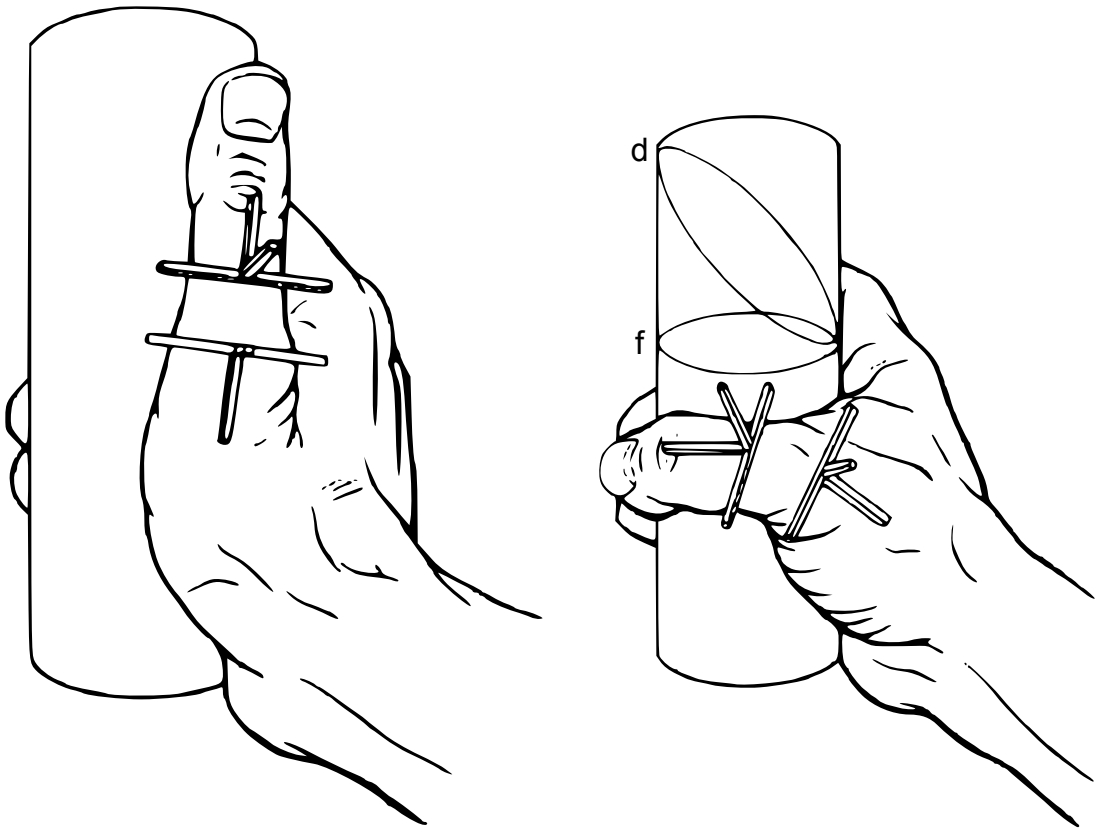

(a) When an object is grasped without the thumb, the object cannot be held securely.

(b) The thumb helps to secure the grasp. Arch (f) on the object is when the thumb MCP joint abduction is active and path (d) if the MCP joint would not be capable of abduction.

Figure 2.4: Difference of the grasp stability when the thumb is employed [9, p. 235].

do not provoke movements of other fingers [11, 12] or vice versa. During functional tasks the thumb is used in a different manner than the other fingers [13] and it is the only digit that can oppose other fingers (primary the index finger). That is the basis for most grasping movements. When an object is grasped with a power grasp the thumb is vital for a stable grasp. If the thumb is not used, as shown in Figure 2.4(a), the grasp loses a lot of its stability as compared to the "normal" power grasp (Figure 2.4(b)).

The kinematic structure of the thumb is more complex when compared to the fingers. That is due to three reasons. *First*, the thumb has more DoF than the fingers. *Second*, the base of the thumb is not aligned with any anatomical plane [14], which makes it difficult to define its movements. That can be also seen in Section 5.2.1, where the primary movement axis is not parallel to any coordinate axes. When measuring the rotation of a hinge joint, which is not aligned with any axes, a rotational component around all three axes will be recorded. Nevertheless, the underlying structure is still one dimensional. The three rotation angles would be perfectly coupled and therefore can be reduced to one

parameter. *Third*, the movement amplitudes of certain joint rotations are rather small, therefore not easily visible. The contribution of those small movements is still important for the thumb function. Those three facts combined make the thumb the most complex system of the five digits [9, p. 208].

The Carpo-Metacarpal joint (Figure 2.2) of the thumb is a saddle joint having 2 DoF. Kinematically this joint can be regarded as a universal joint allowing flexion/extension and abduction/adduction, rotation about a longitudinal axis is prevented by the joint surfaces. The Metacarpal (MCP) joint has 2 joint axes, allowing flexion/extension and abduction/adduction. Little rotation about the longitudinal axis is possible [9], but is normally not regarded as a DoF. Figure 2.4(b) highlights the importance of the abduction/adduction capability of this joint. The arch (f) on the object shows how the finger wraps around the object with normal thumb function. If the MCP joint lacked that ab/adduction capability, the contact area would be more like the elliptic arch (d) which decreases the grasp stability [9, p. 234]. In contrast to the other fingers, the thumb has only two phalangeal bones, which are connected via the Interphalangeal (IP) joint, a hinge joint. In total, these movements sum up to five DoF for the thumb.

2.2 Theory of Grasping

The hand is a complex system and its usage is even more complex. It can be used in a vast variety of tasks. Such as grasping, pushing, holding objects and expressing emotions. As this is an enormous range, the thesis focuses on human grasping with one hand. Still, that is a large and diverse subset. Various authors have tried to structure those movements in order to gain insights on the human hand deployment. This is done by applying different classification principles.

First, there is a rough discrimination for human hand motions into two main groups [15, p. 902]:

Prehensile Movements or movements in which an object is seized and held partly or wholly within the compass of the hand

Non-Prehensile Movements or movements in which no grasping or seizing is involved but by which objects can be manipulated by pushing or lifting motions of the hand as a whole or of the digits individually.

For the scope of this thesis only the prehensile movements are of relevance. In the thesis the terms prehensile movement and grasp will be used interchangeably. Consequently, the focus is on those movements and all other possible hand usages are neglected. A definition of all grasp types that are relevant for this study will be given in Section 3.1.

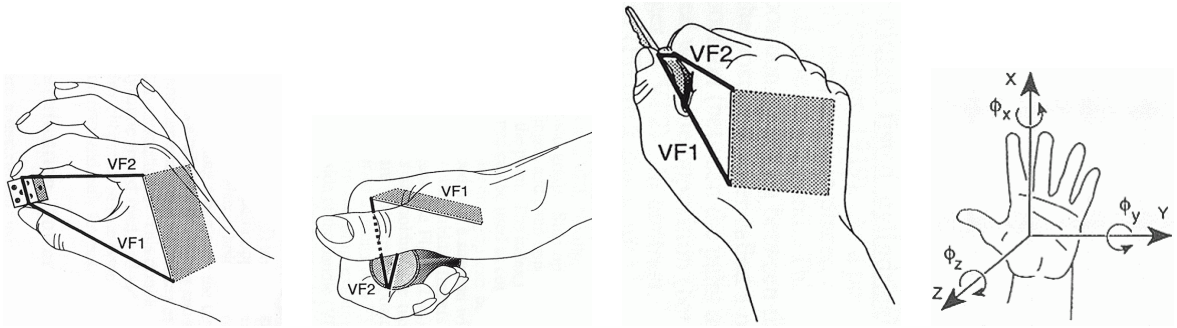

(a) Pad Opposition (b) Palm Opposition (c) Side Opposition (d) Hand Coordinate system

Figure 2.5: Opposition types of the grasping hand [17]. Figures are taken from [18, p. 34]. The abbreviation VF refers to Virtual Finger which is explained in Section 2.2.3.

2.2.1 Opposition types

There are three basic directions relative to the hand coordinate frame, in which the hand can apply forces on the object to hold it securely [16]. Those are [17, p. 286], Figure numbers adapted:

Pad Opposition occurs between hand surfaces along a direction generally parallel to the palm (Figure 2.5(a)). This usually occurs between volar surfaces and the fingers and thumb, near or on the pads. Examples include holding a needle or a small ball. This is the x-axis in the inset in Figure 2.5(d).

Palm Opposition occurs between hand surfaces along a direction generally perpendicular to the palm (Figure 2.5(b)). Examples include grasping a large hammer or screwdriver. This is the z-axis inset in Figure 2.5(d).

Side Opposition occurs between hand surfaces along a direction generally transverse to the palm (Figure 2.5(c)). One holds a key between the volar surface of the thumb and the radial sides of the fingers, or holds a cigarette between the sides of the fingers. This is the y-axis inset in Figure 2.5(d).

2.2.2 Power, Precision, Intermediate Grasp

In every prehensile movement either the power or precision requirement is dominant, even though both sides are present simulaneously. Therefore each grasp can be classified by its need for precison or power [15]. The differentiation is very important, and the idea has influenced most of the authors, as described in Section. 3.2. In Figure 2.6 a sequence

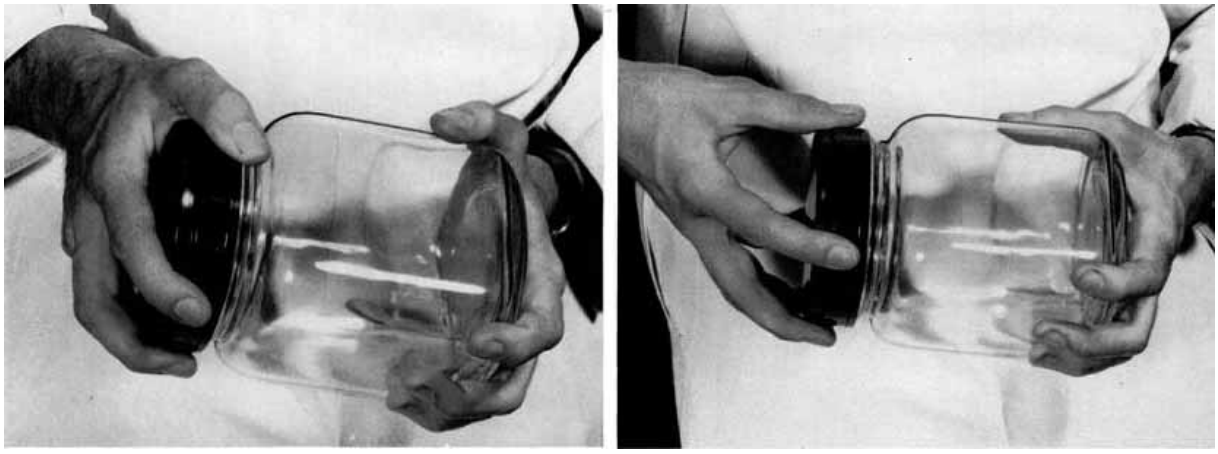

Figure 2.6: A sequence of hand grasps [15]. As the lid gets loose and can be manipulated with less force, the hand changes from a power grasp (left) to a precision grasp (right).

is presented where the hand posture changes from power to precision grasp within the same movement. In the beginning, when the lid of the jar is being opened the dominant requirement is power. When the lid becomes loose, the grasp is changed to a precision grasp, where the ability for delicate movements increases and thus allowing for a faster opening of the lid.

The idea was further developed by Landsmeer [19], who distinguishes between "power grip" and "precision handling". In the power grip, there is a rigid relation between the object and the hand. That means that all movements of the object have to be evoked by the arm. For the precision handling, the hand is able to perform intrinsic movements on the object without having to move the arm. That is the most significant difference between those types [19]. As for our study that difference is somewhat mitigated – we only look at static grasps. That are grasps where the object is in a constant relation with the hand. Nevertheless if a precision grasp is applied to the object, it is (assumed to be) static.

Kamakura [20] later added a third component, the intermediate grasp, where both power and precision are present in roughly the same proportion. This allows for a finer differentiation of grasp types, nevertheless the basic principle stays the same.

2.2.3 Virtual Fingers

In many tasks more than one finger work together as a functional unit, the virtual finger (VF) [21]. Depending on the grasp type, one or more finger or hand proportion can be assigned to one virtual finger. The two virtual fingers oppose each other in the grasp, as it would be the case for a simple two fingered gripper or vice. For example in the case of palm opposition (Figure 2.2.1 B), the palm of the hand is assigned to VF 1 and the four

fingers act against it as VF 2.

If one or more fingers are opposing a task related force or torque, these fingers are assigned VF 3, otherwise VF 3 will not be assigned [17].

2.2.4 Grasp Taxonomies

A big effort has been put into categorizing the human grasp postures. As the literature review in Section 3 will reveal, many different classifications are available and there is no consensus between publications. This seems to be due the fact that each publication has a different focus and that the hand movements are so complex that classifying them is very difficult.

2.3 Artificial Hands

2.3.1 Prosthetic Hands

In contrast to robotic hands, described in Section 2.3.2, prosthetic hands have a limited amount of DoF. This is due to the problems a dextrous hand poses in terms of design, reliability and control. A prosthetic hand has to be rather small (human size), the actuators have to be integrated in the hand itself, because it has to fit to a patient which only lost his hand and not his forearm [22]. Therefore, there is no space to locate the actuators of the hand on the forearm. In addition it has to be very reliable [4], as the patient will use it everyday in a variety of different tasks. Consequently, the hand cannot be designed to fulfill a specific purpose. There are various commercial products available, as will be described further in this section.

The *Otto Bock SensorHand®* [23] is a first generation myoelectric hand [24]. Mechanically the hand has three fingers, which move in a synchronized manner. Therefore, the hand has one DoF. The advantage of the hand is that it is very robust [25] and can develop a strong grip force of about 100 N [23]. To give it a more human like appearance, a covering glove is put over the hand. Figure 2.7(a) shows the hand with and without that glove. The glove also emulates the ring and the little finger, resulting in a 5-digit design. There is a metal bar within the glove which couples fingers four and five to the movements of the middle finger. As they are solely connected via the glove, the movement amplitude decreases from middle to little finger.

The next generation of prosthetic hands by *Otto Bock* is the so called *Michelangelo®* hand [26], Figure 2.7(b). It follows a more human-like kinematic setup and it has 2 DoF. The axes of the finger MCP joints are oriented in a more natural way, where the flexion of the finger also invokes a small adduction. The fingers are slightly abducted

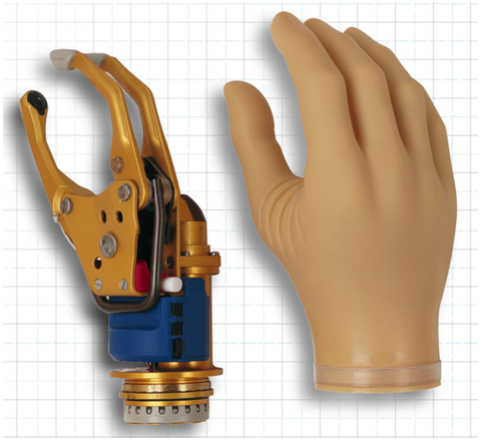

(a) Left: The *Otto Bock SensorHand Speed*® without the glove. The three fingers move in a synchronous manner. Right: The prosthetic glove which covers the hand and gives the hand a five-digit appearance [23].

(b) *Otto Bock Michelangelo*® hand [26].

Figure 2.7: Prosthetic hands by *Otto Bock*.

when the MCP joints of the fingers are extended, whereas when flexed the fingertips touch each other. The first DoF is the main drive which is responsible for a coordinated flexion and extension of the five digits. The second DoF changes the thumb position – it can be abducted or adducted. That allows for two different grasp types, a tip pinch between the thumb and the index and middle finger and the lateral grasp between thumb and the side of the index finger.

The *I-Limb*™ *ultra* Hand by *Touch Bionics*™ has a different kinematic setup and is shown in Figure 2.8. Every finger is actuated by one motor and the MCP and PIP joints of the fingers are coupled. That gives the hand 5 DoF, but that causes a large control problem. Therefore, the hand is controlled in the "classical" way, with one or two electrodes [27]. As all the fingers move simultaneously, or according to a fixed sequence, the hand control space is one-dimensional. In addition to the myoelectrically controlled finger movements, the thumb can be manually adjusted to be in an adducted or abducted position. The setup offers some compliance, as every finger closes independently until it is in contact with the grasped object which stops the movement.

2.3.2 Anthropomorphic Robotic Hands

Many robot hands have been developed in the past and many have had the human hand as paradigm. Depending on the purpose, they have different properties regarding size, sensors, Degree of Freedom etc. Research prototypes tend to have a lot of DoF, but are rarely used outside the university environment. One exception is the *Shadow Dexterous*

Figure 2.8: The *I-Limb*™ *ultra* hand from *Touch Bionics*™ without a covering glove. The kinematic structure of the five digits is identical [28].

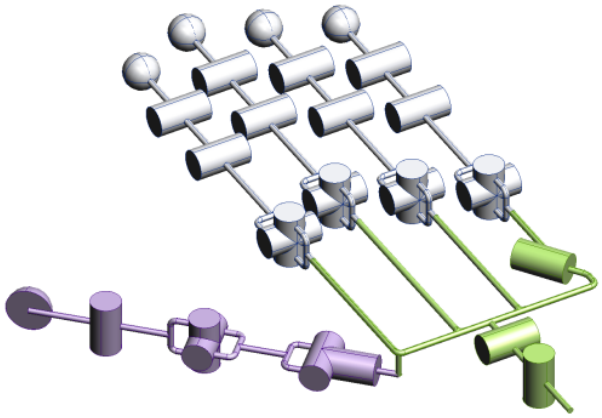

Figure 2.9: The kinematic setup of the *Shadow Dexterous Hand C6*. Each large cylinder represents one joint of the hand [30].

Hand C6 [29] which has 20 DoF and 24 joints. The actuators are 40 pneumatic muscles, which are situated on the forearm. The kinematic setup of the hand is shown in Figure 2.9. The index, middle and ring finger have four joints and the little finger has five joints. The additional joint is the movement of the CMC joint. The PIP and DIP joints of the fingers are coupled, reducing the DoF per finger to 3 and 4 respectively. The thumb has five DoF, two in the CMC and MCP joint, one in the IP joint. Additionally, the wrist offers 2 movement possibilities, summing up to a total of 20 DoF.

The FRH-4 hand [31] built for the mobile assistive robot ARMAR has 8 fluidic actuators. Its general appearance (Figure 2.10) is human-like, it has a size that is comparable to the human hand and the kinematic setup has some similarities. One design goal of the hand was to be anthropomorphic, but another goal was to develop a hand which is suitable for robotic grasping. To meet the second design objective, tradeoffs on the anthropomorphism had to be accepted. One major difference is the palm setup – the

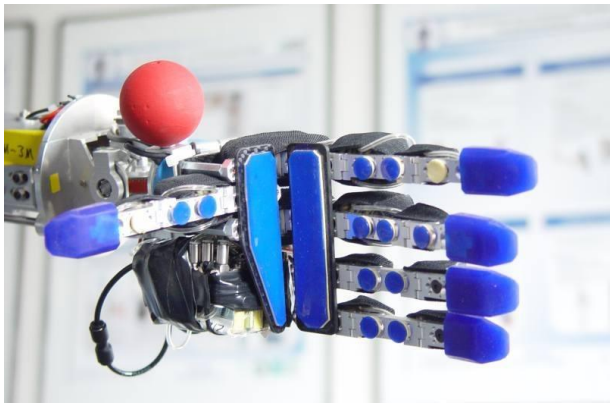

Figure 2.10: The FRH-4 Hand for the mobile assistive robot ARMAR [31].

FRH-4 hand has one DoF in the metacarpus, which allows the palm to flex in the middle. The human hand does not share this feature as there is no joint in the middle of the palm along a transversal axes. Figure 2.10 shows the palm joint in a flexed position. In the extended position, the fingers would point to the upper right corner of the picture. In that case the thumb and the fingers are coplanar. The index and the middle finger both have 2 DoF, one joint represents the MCP joint of the human and the other one is in-between the PIP and DIP joint. The ring and little finger have one combined DoF, that is a common flexion in the MCP joint. All joint axes of the fingers are parallel and the finger segment lengths are 40 mm. The thumb has two actuators, which actuate the CMC joint and the joint between the MCP and IP joint of the thumb. The base of the thumb is exactly opposite and between the index and the middle finger, perfectly opposing those two fingers. This setup is very similar to the SensorHand and fundamentally different to the human hand, where the axes of the thumb are not aligned with the axes of the fingers. Each of the eight DoF has a range of 90 degrees.

2.3.3 Hand Control

The lack of a proper interface between human and machine makes it difficult to detect the intention of the user [3], and therefore the control of the hand is currently the bottleneck in prosthetic systems. The contemporary method of controlling a prosthetic hand is to control one DoF at a time. To control more than one DoF, a sequential control scheme is applied. That method is rather cumbersome and limited to very few independent control signals. More channels require extensive switching between those, being very slow. Advanced methods for prosthetic control have been proposed, however none of them proved reliable enough for commercial application [2, 25].

In the case of robotic hands, the problem is very similar. Anthropomorphic hands, with multiple independent actuators, provide a large potential dexterity. Due to the lack

of proper control algorithms the effective dexterity is much lower, as the controller cannot make use of the potential of the hand [1].

2.3.4 Optimal Hand Designs

Only very recently the interest has shifted to simpler hands with only a few DoF. However, they are smartly designed so that they can fulfil their assigned tasks [32]. How different design parameters influence the dexterity of a kinematic hand setup is largely unknown [33] and considered a difficult task [34]. Due to the mechanical complexity of the hand itself and the complex hand-object interaction it is difficult to assess the hand performance without realization of the design, as analytical tools are limited to few special cases.

One approach [35, 36] is specialized in underactuated kinematic hand setups. Feasible grasping postures are manually defined for a given kinematic hand setup. This implies the assumption that all joints can be controlled independently. In the next step the actuation parameters resulting in the largest number of stable grasps in the predefined pool are chosen. In that sense this is the optimal underactuated hand design. In [36] a prototype was built for a simple symmetric 2 finger gripper. For this special case it was possible to calculate a global optimum solution. For more complex embodiments the goal function will become more difficult to handle, having multiple local minima and therefore calculation will become non-trivial. Additionally, in the current implementation the set of grasps is created manually, prohibiting large scale usage.

An approach using postural synergies is presented in [37]. A certain number of in hand rigid-body object motions and internal forces can be applied to the object depending on the number of synergies (defined as basis vectors of a linear subspace) used to drive the hand. It can be shown that with an increasing number of synergies more movements and forces become controllable. For example, having three point contacts on the object and controlling the hand with one synergy, one internal force is controllable. Increasing the number of synergies up to three will render up to three internal forces controllable. A further increase in the number of synergies will allow for intrinsic movements. Finally, if the number is increased even higher redundant movements will be possible. This analysis is a good tool to judge how complex a hand has to be in order to achieve a desired degree of dexterity. Nevertheless, this tool is limited to a linear subspace analysis and therefore to joint couplings in a linear combination sense. Nonlinear couplings or other complex joint coordination patterns cannot be modeled using this approach. Further, this does not produce hints on the actual design of a kinematic hand setup.

Using the tendon driven Anatomically Correct Testbed (ACT) hand, Malhotra and Matsuoka [38] investigate how tendon coordination patterns influence the positional precision of the hand. In the fully actuated hand the only error of the controller is present,

which acts as the baseline. The decrease in precision is measured after tying various tendons to the same actuator. Without large penalties on the fingertip precision a small reduction in actuators is possible. Controlling 20 tendons with only 16 motors results in an increase of the error of about 30 % to the fully actuated hand. When each finger is driven only by 2 actuators, the error is twice that of the fully actuated hand.

A more specialized approach is taken in [33], where the focus is to optimize the hand for a specific set of objects with simple shape. When grasping blindly into a box of such objects, the hand should be designed in such way that only a few hand-object configurations are possible. Finally, the goal is that only one configuration results in a successful grasp. In that case no sensors would be needed to determine how the object is grasped with the hand. The relative orientation of the object and the hand will be known as only one configuration results in a successful grasp. The evaluation method is complicated and extensive as it is partly based on real experiments or complex simulations.

The experimental approach of [39] restrains different fingers and finger combinations by tying them to a fixed structure. Then the performance of those altered human hands is measured with standard human hand dexterity tests (e.g. box and block test). The result is that the thumb and the middle finger are most important for the grasping performance. The best results were obtained when the little finger was restrained, which was taken as a sign that for that simple grasps the finger did not contribute to the overall dexterity. The results are worse when the index and the middle finger are restrained.

2.4 Kinematic Chains

A kinematic chain is a series of rigid bodies connected by joints. For the thesis that is an important concept, because a hand can be modeled as five independent kinematic chains. Each finger is represented by one chain, where the joints of the chain correspond to the actual joints of the hand. The hand models presented in the thesis are defined in the fashion introduced here.

2.4.1 Degrees of Freedom

There are different definitions for the number of Degrees of Freedom (DoF) of a system and they depend upon the area the definition belongs to. For this thesis the following definition is suitable [40, p. 133]:

"The number of degrees of freedom of a system is the number of independent variables that must be specified to define completely the condition of the system. In the case of kinematic chains, it is the number F of independent pair variables needed to completely define the relative positions of all links."

A rigid body in a 3D space has 6 DoF - three for translation and three for rotation. The specification of position and rotation in one parameter set will be referred to as *pose*.

Given a kinematic chain where all joints are actuated independently, the DoF will be equal to the number of joints. For the thesis, being in accordance with the Denavit Hartenberg view of modeling kinematic chains, each joint is represented by one axis about which the rotation takes place. Accordingly, a spherical joint is modeled as three joints where the joint axes intersect in the center of the joint. Additionally, the six DoF which define the pose in space are disregarded as the global orientation and position of the hand is not of interest for the study.

If constraints on the movement are introduced, the number of DoF is reduced. The reduction in DoF depends on the constraints' type. For example, if the body is constraint to planar motion, the movements are restricted to 2D. In that case the body has 3 DoF – two for translation and one for rotation about the axis perpendicular to the plane. If two joints of the kinematic chain are coupled, the DoF are reduced by one. That is due to the fact that one parameter will define the rotation of both joints and is therefore sufficient.

Care has to be taken when talking about Degrees of Freedom in human hand models. Often the specification of DoF is not correct and corresponds to the number of joints. As some of the joints might be driven by the same actuator, a coupling between the joints is introduced. From a mechanical perspective the number of actuators corresponds to the number of degrees of freedom. That discrepancy between joints and DoF can even increase if the hand has mechanically multiple DoF, but they are all controlled in synchronization. That leads to a hand with a large number of joints, but with a small number of DoF.

The same principle applies to the human hand. Depending on the publication, around 23 (with a range of 21-31) joint movements can be identified. The first assumption would be that the hand has as many DoF as joints. The fact is that, due to mechanical and neural limitations, the joints of the hand are coupled to some degree. Consequently, not all joints can be moved in total isolation without invoking a movement in other joints. In the high dimensional joint space, a manifold exists where the actual human hand movements take place. The minimal dimension with which the manifold can be described will be equal to the DoF of the hand. Those couplings are non-obvious and cannot be modeled explicitly. Therefore, data driven approaches are used to determine the dimensionality of the human hand. Various studies have shown that with only a few basis vectors most of the hand movements can be described with sufficient precision (see Section 2.5.1). That reveals that the actual number of Degrees of Freedom is much smaller than the number of joints. That fact is also exploited later in the thesis, as this is the justification for the dimensionality reduction applied to the human grasping dataset.

2.4.2 Denavit - Hartenberg Formalism

The convention was first proposed by Denavit and Hartenberg [41]. It is a method to unambiguously describe a kinematic chain with four parameters per link/joint. Possible joint types which connect the links are of type revolute and prismatic. A revolute joint allows the rotation about one axis, whereas a prismatic joint defines the translation along an axis. The number of parameters needed to determine the relation between two links is reduced from 6 to 4 by to the introduction of special conventions [42, p. 65]. The formalism allows to quickly determine the transformation matrices which transform from the base coordinate system to the end effector frame. Calculating the end effector frame with given joint angles is called forward kinematics. The Denavit Hartenberg (DH) notation is used to define the hand models in Section 4 and Section 5.

The four DH parameters are the following [42, p. 70-71]:

$a_i =$ distance along x_i from o_i to the intersection of the x_i and z_{i-1} axes.

$d_i =$ distance along z_{i-1} from o_{i-1} to the intersection of the x_i and z_{i-1} axes. d_i is variable if joint i is prismatic.

$\alpha_i =$ the angle between z_{i-1} and z_i measured about x_i.

$\theta_i =$ the angle between x_{i-1} and x_i measured about z_{i-1}. θ_i is variable if joint i is revolute.

The Figure corresponding to the definition is presented in Figure 2.11. A more elaborate description on the system can be found in [42]. It also defines the parameters in more detail, in specific how the sign of the values is determined correctly.

The transformation matrix A_i corresponding to link i is given by the following relation:

$$A_i = Rot_{z,\theta_i} Trans_{z,d_i} Trans_{x,a_i} Rot_{x,\alpha_i} = \begin{pmatrix} \cos\theta_i & -\sin\theta_i \cos\alpha_i & \sin\theta_i \sin\alpha_i & a_i \cos\theta_i \\ \sin\theta_i & \cos\theta_i \cos\alpha_i & -\cos\theta_i \sin\alpha_i & a_i \sin\theta_i \\ 0 & \sin\alpha_i & \cos\alpha_i & d_i \\ 0 & 0 & 0 & 1 \end{pmatrix} \tag{2.1}$$

Finally, the full transformation from the base frame to the end effector frame is given by multiplying all the transformation matrices corresponding to the links l_i.

$$H = T_n^0 = A_1(l_1) \cdot \ldots \cdot A_n(l_n) \tag{2.2}$$

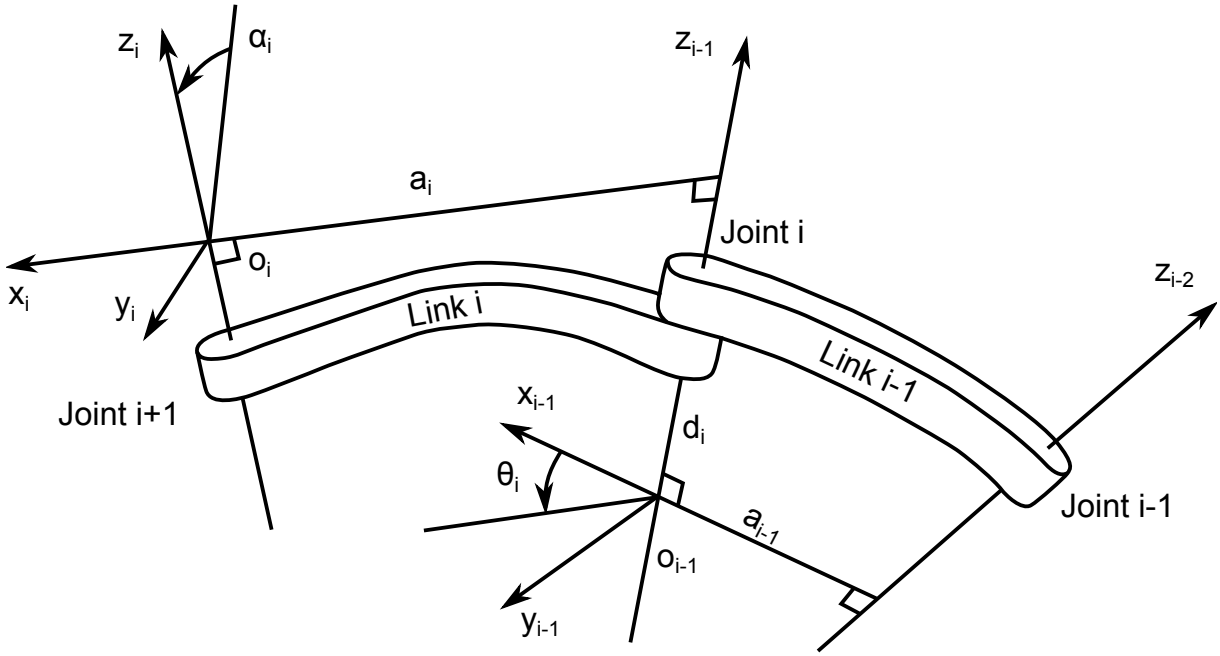

Figure 2.11: Coordinate system assignment for the DH convention [42].

2.4.3 Human Hand Models

A lot of effort has been put into developing a kinematic model of the human hand. There are many applications for such a hand model. They range from the field of biomechanics [43–47], animation of the human hand [48–55], hand tracking [56–59], hand posture prediction [60, 61] to virtual grasping experiments [62, 63]. There is no real consensus about the number of Degrees of Freedom the hand has, or even which joint axes are assigned to a specific joint.

Table. 2.1 shows a comparison of different human hand models. The average number of DoF assigned to the hand is about 23. In most cases the thumb CMC and MCP joint are assigned two DoF; one for flexion/extension and one for abduction/adduction. The thumb IP joint is modeled as a hinge joint, offering only flexion/extension.

The kinematic setup from the fingers is consistent throughout the publications. The MCP joint is a two axis joint with flexion/extension and abduction/adduction and the PIP and DIP joints offer only flexion/extension. The biggest variation is whether the palm is modeled as rigid body (10 cases), or if the CMC joints of the fingers are assigned some rotational freedom (6 cases). Especially for spherical grasps this freedom becomes important. It allows the palm to form an arch, so that the hand can adapt better to the shape of the object.

In mathematical terms, a human hand model is composed of five independent kinematic chains, each representing one digit. The kinematic structure is defined by the joints assigned to the hand model, as described above. In most cases Denavit Hartenberg (DH)

parameters are used to calculate the forwards kinematics. To define such a model, many parameters have to be determined:

- The pose of the bases of digits in the hand coordinate frame. That specifies how the starting point of the kinematic chain is translated and rotated in space.
- The kinematic setup of the hand. The position and orientation of the joint axes and the segment lengths have to be specified. Those parameters can be represented in a structured way with the DH convention.
- Range of motion of the joints.
- Optional: Coupling functions which connect joints and reduce the number of DoF of the hand.

Determining those parameters is not trivial. Most models generate those parameters by measuring one hand only. For example a Computed Tomography (CT) scan of a human hand can be used to determine the parameters [52]. A different approach is to use a system based on optical surface markers to determine the rotational centers of the human hand joints [64]. Unfortunately, such a system has never been used to perform a large scale analysis on several specimen. To the best knowledge of the author, the only publication which measures anthropomorphic parameters and expresses them as a function of hand width and hand length is [44]. The kinematic parameters of cadaver hands were measured and means to scale them according to the hand length and width are presented. As this study is composed of only six hands, it might not represent the complete human population.

			Average	Rijpkema 1991	Buchholz 1992	Lee 1995	Yasumuro 1999	Lin 2000	Kapandji 2006	Albrecht 2003	Wan 2004	Pitarch 2005	Veber 2006	Jones 2006	Choi 2008	Rezzoug 2008	Cobos 2008	Sancho - Bru 2003	Lee 2005
Thumb	CMC	f/e	1.0	1	1	1	1	1	1	1	1	1	1	1	1	1	-	-
		Ab/Ad	1.0	1	1	1	1	1	1	1	1	1	1	1	1	1	-	-
		Rot	0.2	0	1	0	0	0	0	1	0	0	0	0	0	1	0	-	-
	MCP	f/e	1.0	1	1	1	1	1	1	1	1	1	1	1	1	1	1	-	-
		Ab/Ad	0.8	1	1	1	1	1	1	1	1	1	0	1	1	0	0	-	-
		Rot	0.3	0	0	0	0	0	1	1	0	0	1	0	1	0	0	-	-
	IP	f/e	1.0	1	1	1	1	1	1	1	1	1	1	1	1	1	1	-	-
Index	CMC	f/e	0.1	0	0	0	0	0	0	0	0	0	0	0	0	0	1	1	0
	MCP	f/e	1.0	1	1	1	1	1	1	1	1	1	1	1	1	1	1	1	1
		Ab/Ad	1.0	1	1	1	1	1	1	1	1	1	1	1	1	1	1	1	1
		Rot	0.1	0	0	0	0	0	0	1	0	0	0	0	0	0	0	0	0
	PIP	f/e	1.0	1	1	1	1	1	1	1	1	1	1	1	1	1	1	1	1
	DIP	f/e	1.0	1	1	1	1	1	1	1	1	1	1	1	1	1	1	1	1
Middle	CMC	f/e	0.1	0	0	0	0	0	1	0	0	0	0	0	0	0	1	1	0
	MCP	f/e	1.0	1	1	1	1	1	1	1	1	1	1	1	1	1	1	1	1
		Ab/Ad	1.0	1	1	1	1	1	1	1	1	1	1	1	1	1	1	1	1
		Rot	0.1	0	0	0	0	0	0	1	0	0	0	0	0	0	0	0	0
	PIP	f/e	1.0	1	1	1	1	1	1	1	1	1	1	1	1	1	1	1	1
	DIP	f/e	1.0	1	1	1	1	1	1	1	1	1	1	1	1	1	1	1	1
Ring	CMC	f/e	0.3	0	0	0	0	0	1	1	0	1	0	0	0	0	1	1	0
		Ab/Ad	0.1	0	0	0	0	0	0	1	0	1	0	0	0	0	0	0	0
	MCP	f/e	1.0	1	1	1	1	1	1	1	1	1	1	1	1	1	1	1	1
		Ab/Ad	1.0	1	1	1	1	1	1	1	1	1	1	1	1	1	1	1	1
		Rot	0.1	0	0	0	0	0	0	1	0	0	0	0	0	0	0	0	0
	PIP	f/e	1.0	1	1	1	1	1	1	1	1	1	1	1	1	1	1	1	1
	DIP	f/e	1.0	1	1	1	1	1	1	1	1	1	1	1	1	1	1	1	1
Little	CMC	f/e	0.4	0	0	0	1	0	1	1	0	1	0	0	0	0	1	1	0
		Ab/Ad	0.2	0	0	0	1	0	0	1	0	1	0	0	0	0	0	0	0
	MCP	f/e	1.0	1	1	1	1	1	1	1	1	1	1	1	1	1	1	1	1
		Ab/Ad	1.0	1	1	1	1	1	1	1	1	1	1	1	1	1	1	1	1
		Rot	0.1	0	0	0	0	0	0	1	0	0	0	0	0	0	0	0	0
	PIP	f/e	1.0	1	1	1	1	1	1	1	1	1	1	1	1	1	1	1	1
	DIP	f/e	1.0	1	1	1	1	1	1	1	1	1	1	1	1	1	1	1	1
		DOF	22.8	21	22	21	23	21	25	31	21	25	21	21	22	21	24	20	16

Table 2.1: Comparison of available human hand models. "1" marks that the hand has this DoF, whereas "0" denotes a missing capability. Only the information of Kapandji is an anatomy book. Due to space restrictions only the first author of each publication is printed. The two models on the right side did not model the thumb, therefore the thumb section is empty. They are excluded from the "average" column which calculates the mean over all other models. Finally, the bottom row shows the number of DoF for each model. "f/e" is flexion/extension of the joint, whereas "Ab/Ad" means Abduction/Adduction and "Rot" a rotation along an longitudinal axis. The models referenced in the table are in order from left to right [9, 44, 46–51, 53, 54, 56–58, 60, 61, 65]

2.5 Unsupervised Machine Learning

The term unsupervised machine learning refers to a method to find hidden structure within data. The data is unlabeled, thus there is no information on specific classes a data point belongs to which can be used to define an error function. One method, to find structure within the data is to apply dimensionality reduction algorithms in order to represent the data in a lower dimensional space. Such a low dimensional space is referred to as latent space. The shape of such a space might deliver deeper insights into the structure of the data. Such an approach is in particular useful if dimensions of the input space are coupled, thus reducing the intrinsic dimensionality of the dataset.

Due to neural and anatomical limitations, humans cannot move their finger joints independently. There is a large degree of interconnection between joints of the same and other digits. The thumb is the digit with the highest independence, followed by the index finger [11–13]. Nevertheless most joints cannot be moved in an isolated manner, be it intra- or interdigital movements. This fact reduces the intrinsic dimensionality of the human hand movements. If all joint axes could be moved completely independent, the number of DoF would be equal to the number of joint axes. As human finger movements are coupled, certain regions in the high dimensional space simply cannot be reached. Consequently, a subspace exists within the high dimensional space where the actual human hand movements are situated. The shape of the subspace or manifold is unknown, thus it is referred to as the latent (hidden) space. The dimension of the latent space will always be lower or equal than the dimension of the space which parameterizes the human hand postures. Various Dimensionality Reduction (DR) algorithms can be applied to find such a latent or low dimensional embedding suitable for a given task. Most research was done with Principal Component Analysis (PCA), but there are also other algorithms which can be applied for that purpose. [66]

2.5.1 Principal Components Analysis

The most prominent and widely used method for dimensionality reduction is Principal Component Analysis (PCA). This algorithm seeks a linear subspace which retains most of the variance in the dataset [67]. It has been applied in a wide spectrum of research areas [13, 68–71] and the principle behind it is simple but powerful.

Theory

The data matrix $\mathbf{Y}$ stores N observations in each row, with D variables. Therefore, the complete matrix is $\mathbf{Y} \in \mathbb{R}^{N \times D}$. The data matrix will then be centered, so that the mean of each column is zero [72]. Additionally to centering the data should also be scaled. This

can be done either by dividing each dimension by its variance or its maximum. This step gives each dimension a similar variance, thus each dimension is treated equally. Generally speaking, the scaling determines the relative importance of one variable in respect to the others. A priory knowledge can be incorporated into the system by weighting the dimensions of the high dimensional space differently.

To retain the Principal Components (PCs) the following eigenproblem has to be solved [73], where $\text{cov}(\mathbf{Y})$ is the covariance matrix of $\mathbf{Y}$ and $\mathbf{u}_i$ is the i-th eigenvector with a corresponding eigenvalue of λ_i.

$$\text{cov}(\mathbf{Y})\mathbf{u}_i = \lambda_i \mathbf{u}_i \tag{2.3}$$

The eigenvectors are then sorted by the value of their corresponding eigenvalues λ_i. The eigenvector with the highest eigenvalue is the most important one as it shows the direction in the data with maximal variance. The second eigenvector is perpendicular to the first one, pointing into the direction with the largest remaining variance. So the first q eigenvectors span a linear subspace in the original space with a dimension of q. To project the data to a subspace, the following mapping can be applied, where $\mathbf{M} \in \mathbb{R}^{D \times q}$ is the mapping corresponding to the linear mapping of the first q eigenvalues. $\mathbf{X} \in \mathbb{R}^{N \times q}$ is the data matrix containing the low dimensional locations of the points and is obtained by

$$\mathbf{X} = (\mathbf{Y} - \overline{\mathbf{Y}})\mathbf{M}. \tag{2.4}$$

Each row of the matrix $\overline{\mathbf{Y}}$ contains the means of the D variables. The rows are repeated N times to form a $N \times D$ matrix. That step guarantees that the mean of each dimension is zero.

The number of PCs which should be used depends on the intrinsic dimensionality of the dataset and the desired level of accuracy. When the subspace is linear, or close to linear, the method is guaranteed to find the correct subspace. On the other hand, when the data lies on some nonlinear manifold, PCA might have troubles finding a proper subspace, as it only looks for linear variance in the data [74].

Application to Grasping

Principal Component Analysis (PCA) can be used to gain deeper insights into the human grasping movements [68]. Subjects are asked to imagine to grasp an object and a Cyberglove is used to record the hand postures. Those preshapes are measured for a large set of different objects. The analysis showed that the first few PCs accounted for the vast majority of variance in the dataset. On average the first three PCs accounted for about 90 %

of the variance in the dataset. There are differences in literature about the actual number of Principal Components that account for 90 % of the variance but that can be explained due to different measurement setups and dimensionality of the data spaces. When only four fingers are taken into account and simple movements are performed, the first PC is dominant. In that case it alone contributes about 90 % of the variance [71]. This seems to be due to the stronger coupling between the fingers and the reduced dimensionality of the space, as the data of the thumb is missing. Similarly, when only a few specific tasks are recorded using a 15 Degree of Freedom Cyberglove, only four PCs are needed to reach the 90 % threshold [70]. When the hand is employed in an every day situation, composed of a variety of different hand movements, the hand movements are of higher dimension. In that case therefore 8 PCs are needed to explain 90 % of the variance [13].

Given different datasets which consist of a larger set of human grasping movements (not restricted to specific grasp types), the first two PCs are very similar [13, 68, 75]. Figure 2.12 presents a comparison of different literature sources. Commonly, the first one is a coupled opening and closing of the full hand. It employs mostly the Metacarpal joints of the fingers and the Carpo-Metacarpal joint of the thumb. The other joints stay in a rather moderate flexion throughout the complete movement. The second Principal Component modulates primarily the bending of the fingers, especially of the index finger. Nevertheless this component shows more variation than the first. Higher PCs will probably be unstable. However, the fact that the first two PCs are very similar suggests that there is a common 2D subspace for all human hand movements.

Eigengrasps

The term eigengrasp refers to a basis vector of a linear subspace in the joint space [63]. That low-dimensional basis of grasp postures is positioned in such a way that moving within that subspace will cover the most important part of the hand shapes. The advantage is that only a few control signals are needed to control a complex hand with many DoF. Such an eigengrasp space is commonly obtained by PCA, thus the first PCs form the eigengrasps.

The eigengrasp concept can be applied to a grasp planning system [35, 63]. The first two Principal Components are used to define the hand preshape for grasping an object. This restricts the space very much and therefore simplifies the search process for a suitable hand preshape for grasping. The system searches in the low dimensional space for a preshape which matches the presented object the best. When this shape is found, the system closes all fingers in a synchronized manner, until the finger movement is stopped by a contact with the object. When the hand is closed, it has to leave the subspace, to find a hand posture which can conform with the object. An additional advantage of

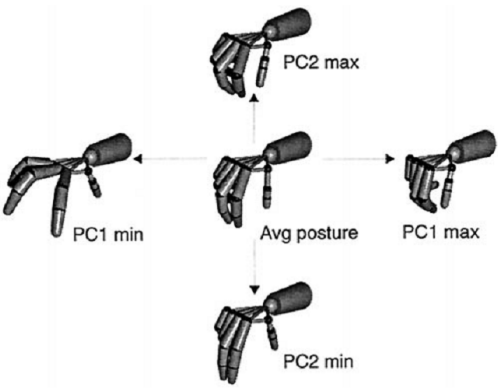

(a) Modulation of the hand posture when moving along the first two PCs according to [68].

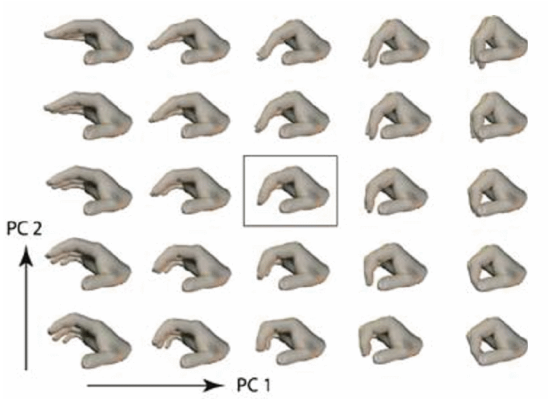

(b) Modulation of the hand posture when moving along the first two PCs according to [13].

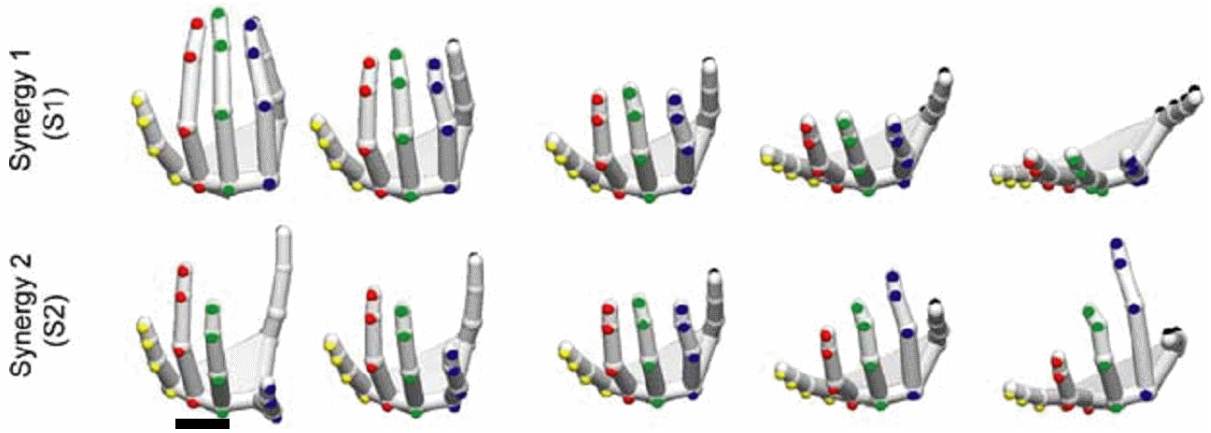

(c) Modulation of the hand posture when moving along the first two PCs according to [75]. Synergy 1 and 2 refer to the first two PCs.

Figure 2.12: Comparison of the first two Principal Components. All three change the hand posture in a similar fashion.

the system is that the planner is independent of the hand design. Simply the first two PCs have to be specified in the embodiment specific hand space. The system itself is completely independent of the hand kinematics. Up to now the focus has been proving the applicability of the system. Determining the optimal linear subspace for a given task has never been done.

2.5.2 Isomap

Isomap is a nonlinear method for dimensionality reduction [74]. The algorithm tries to preserve the pairwise geodesic distance between points, which is the distance measured on the lowdimensional manifold. As an approximation of the true distance, it is calculated by finding the shortest path between neighboring data points. The distance between all points is calculated and this information is fed to the Multi Dimensional Scaling algorithm which calculates the low dimensional representation of the data. A major weakness is the topological instability of the algorithm [76]. If the data is disrupted by noise, or the manifold is sparsely populated, a shortcut might occur. This means that the presumed neighboring point is not close, as it belongs to another branch and the actual distance along the manifold would be much bigger. Such a distance is obviously wrong and corrupts the result.

Isomap can be used to control a robotic hand [77]. A dataset with different human hand movements (tapping, 2 power grasps and 3 precision grasps) is measured with a Vicon optical marker capture system and consists of approx. 500 points. The latent space is constructed using Isomap. As each point in the low dimensional space corresponds to a hand posture, a simple control of a complex hand is possible. By moving a point in the two dimensional latent space, a robotic hand can be controlled. Nevertheless, the amount of different movements in the training dataset was limited, and therefore the hand was not able to perform complex movements.

2.5.3 Locally Linear Embedding

Locally Linear Embedding (LLE) is also a nonlinear dimensionality reduction algorithm [78]. In contrast to PCA and Isomap, Locally Linear Embedding is a local technique. It also constructs a neighborhood graph, but in contrast to Isomap it only tries to recover the local structure of the data [76]. Each datapoint is constructed as a linear combination of its neighbors. In the lowdimensional space LLE tries to find the weights of the linear combinations which are most similar to the highdimensional ones. It is less sensitive to short circuiting since only a small proportion of the data is altered if it occurs. As in the case with Isomap, LLE is weak if a dataset contains holes or is altered by large amounts

of holes [76].

2.5.4 Gaussian Process Latent Variable Models

Gaussian Process Latent Variable Model (GP-LVM) is a probabilistic generative method for dimensionality reduction. Recently GP-LVM and its variants have proved their usefulness in a handful of human motion modeling applications [79–82]. They have proved superior to other nonlinear dimensionality reduction techniques when dealing with noise and incomplete data [83].

Theory

Let D denote the dimension of the data space and q the dimension of the latent space. Given N observations, the matrix containing the data points is denoted $\mathbf{Y} \in \mathbb{R}^{N \times D}$ and the matrix of the corresponding points in the latent space is $\mathbf{X} \in \mathbb{R}^{N \times q}$. The marginal likelihood P of the datapoints, given the latent positions and the hyper parameters θ, is a product of D independent Gaussian processes [84]:

$$P(\mathbf{Y}|\mathbf{X}, \theta) = \prod_{j=1}^{D} \frac{1}{(2\pi)^{\frac{N}{2}} |\mathbf{K}|^{\frac{1}{2}}} e^{-\frac{1}{2} y_j^T \mathbf{K}^{-1} y_j} \tag{2.5}$$

where $\mathbf{y}_j \in \mathbb{R}^{N \times 1}$ is the jth column of the data matrix and $\mathbf{K} \in \mathbb{R}^{N \times N}$ is the covariance matrix. The matrix defines the notion of distance between the points in the latent space and is dependent on the hyper parameters; thus $\mathbf{K} = \mathbf{K}(\mathbf{X}, \theta)$.

To obtain the latent representation of $\mathbf{Y}$ one has to maximize Eq. (2.5) with respect to $\mathbf{X}$ and θ. In general, this optimization has many solutions since the function is not convex.

Covariance Functions

The covariance matrix K in Eq. (2.5) is determined by the covariance or kernel function k:

$$\mathbf{K}_{i,j} = k(\mathbf{x}_i, \mathbf{x}_j) \tag{2.6}$$

The choice of the covariance function is critical, since it defines the behavior of the solution. This is an advantage of the method, since it allows adaptation to the specific needs of the task and the dataset at hand. The kernel function needs to generate a valid covariance matrix, i.e. a positive semidefinite kernel matrix. Therefore, the class of valid kernels is the same as the class of Mercer functions. For practical purposes it should also be possible to calculate the gradient of the kernel with respect to the latent space, since

gradient based optimization is used to calculate the maxima of Eq. (2.5). A special case is the linear kernel

$$k(\mathbf{x}_i, \mathbf{x}_j) = \alpha_L \mathbf{x}_i \mathbf{x}_j \tag{2.7}$$

since the solution of the optimization is then identical to the PCA solution [84]. Most commonly, the covariance matrix is determined by a sum of several different kernels, like the Radial Basis Function (RBF), bias and noise kernels. The RBF kernel is defined as follows:

$$k(\mathbf{x}_i, \mathbf{x}_j) = \alpha_{RBF}\ e^{-\frac{\gamma}{2}(\mathbf{x}_i - \mathbf{x}_j)^T(\mathbf{x}_i - \mathbf{x}_j)} \tag{2.8}$$

where α defines the output variance and the inverse kernel width γ controls the smoothness of the function. If γ is set very large, the function may fluctuate strongly, since the kernel is narrow and tends to overfit the data. By using a smooth covariance function like the RBF kernel, a preference towards smooth generative mappings in the GP prior is encoded. This implies that points close in the latent space will remain close in the observed space (when projected using the mean prediction of the GP). Convex kernels like the RBF kernel create a smooth mapping from latent to data space in the sense that it enforces that nearby points in the latent space will stay close in the data space. However, it is not guaranteed that the inverse is true, i.e. points close in the observed space remain close in the latent space. This is further discussed in the next section.

A constant offset can be added to a covariance function by introducing the bias kernel:

$$k(\mathbf{x}_i, \mathbf{x}_j) = \alpha_B \tag{2.9}$$

It is often desirable to model noise. This is commonly done using Kronecker's delta function. The amount of noise is controlled via α.

$$k(\mathbf{x}_i, \mathbf{x}_j) = \alpha_N \delta_{ij} \tag{2.10}$$

The kernel used in the thesis is a sum of an RBF, bias and noise term. The covariance function is therefore

$$k(\mathbf{x}_i, \mathbf{x}_j) = \alpha_{RBF}\ e^{-\frac{\gamma}{2}(\mathbf{x}_i - \mathbf{x}_j)^T(\mathbf{x}_i - \mathbf{x}_j)} + \alpha_B + \alpha_N \delta_{ij}. \tag{2.11}$$

The parameters α_{RBF}, α_B and α_N define the relative importance of those three terms. The RBF term has an additional parameter which is the inverse width γ. Those parameters form the hyper parameters θ which are subject to optimization.

Back Constraints

As stated above, a GP-LVM in its basic form does not guarantee that a smooth inverse exists to the generative mapping ([84] p.19). However, this can be incorporated into the model by representing the latent locations $\mathbf{x}_i$ in terms of a smooth parametric mapping g_j from the observed data $\mathbf{y}_i$ [85],

$$x_{ij} = g_j(\mathbf{y}_i, a) = \sum_{n=1}^{N} a_{jn} k_{bc}(\mathbf{y}_i, \mathbf{y}_n) \tag{2.12}$$

where k_{bc} is the back constraint kernel. This means that the maximum likelihood solution of these parameters a rather than the latent locations are sought. This is referred to as a back-constrained GP-LVM. In addition to constraining the latent location to preserve the local smoothness of the observed data, previously unseen data can be projected onto the latent space in an efficient manner by pushing them through this back-mapping.

In the thesis, the back constraint kernel k_{bc} is an RBF kernel. The parameters of the kernel are not subject to optimization, consequently they have to be set by hand. The variance α_{RBF} is set to one and the inverse width is varied to find a value that fits to the dataset.

Visualization of Uncertainty

When the GP-LVM latent space is plotted there is a background with varying intensity visible. As Equation (2.5) is a product of independent Gaussian Processes there is not only a mean but also a variance connected to the latent location. The variance can be used to create the black/white background image - the lighter the pixel, the higher the precision of the reconstruction of the latent point [86].

Chapter 3

Comprehensive Grasp Taxonomy

Literature provides a large set of different human grasp taxonomies, which range from robotics and medicine to biomechanics. Depending on their intended use and the area of origin, they list different grasp types. There is no consensus about grasp types that are commonly used by humans and how they can be organized in a meaningful way. The goal of this Chapter is to determine the largest set of grasp types that can be found in the literature. That grasp taxonomy defines the sub set of all human hand movements that are of relevance for the thesis.

Section 3.1 defines what grasp types are of relevance for the thesis. Then all literature sources are listed in Section 3.2 and how they are further processed is presented in Section 3.3. Based on that analysis a list of grasps is extracted in Section 3.4 and arranged in a new classification in Section 3.5. Finally a discussion is given in Section 3.6.

3.1 Grasp Definition

The human hand can be used in a variety of different tasks, not only prehension. Additionally there is no consensus in literature on how a human grasp is defined. Therefore a definition of relevant hand movements is needed. Only human grasp types are considered, which conform to the grasp definition [87]:

> "A grasp is every static hand posture with which an object can be held securely with one hand, irrespective of the hand orientation."

For the remainder of the thesis the term grasp will refer to all kind of grasps, not only ones that are in accordance with the grasp definition. The context will clarify whether grasps that conform with the definition are meant.

The definition also implies that the grasp stability has to be guaranteed irrespective of the relative force direction between hand and object.

The definition rules out:

Intrinsic Movements: They are excluded because the object is not in a constant relationship to the hand.

Bimanual Tasks: Only one hand is to be used.

Gravity dependent grasps: They are ruled out, because the hand orientation is vital to the grasp stability. If one turns the hand, the object may fall down, which is not irrespective of the force direction. Grasps being excluded here are, amongst others, the Hook Grasp and the Flat Hand Grasp.

It is interesting to note that grasping a glass of water still fits into that definition. The glass is sensible to the orientation of the hand, but this is not because the grasp would lose its stability if the hand rotates. Just the water would be poured out – so the orientation of the hand is constrained by the object itself, not by the grasp stability.

3.2 Compared Taxonomies

This section gives a short overview of the literature sources taken into consideration and the intended application of the taxonomies. They will be compressed later in the comparison sheet and based on them a new taxonomy is built (Section 3.5). The literature sources are presented in chronological order.

3.2.1 Schlesinger

Schlesinger [88] was the first to create a classification of human hand grasps. He comes up with six major human hand grasps, which were later summarized by Taylor and Schwarz [89]. The grasps are depicted in Figure 3.1. The Taxonomy covers a lot of different hand postures, but does not go into detail too much.

3.2.2 Slocum and Pratt

Coming from the field of rehabilitation, Slocum and Pratt [90] give an overview on hand function and propose a system on which the amputation of parts of the hand could be assessed. In their opinion it is important to know to which degree the function of the hand is altered. It is important for the appraisal by insurance companies, and to have a basis on which medical treatment can be planned. This has to be seen in the light of the period of the publication; in 1946 the Second World War had just ended and there was a large need for treatment of people with hand injuries.

In their opinion there are three fundamental hand functions [90] p. 491:

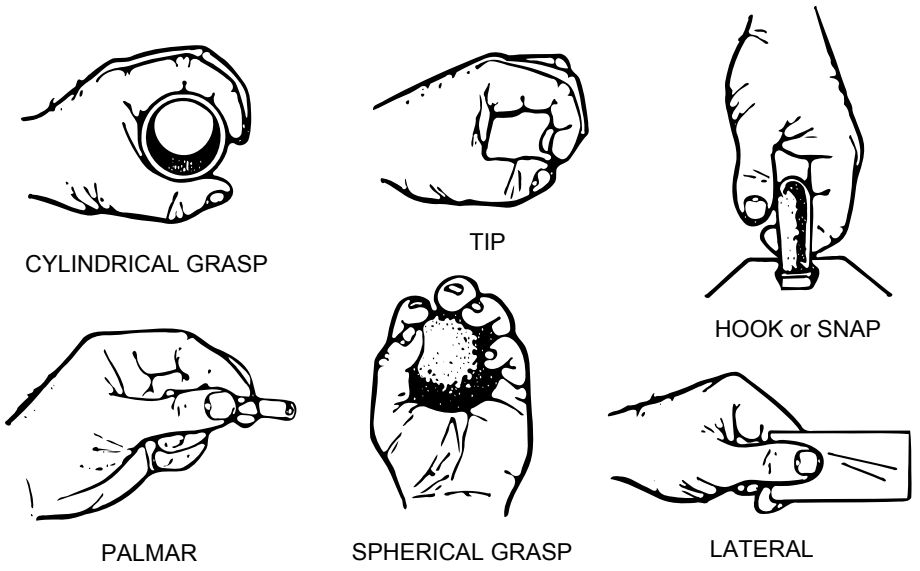

Figure 3.1: The taxonomy of Schlesinger [88], summarized by Taylor [89].

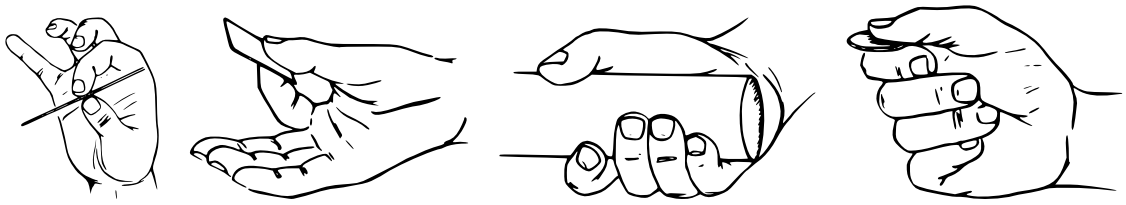

(a) Precision Pinch (b) Pulp Pinch (c) Key Pinch (d) Hook Grip

Figure 3.2: Different human grasps as listed by Cooney and Chao [91].

Grasp "Grasp may be defined as the combined action of the fingers against the opposed thumb and the palm of the hand."

Pinch "Pinch is the apposition of the pad of the thumb against the pads of the opposing fingers."

Hook "Hook is simply what the word implies: The fingers are flexed so that their pads lie parallel and slightly away from the palm, forming a hook."

3.2.3 Cooney and Chao

The grasps named by Cooney and Chao [91] are only grasps where the thumb is in functional use. In those positions they analyze the anatomy of the thumb to assess the kinematics and the forces within the thumb skeleton and muscular system. The four positions referenced are shown in Figure 3.2.

3.2.4 Kamakura et. al

The taxonomy created by Kamakura et. al [20] is one of most complete ones available. Humans, grasp a large set of different objects, are analyzed, comparing their static grasp postures and contact area. The assumption is that there are common grasping patterns present in human grasping actions. According to Kamakura et. al those patterns are dependent on the shape and function of the object, the habits of the person and also chance. Seven subjects are asked to grasp 98 common objects and pictures of the grasps are taken from different viewpoints for later analysis. Overall, 14 different grasp types are extracted and arranged in four different categories, where a grasp was considered to be the same when the posture of the hand as well as the contact area showed similarities:

Power Grip (Figure 3.3) Within that category, a wide area of the hand is in contact with the object, including the palm and the volar side of the fingers.

Intermediate Grip (Figure 3.4) This group is in an intermediate position between "Power Grip" and "Precision Grip". The palm is not included as contact area and the flexion of the fingers is moderate.

Precision Grip (Figure 3.5) The object is held between the volar side of the fingers and the pulp of the thumb and the flexion of the fingers is small.

Grip involving no thumb (Figure 3.6) The only representative of this group is the adduction grip, where the object is grasped between two fingers.

3.2.5 Lister

Lister [92] focuses on hand reconstruction after injury. Therefore he defines eight basic positions which make up most of the hand maneuvers which help to assess the hand function of a patient. Figure 3.7 shows the grasp types he found. All grasp types except the "hook grip" and the "flat hand" are within our grasp definition.

3.2.6 Elliott and Connolly

Elliott and Connolly [93] focus on manipulative movements of the hand. In principle that would put the grasps out of the scope of the analysis (see Section 3.1 for the grasp definition). A "workaround" was used: The manipulative movements were described as having a starting and an end posture, and those two snapshots are presented in the publication. Each of those postures are assumed to be a static hand posture and that allows to fit them into the grasp definition. It is obvious that if a hand is able to grasp an object and perform intrinsic manipulation, it can grasp that object with that pattern in a static manner as well. The relevant hand postures are depicted in Figure 3.8.

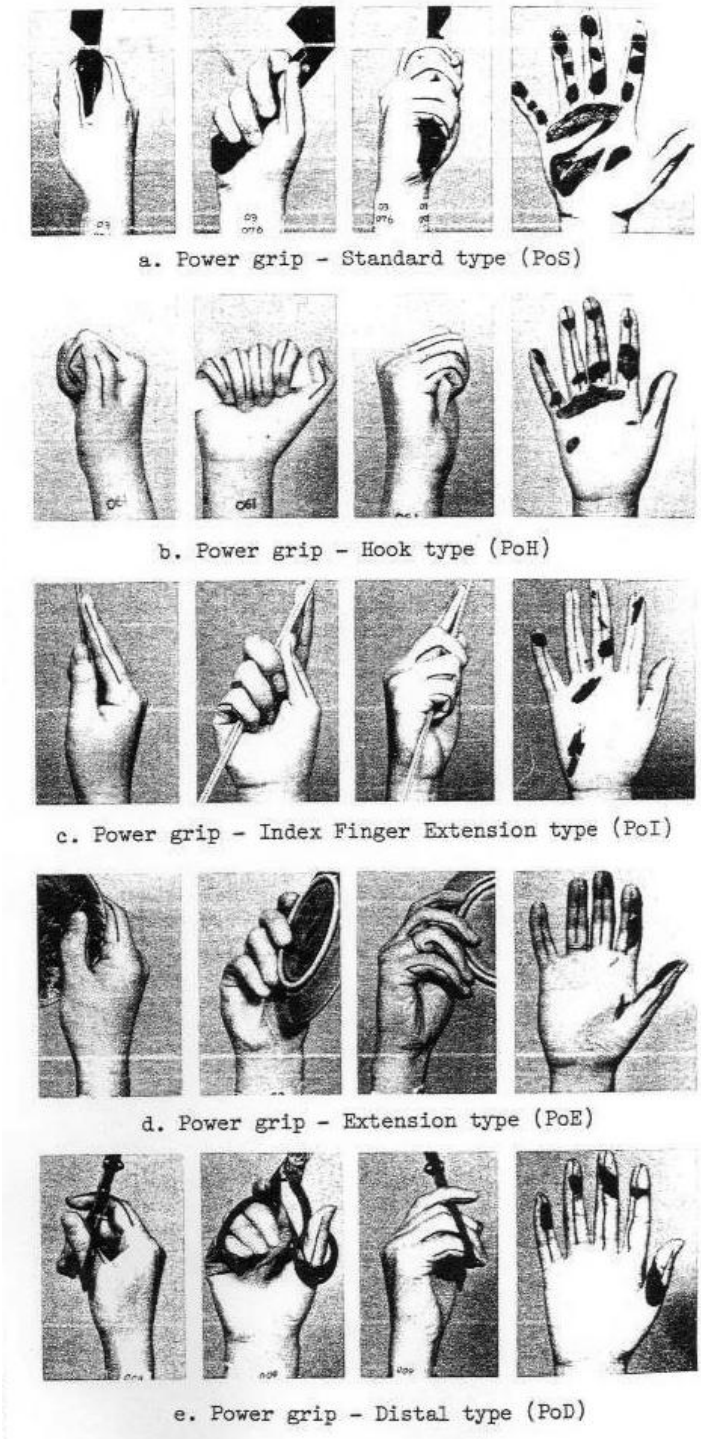

Figure 3.3: The "Power Grip" category, from Kamakura et. al [20]. The right column shows the contact area of the object with the hand and the other three columns show the grasp from different views.

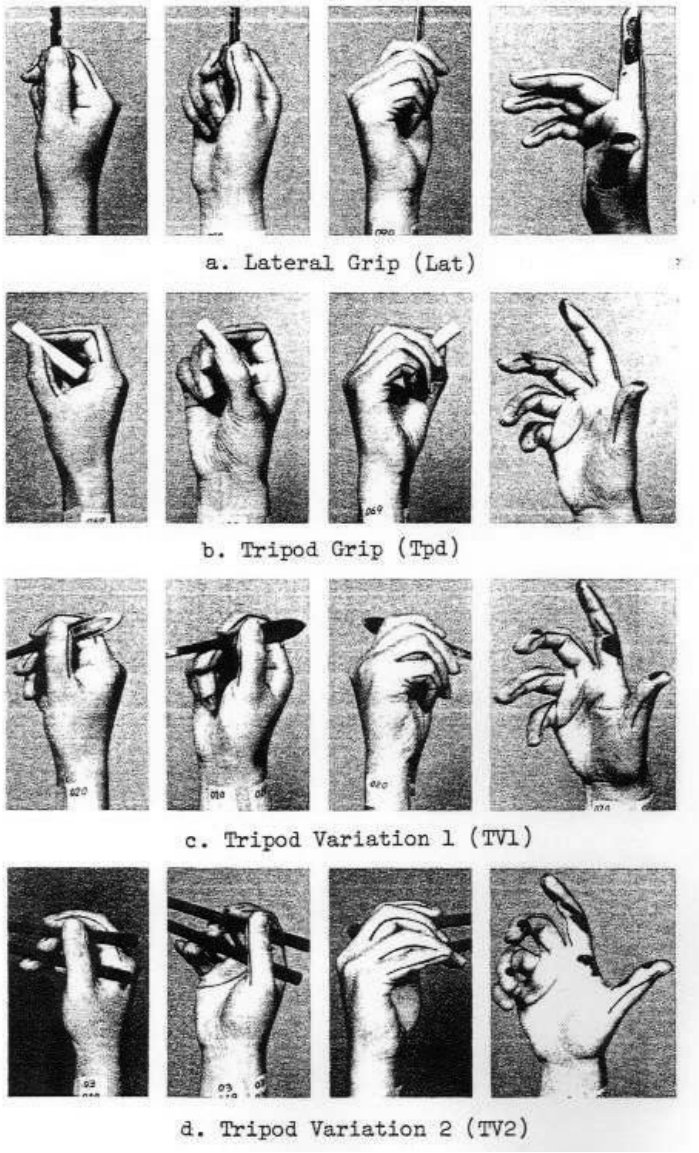

Figure 3.4: The "Intermediate Grip" category, from Kamakura et. al [20]. The right column shows the contact area of the object with the hand and the other three columns show the grasp from different views.

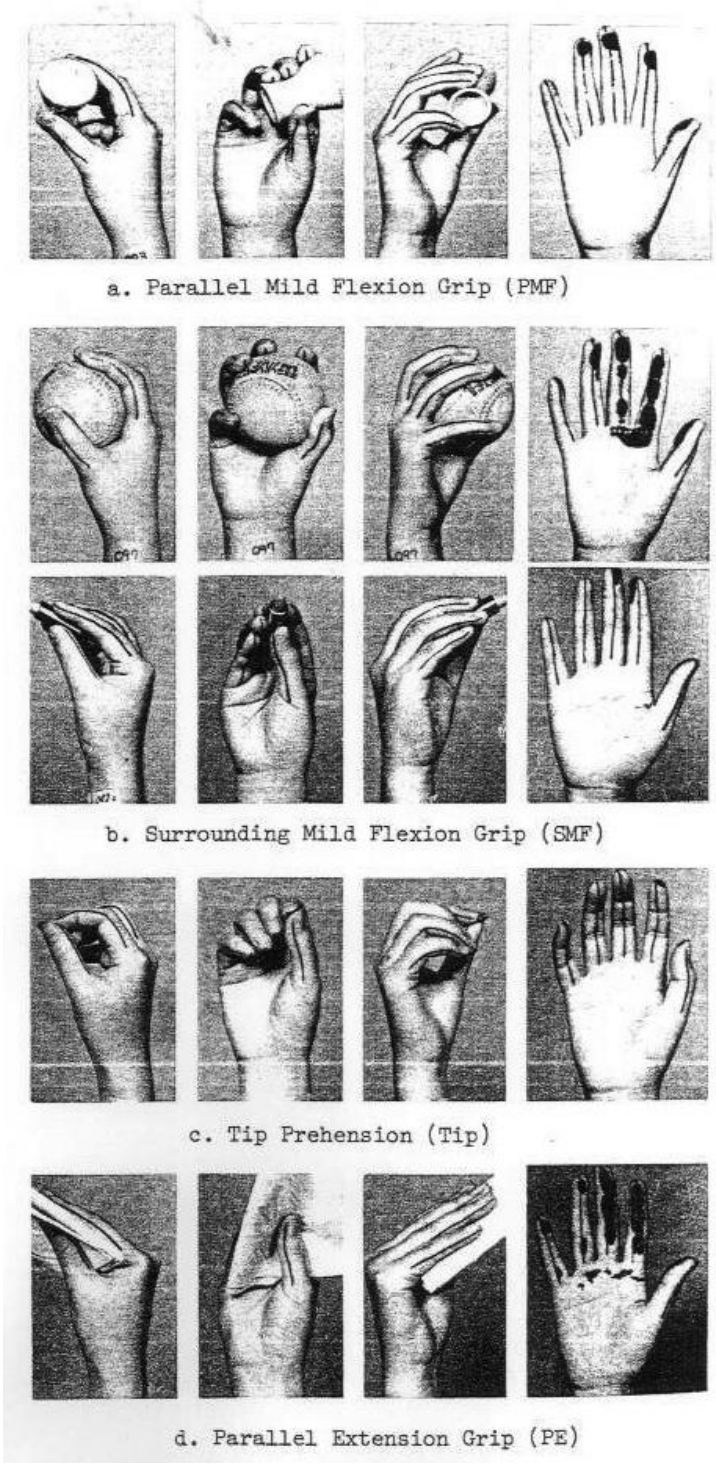

Figure 3.5: The "Precision Grip" category, from Kamakura et. al [20]. The right column shows the contact area of the object with the hand and the other three columns show the grasp from different views.

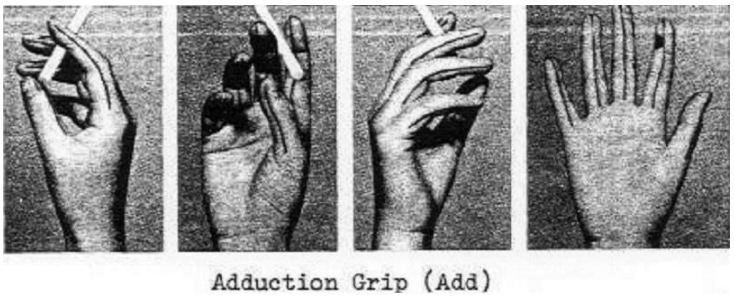

Figure 3.6: The "Grip involving no thumb" category, from Kamakura et. al [20]. The right image shows the contact area of the object with the hand and the other three columns show the grasp from different views.

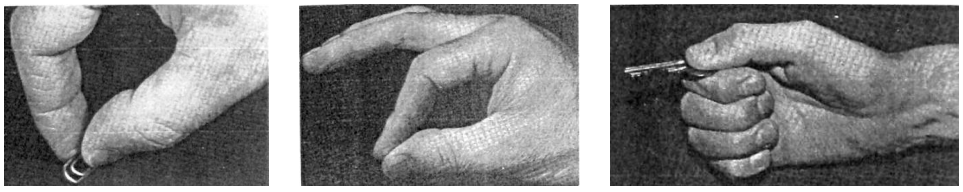

(a) Precision Pinch (b) Pulp Pinch (c) Key Pinch

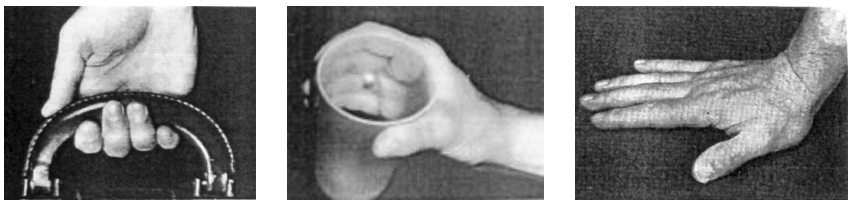

(d) Hook Grip (e) Span Grasp (f) Flat Hand

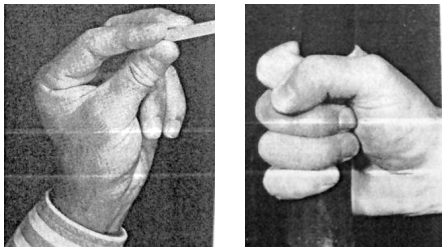

(g) Chuck Grip (h) Power Grasp

Figure 3.7: The eight basic positions of the hand as defined by Lister [92]. Except the "Hook Grip (d)" and the "Flat Hand (f)" all grasps are well within our grasp definition.

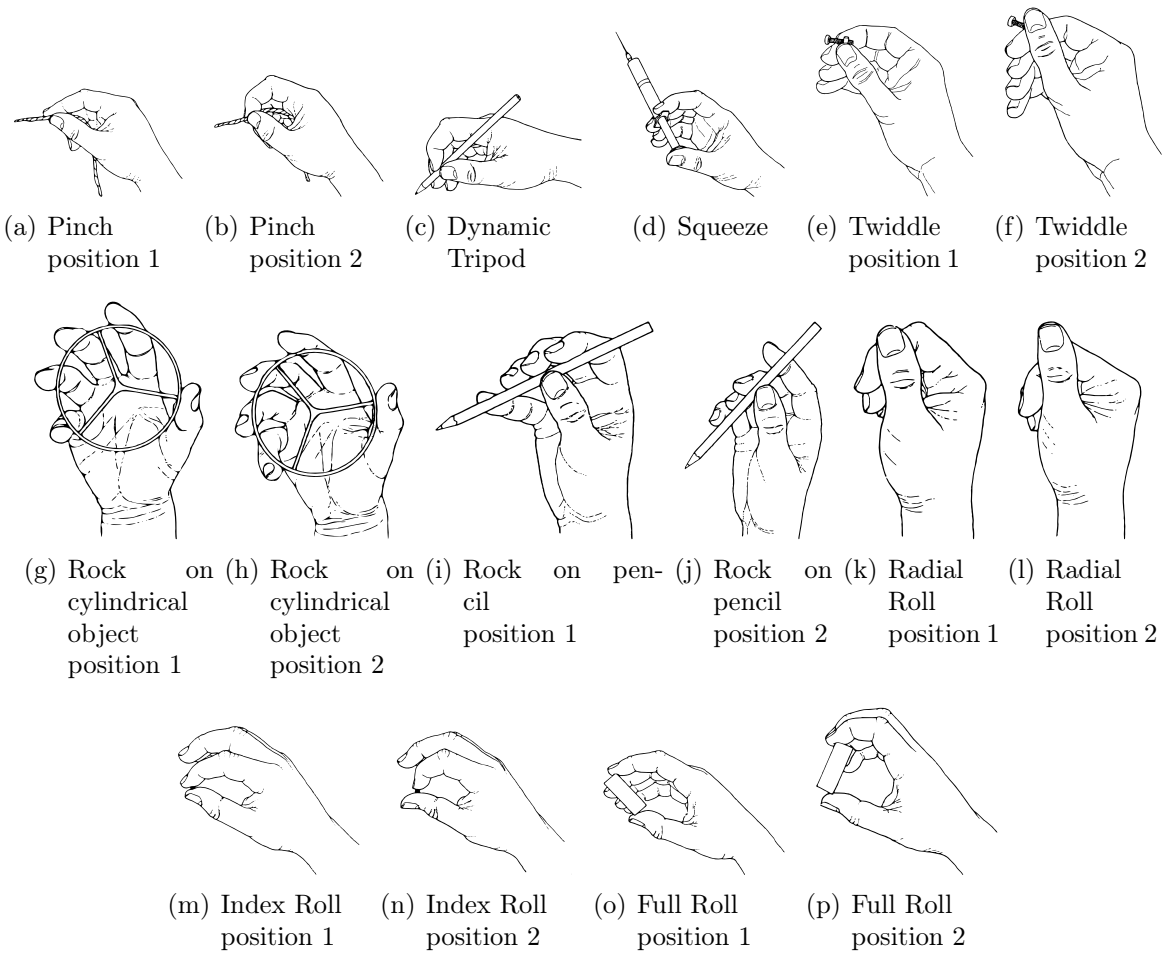

(a) Pinch position 1 (b) Pinch position 2 (c) Dynamic Tripod (d) Squeeze (e) Twiddle position 1 (f) Twiddle position 2

(g) Rock on cylindrical object position 1 (h) Rock on cylindrical object position 2 (i) Rock on pencil position 1 (j) Rock on pencil position 2 (k) Radial Roll position 1 (l) Radial Roll position 2

(m) Index Roll position 1 (n) Index Roll position 2 (o) Full Roll position 1 (p) Full Roll position 2

Figure 3.8: Hand positions as defined by Elliott and Connolly [93]. The postures depicted here were taken to be static to fit into the grasp definition.

(a) Encompass Grasp (b) Lateral Grasp (c) Precision Grasp

Figure 3.9: Grasps named by Lyons [94]

3.2.7 Lyons

The grasp-set of Lyons [94] includes only three grasp types, which is less than in most of the other classifications, but they are intended to be a basis for a dexterous robot gripper and should be adapted in a flexible way. The set of grasp include the *Encompass Grasp* which is found in most of the grasp taxonomies. Interestingly, the *Lateral Grasp* is different from the other sources. Normally the index finger would be in a rather flexed position, and the thumb would oppose the side of the index finger. The contact point of index finger with the thumb would be near the PIP joint of the index. Here this grasp is similar to the *Parallel Extension Grip* of Kamakura (Section 3.2.4), the *Extension* of Light (Section 3.2.11) or the *Lumbrical Grasp* named by Edwards (Section 3.2.13). The index finger is rather straight, only with flexion in the MCP joint and the thumb is not opposing the side of the index, but rather on the volar side of the finger. The grasp itself is used for grasping flat objects.

3.2.8 Kroemer

Kroemer [95] presents a list of hand-handle couplings. They can be interpreted as grasp types and most of them are well within the definition of a grasp. The only exception is the "Finger Palmar Grip" (Hook Grip) (Figure 3.10(c)) which is not independent of hand orientation. The relevant grasp types are shown in Figure 3.10.

3.2.9 Cutkosky

Cutkosky [96][97], coming from the field of robotics, published a taxonomy which includes 16 different grasping patterns. He states that the most prominent feature of a grasp is not the appearance, but the task itself. That is in conformity with [15]. Beginning at

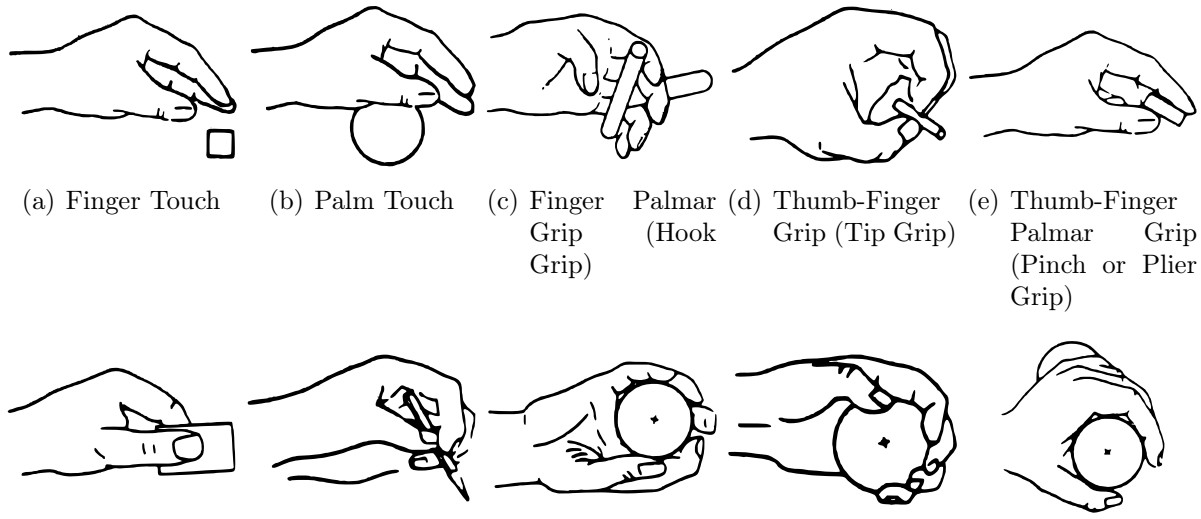

(a) Finger Touch (b) Palm Touch (c) Finger Palmar Grip (Hook Grip) (d) Thumb-Finger Grip (Tip Grip) (e) Thumb-Finger Palmar Grip (Pinch or Plier Grip)

(f) Thumb-Forefinger Side Grip (Lateral Grip or Side Pinch) (g) Thumb-Two-Finger Grip (Writing Grip) (h) Thumb-Fingertips Enclosure (Disk Grip) (i) Finger-Palm Enclosure (Collet Enclosure) (j) Power Grasp

Figure 3.10: Grasp types defined by Kroemer [95]. Except the "Finger Palmar Grip", all grasps are within the grasp definition.

the top in Figure 3.11, the first distinction of a grasp is whether a grasp is a power or precision grasp. The next level differentiates between the rough shape of an object – is it compact or of prismatic appearance. On the last level, the size of the object determines the precise shape of the grasp. As indicated by the vertical arrow on the left side, moving from top to bottom of the Figure, the task is defined more precisely. At the top only rough information is present, whereas on the bottom complete knowledge of the object is available. On the horizontal axis the difference is based on the precision requirements and therefore also the size of the object – it is more likely that small objects are grasped with precision grasps.

3.2.10 Kang and Ikeuchi

Kang and Ikeuchi [99, 100] created a grasp taxonomy based on their proposed contact web. This web defines which finger parts are in contact with the object and by that the position in the taxonomy is defined. The rough classification differentiates between a non-volar-grasp (Figure 3.12(a)) and a volar-grasp (Figure 3.12(b)). Volar grasps include the palm surface in the grasp and they are all power grasps. Non-volar-grasps are mostly precision grasps, where the one exception is the lateral pinch.

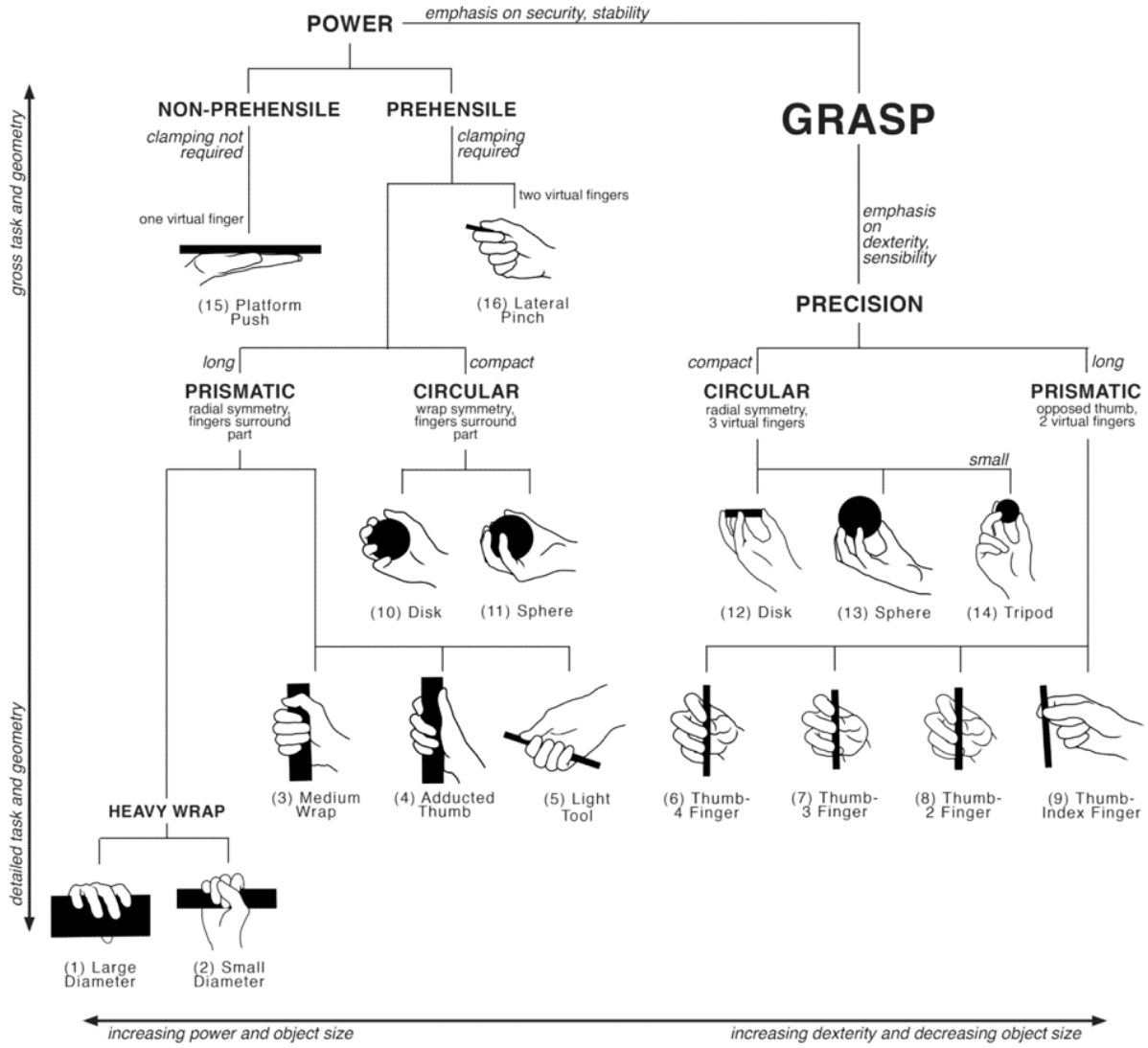

Figure 3.11: The 16 different grasp types referenced by Cutkosky [97]. Image taken from [98].

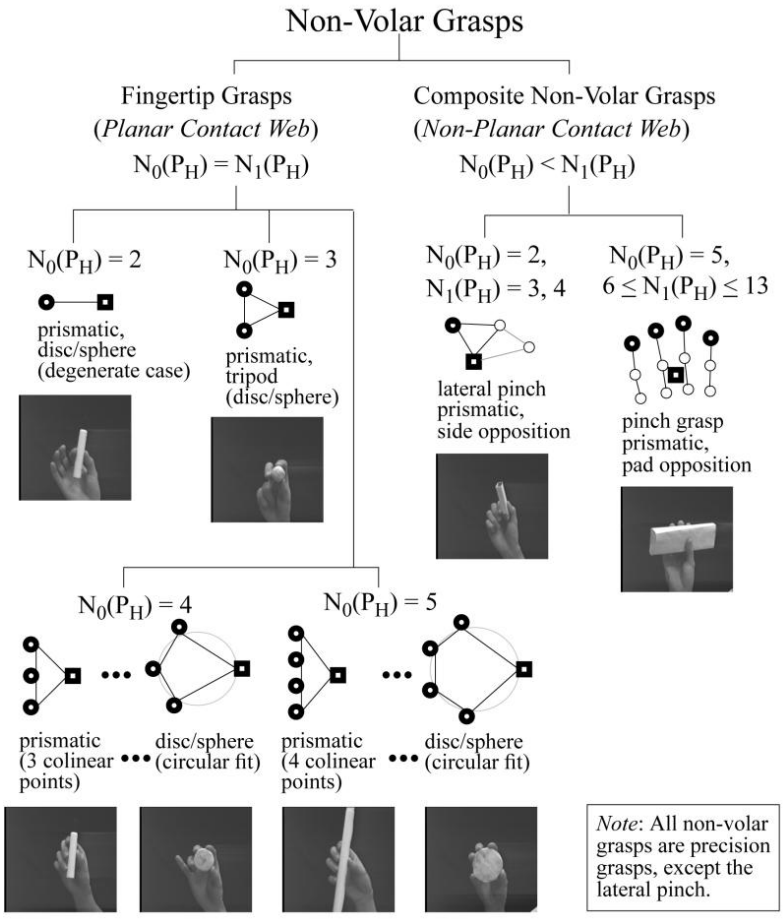

(a) Non-Volar Grasps

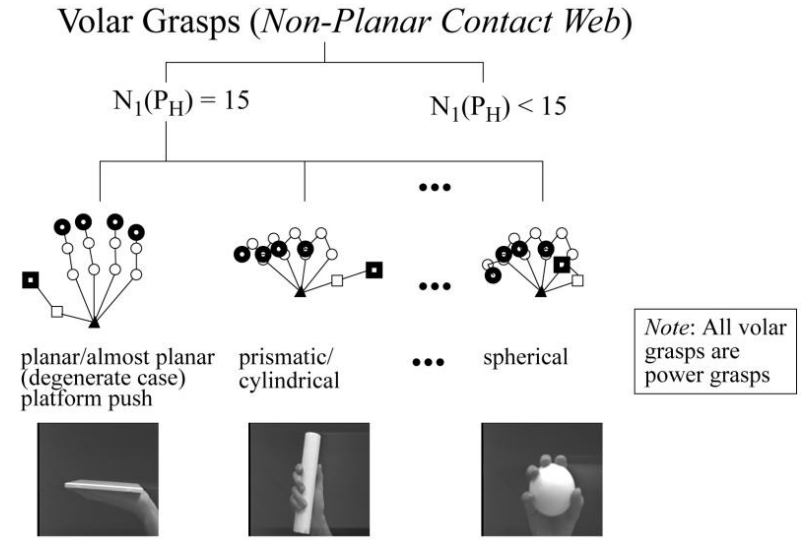

(b) Volar Grasps

Figure 3.12: Overview of the grasps as defined by [99] and [100]. Non-Volar Grasps do not include the palm as contact area, whereas Volar Grasps do include the palm. $N_0(P_H)$ = number of fingers in contact with object; $N_1(P_H)$ = total number of contact points.

3.2.11 Light et al.

Light et al. [101, 102] focus on a standardized test to assess human and prosthetic hand function. For the natural hand they state that there are six distinct functional positions of the hand as depicted in Figure 3.13. The function of the injured hand is then compared to the healthy hand function, as defined by the six functional positions, to assess the loss of functionality of the impaired hand.

Commonly the "Tip Pinch" is defined as the precision grasp which opposes the thumb and the index finger. They are the only source where the thumb is opposing the middle finger. This grasp is rarely applied, nevertheless it is possible, as from a function perspective those two grasps are very similar. This grasp is regarded as the equal grasp to the "normal" Tip Pinch, where the index finger is used.

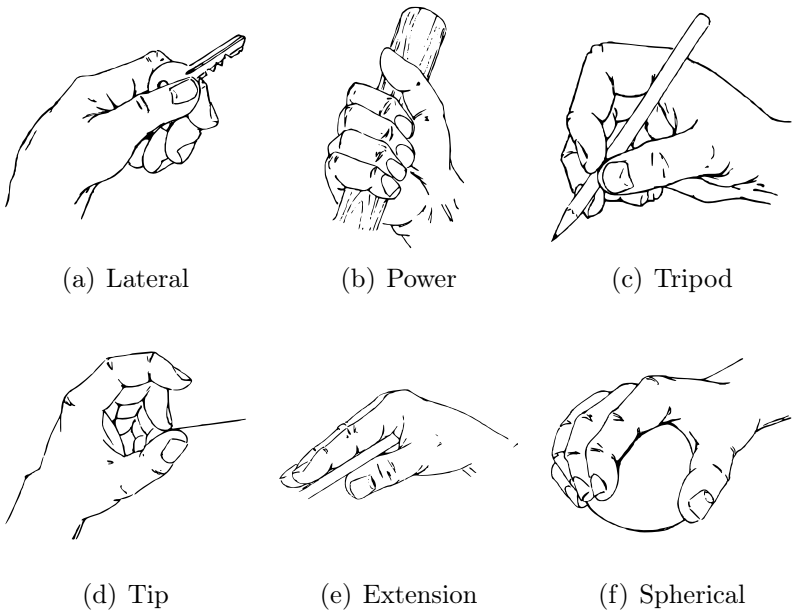

(a) Lateral (b) Power (c) Tripod

(d) Tip (e) Extension (f) Spherical

Figure 3.13: The six distinct function hand positions of the human hand according to Light et al. [101]

.

3.2.12 Exner

From the field of developmental medicine, Exner [103] found multiple grasp types which help to assess the development of a child. Depending on the age at which an infant uses specific grasp types, the overall motoric development can be deduced. Figure 3.14 shows the grasp defined by Exner.

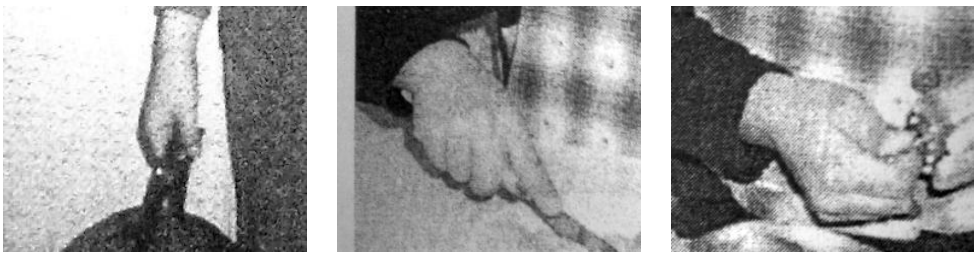

(a) Hook grasp (b) Power Grasp (c) Lateral Pinch

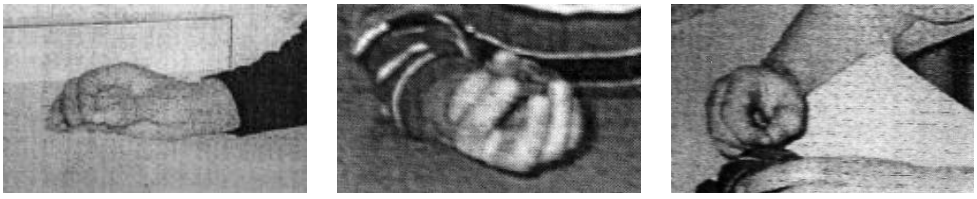

(d) Pincer grasp (e) Three-jaw chuck (f) Tip Pinch

(g) Spherical grasp (h) Cylindrical grasp (i) Disc grasp

Figure 3.14: Grasp types as defined by Exner [103].

3.2.13 Edwards et al.

The book of Edwards et al. [104] lists many different grasp types. It is a comprehensive work, focusing on the development of human hand function. The power grasps are presented in Figure 3.15, the grasps in-between Power and Precision Grasps are shown in Figure 3.16, the precision grasps are presented in Figure 3.17. Finally the Miscellaneous and Nonprehensile grasps can be found in Figure 3.18. Most of them are in accordance with the definition of a relevant grasp. The ones excluded are the "Reverse Transverse Palmar Grasp", the "Hook Grasp", the "Raking Grasp" and the class of "Nonprehensile Movements". Overall this results in 20 grasps that conform with the grasp definition and which are therefore taken into account. The list of grasps is very extensive and has four grasp types which are not listed in any other publication. This includes the "Palmar Grasp", "Ring Grasp", "Ventral Grasp" and "Inferior Pincer Grasp". It is one of the few publications which lists an intermediate category between power and precision grasps. The membership of grasps belonging to that group is different to Kamakura (Section 3.2.4), no grasp type is named by both authors as intermediate grasp.

(a) Cylindrical Grasp

(b) Hammer Grasp

(c) Oblique Palmar Grasp

(d) Opposed Palmar Grasp, only the upper grasp is of relevance.

(e) Palmar Grasp

(f) Reverse Transverse Palmar Grasp, according to the grasp definition identical to cylindrical grasp.

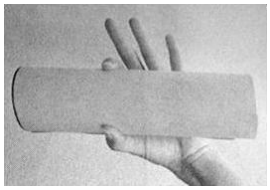

(g) Ring grasp

(h) Spherical grasp

Figure 3.15: Power grasps as defined by Edwards et al. [104].

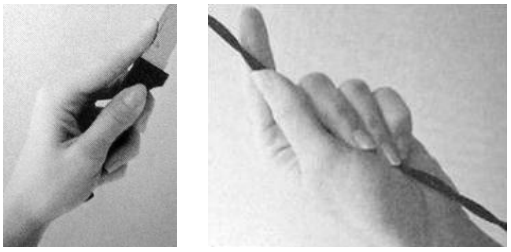

(a) Diagonal Volar Grasp (b) Ventral Grasp

Figure 3.16: Combination of Power and Precision grasps as defined by Edwards et al. [104].

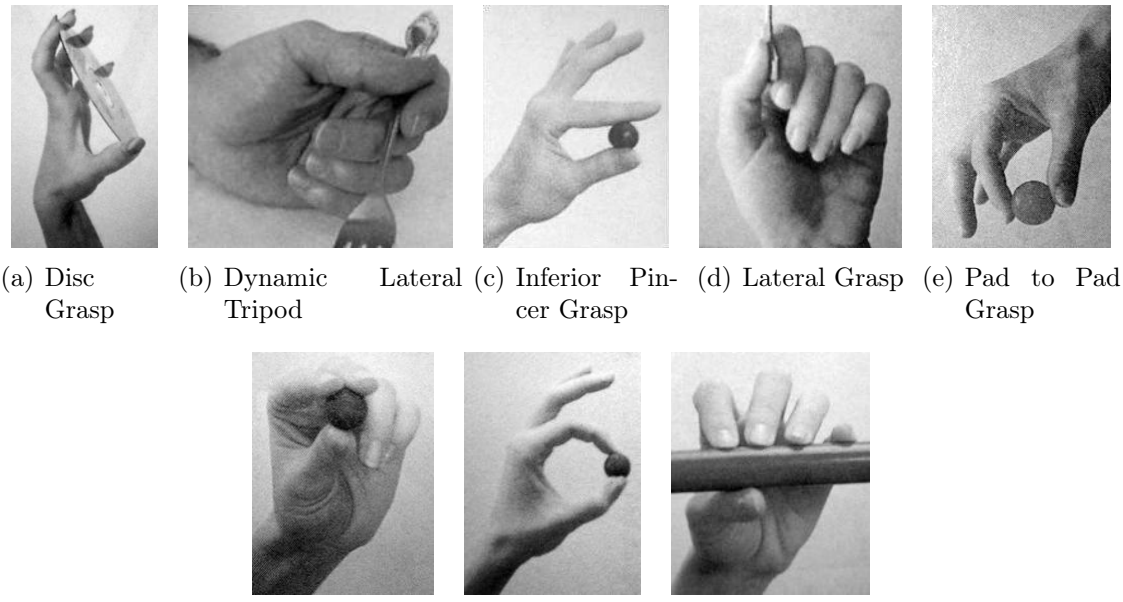

(a) Disc Grasp (b) Dynamic Lateral Tripod (c) Inferior Pincer Grasp (d) Lateral Grasp (e) Pad to Pad Grasp

(f) Three Jaw Chuck (g) Tip Pinch (h) Transverse Digital Grasp

Figure 3.17: Precision grasps as defined by Edwards et al. [104].

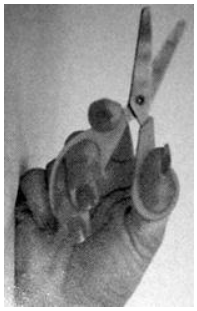

(a) Functional Scissors Grasp

(b) Hook Grasp, this grasp does not fit into the grasp definition.

(c) Interdigital Grasp

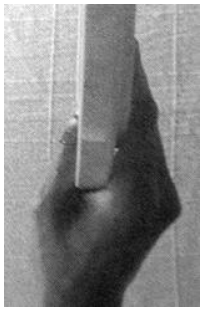

(d) Lumbrical Grasp

(e) Raking Grasp, this grasp does not fit into the grasp definition.

(f) Class of Nonprehensile Movements

Figure 3.18: Miscellaneous (a-e) and Nonprehensile (f) grasps as defined by Edwards et al. [104].

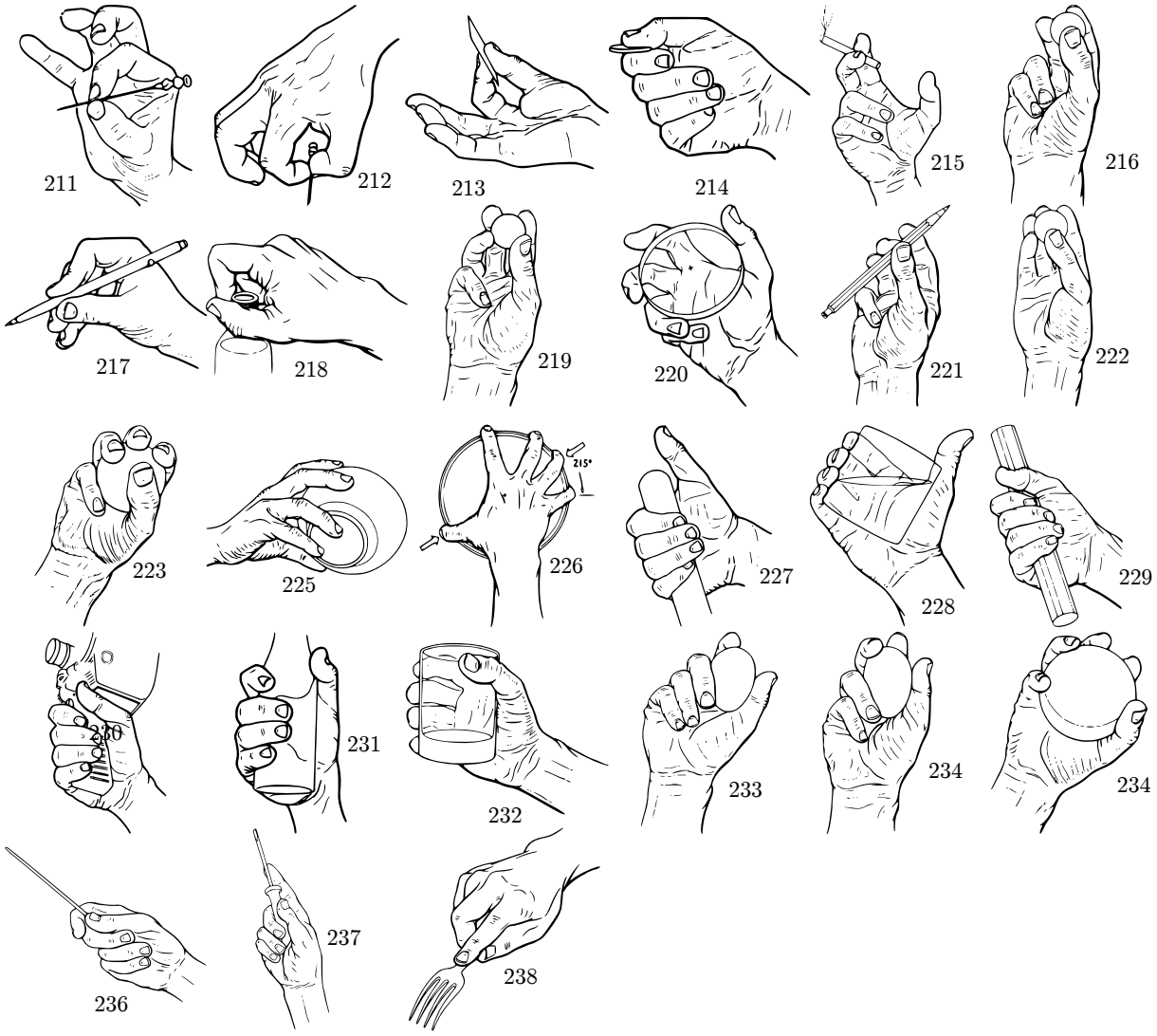

Figure 3.19: Grasp Types defined by Kapandji [9]. The corresponding classification can be found in Table 3.1.

3.2.14 Kapandji

Kapandji [9] gives a large set of grasp types which are classified mainly by the number of fingers used. Table. 3.1 shows all grasps named by Kapandjii. Only the category "Static Graps" is relevant for the research, since it is in accordance to our definition of a grasp (see Section 3.1). Overall, it offers a great amount of different grasp types. The pictures corresponding to the grasp types can be found in Figure 3.19. The grasps were classified by the hand parts in contact with the object. This can be either the fingers, the palm or both ("Symmetrical Grasps"). Within these categories there are additional properties which focus on the number of fingers in use.

Main Category	Sub Category			Grasp Name	Ref Picture
Static Grasps	Finger Grasps	bidigital (precision)	Pliers Grasp Thumb Grasp	Tip Grasp	211,212
				Tip Grasp	213
				Pad-Side Grasp	214
				Interdigital Grasp	215
		pluridigital	Tridigital	Pad Grasp Writing	216,217
				Screw Cap	218
			Tetradigital	Sperical Object	219
				"Disk Grip"	220
				"Thumb 3 Finger"	221
			Pentadigital	Pad Grasp	222
				Pad Grasp + Palm	223
				Bowl Grasp	225
				Large Disk	226
	Palmar Grasps			Finger-Palm	227,228
			Palmar Grasp	Zylindrical Objects	229,230,231,232
				Round Objects	233,234,235
	Symmetrical Grasps			Stick	236
				Screw Driver, Fork	237,238
Gravity Dependent				Tray	
				Spoon	
				Bowl, two handed	
				Edge Grasp	
Dynamic Grasps				Spin Top	
				Marbel	
				Lighter	
				Spray	
				Scissors	
				Chopsticks	
				Knot	
				Violin Player	

Table 3.1: Classification of the grasp types according to Kapandji [9]. Since the publication used is German, the names of the classes/grasp were translated to English. Only the "Static Grasps' are relevant for our research, as they are in accordance with the grasp definition. The grasp pictures corresponding to the "Ref. Picture" number are in Figure 3.19.

3.3 Comparison Sheet

To compare the literature sources a comparison sheet is created which helps to find similarities between sources [87]. In total, 14 literature sources are compared, Section 3.2 gives a more detailed description of those. Within the comparison sheet, columns store equal grasps, whereas rows store all grasp types defined by an author. Grasps that are defined by the author as power, precision or intermediate, are marked with a color code. Yellow is denoting a power grasp, green a precision grasp and yellow/green an intermediate grasp as defined in [15–17]. Red is marking grasps that are not conforming to the definition of a grasp. On top of every column there is a small box which shows the properties of that grasp type:

- The opposition type; if the assignment is inconsistent or not defined in literature, its type is determined according to Section 2.2.1
- The virtual finger assignment
- The name of the grasp which we will use later (grasp names are not consistent in literature)
- The number of entries of the grasp, ie. number of authors referencing the grasp.

Since the whole sheet is too large for depiction, Table 3.2 shows a small excerpt of the sheet and the complete table can be downloaded at [105]. This arrangement helps to assess the consistency between different authors. The grasp type which was named by most authors was the "Lateral Grasp" with 12 entries. This might be due to the fact that this grasp is very specific and was not further divided into multiple "sub" grasps. This was the case for full hand power grasps, where some authors divided this grasp into multiple types and others listed just one. Overall 147 grasp examples were found in the considered literature sources. Those grasp examples could be compressed to 45 different grasp types. A further classification based on our grasp definition (Section 3.1) revealed only 33 valid grasp types.

3.4 Grasp List

To further process the relevant grasp types they were put into a grasp list and their properties were added. Description on the properties "Type", "Opposition Type" and the concept of virtual fingers were defined in [15–17, 20]. The thumb position was introduced as additional property. It can be either in an abducted or adducted position. The list is shown in Table 3.3 and a further description on the columns of the list is given below.

Type Defines the rough type of the grasp. It can be Power, Precision or Intermediate.

	Palm **VF1: P** **VF2: 2-5** **VF3:**	**Palm** **VF1: P** **VF2: 2-5** **VF3:**	**Palm** **VF1: P** **VF2: 2-5** **VF3:**	**Palm** **VF1: P** **VF2: 2-5** **VF3: 1**	**Palm** **VF1: P** **VF2: 2-5** **VF3: (1)**	**Pad** **VF1: 1** **VF2: 2-5** **VF3:**
	Large Diameter	Small Diameter	Medium Wrap	Adducted Thumb	Light Tool	Thumb-4 Finger
Cutkosky 1986 1989						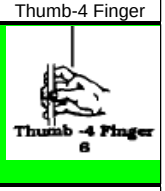
Kamakura 1980			Standard Type 			
Kapandji 1982	zylindrische Gegenstände 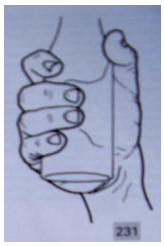 		zylindrische Gegenstände 			
Lister 1984	Span Grasp 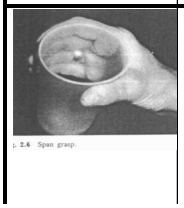	Power Grasp 				

Table 3.2: The sheet is used for comparison of different grasp taxonomies. This is just a small excerpt of the whole sheet. Each row stores the grasp types listed by one author and each column stores equal grasp types. The top row is used to present some information about the specific grasp type. The complete table can be downloaded online [105].

Opposition Type Depends on which proportions of the hand act against each other to fixate the object. It can be either the palm (palm opposition), the fingerpads (pad opposition) or the side of a finger (side opposition)

Thumb Position Position of the thumb in the specific grasp type. It can be either abducted or adducted.

VF1 The first Virtual Finger (VF).

VF2 The second virtual finger, which acts against VF1.

VF3 Some grasp types also use a third virtual finger.

\# The number tells how often this grasp type was named in the literature sources. This can be a very rough estimation of the importance of that grasp.

Compared to the taxonomies in the literature this is a much more comprehensive list. The publications which name the largest number of grasps are Kapandji [9] and Edwards [104], each with 24 grasp types. The taxonomy of Cutkosky [97], which is widely used in the field of robotics, lists 16 different grasps. Even this very basic comparison shows the difference to our taxonomy which incorporates a much higher number of grasp types.

3.5 Comprehensive Taxonomy

The grasps were then arranged in a taxonomy which is depicted in Table 3.4. The differentation in the columns is done by the power/precision requirements. The next finer differentiation is depending on whether the opposition type is *Palm*, *Pad* or *Side Opposition*. The opposition type is also defining the VF 1: In the case of *Palm Opposition* the palm is mapped into VF 1, in *Pad* and *Side Opposition* the thumb is VF 1. The only exception to this "rule" is the *Adduction Grasp*, where the thumb is not in contact with the object.

The position of the thumb is used to differentiate between the two rows: the thumb CMC joint can be in an either adducted or abducted position. This is a new feature introduced in the comprehensive taxonomy.

Nr.	Name	Picture	Type	Opp. Type	Thumb Pos.	VF1	VF2	VF3	#
1	Large Diameter		Power	Palm	Abd	P	2-5		10
2	Small Diameter		Power	Palm	Abd	P	2-5		3
3	Medium Wrap		Power	Palm	Abd	P	2-5		6
4	Adducted Thumb		Power	Palm	Add	P	2-5	1	2
5	Light Tool		Power	Palm	Add	P	2-5	(1)	2
6	Prismatic 4 Finger		Precision	Pad	Abd	1	2-5		4
7	Prismatic 3 Finger		Precision	Pad	Abd	1	2-4		4
8	Prismatic 2 Finger		Precision	Pad	Abd	1	2-3		2
9	Palmar Pinch		Precision	Pad	Abd	1	2		12

Nr.	Name	Picture	Type	Opp. Type	Thumb Pos.	VF1	VF2	VF3	#
10	Power Disk		Power	Palm	Abd	P	2-5		3
11	Power Sphere		Power	Palm	Abd	P	2-5		8
12	Precision Disk		Precision	Pad	Abd	1	2-5		5
13	Precision Sphere		Precision	Pad	Abd	1	2-5		6
14	Tripod		Precision	Pad	Abd	1	2-3		8
15	Fixed Hook		Power	Palm	Add	P	2-5		2
16	Lateral		Inter-mediate	Side	Add	1	2		12
17	Index Finger Extension		Power	Palm	Add	P	3-5	2	4
18	Extension Type		Power	Pad	Abd	1	2-4		1

Nr.	Name	Picture	Type	Opp. Type	Thumb Pos.	VF1	VF2	VF3	#
19	Writing Tripod		Precision	Side	Abd	1	3		6
20	Parallel Extension		Precision	Pad	Add	1	2-5		5
21	Adduction Grip		Inter-mediate	Side	Abd	1	2		3
22	Tip Pinch		Precision	Pad	Abd	1	2		9
23	Lateral Tripod		Inter-mediate	Side	Add	1	3		1
24	Sphere 4 Finger		Power	Pad	Abd	1	2-4		1
25	Quadpod		Precision	Pad	Abd	1	2-4		2
26	Sphere 3 Finger		Power	Pad	Abd	1	2-3		1
27	Stick		Inter-mediate	Side	Add	1	2		1

Nr.	Name	Picture	Type	Opp. Type	Thumb Pos.	VF1	VF2	VF3	#
28	Palmar		Power	Palm	Add	1	2-5		1
29	Ring		Power	Pad	Abd	1	2		1
30	Ventral		Inter-mediate	Side	Add	1	2		1
31	Inferior Pincer		Precision	Pad	Abd	1	2		1
32	Distal Type		Power	Pad	Abd	1	2-5		2
33	Tripod Variation		Inter-mediate	Side	Abd	1	3-4		1

	Power	Palm	
	Intermediate	Side	
	Precision	Pad	
			Abducted
			Adducted

Table 3.3: Grasp list based on the literature review. In total 33 different grasp types could be extracted. They are shown in this list together with their properties [87, 105]. The pictures of the grasp types were created by Javier Romero, using Poser 7 a commercial modeling software. "P" denotes that the palm serves as one Virtual Finger (VF). "(1)" is a sign that the thumb can act optionally as virtual finger.

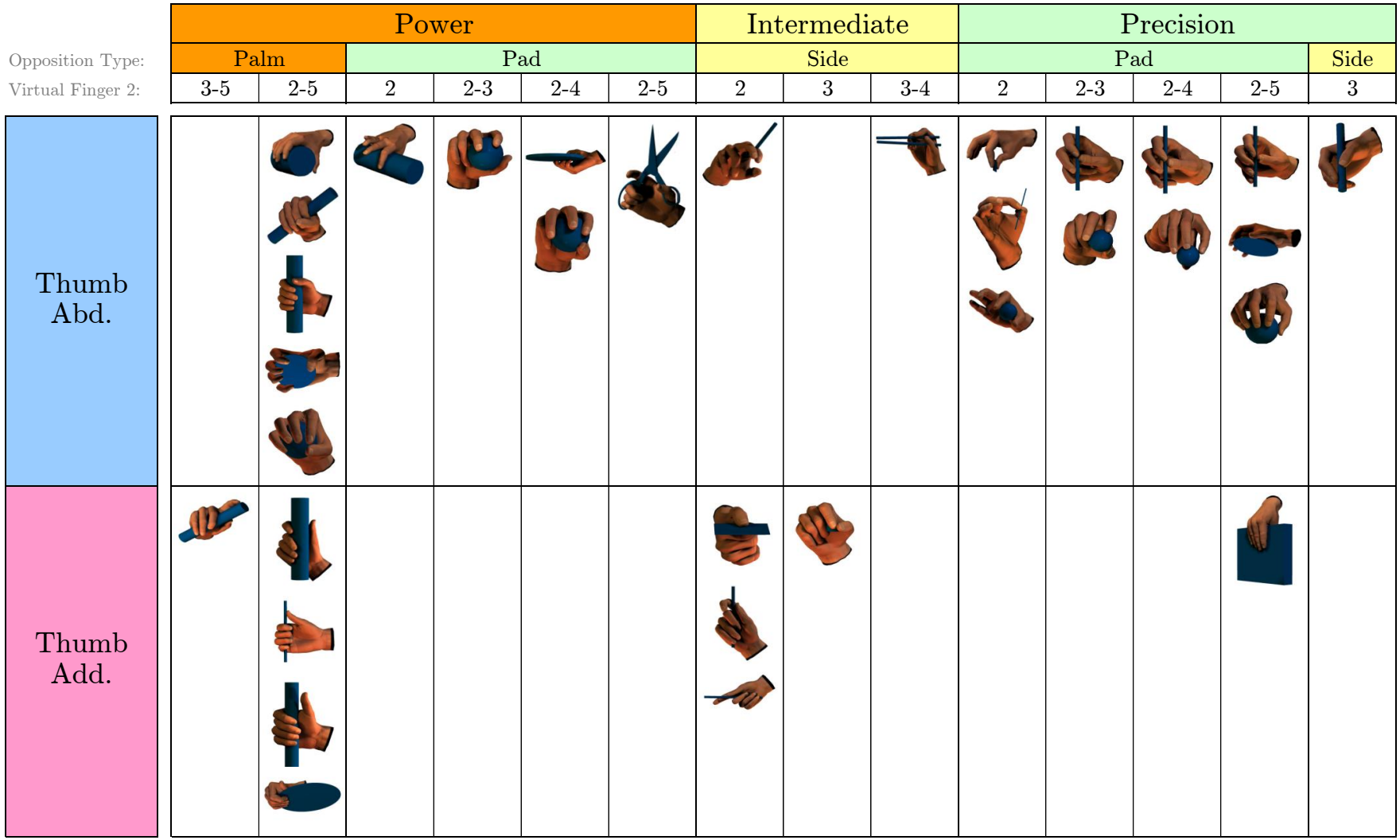

Table 3.4: Comprehensive Grasp Taxonomy which includes 33 different grasp types. Some cells are populated with more than one grasp type. They can be merged to one grasp if there is less need for precision [87].

Merging of grasps within one cell

Many grasps have similar properties (opposition type, thumb position etc.), therefore some cells are populated with more than one grasp. The sole difference between such grasps within one cell is the shape of the object. This offers the possibility to reduce the set of all 33 grasps down to 17 grasps by merging the grasps within one cell to a corresponding "standard" grasp. Depending on the task, this offers the possibility to choose between two different levels of accuracy of the grasp classification.

As a comparison, the classification of Cutkosky [97] has 15 different grasp types that fit into our definition of a grasp. This is close to the amount of grasps the reduced taxonomy has. However, our comparison shows that even though the number of grasps is nearly the same, the classification is very different. When the grasps from [97] are classified according to the presented scheme, the grasps only populate 7 cells. That is a reduction by more than half. As [97] mainly differ grasps by the object properties this reduction is only natural. The differentiation between object properties is done within one cell.

On the other hand, Kamakura [20] has no multiple entries in one cell. That is especially reassuring because humans were observed grasping 98 different objects with static grasps. That is very close to natural human hand usage and therefore it is reassuring that the comprehensive taxonomy has a similar result. The study was performed in restricted conditions, consequently there is no information about the occurrence of grasps in unconstrained conditions. The grasp types used by humans should be the same in constrained and unconstraint conditions, as it can be assumed that humans always use the same grasping patterns. The occurrence frequency might shift in laboratory conditions, since the subjects are exposed to situations which might be very unlikely in real life.

Analysis of Power and Precision Grasps

Of the 14 authors represented in the survey only four classified their grasps as power, precision and/or intermediate grasps. They showed a large consensus about the allocation of the categories. In total 16 grasps can be compared based on that assignment. Of them, 13 grasps showed total consensus, which is an conformity of 81%. Interestingly, the lateral grasp was classified either as precision grasp [97, 100]; intermediate [20]; or power grasp [104]. So it seems that this grasp takes an intermediate stage between power and precision, what Iberall [17] also acknowledges. This "in between" state of the grasp is represented within our taxonomy since it is put into the intermediate category.

Some inconsistency was found in the tripod grasps ("real" tripod and writing tripod), since Kamakura [20] classified them as intermediate grasps, apart from that it was classified as precision. Because of the dominant need for delicate handling, these grips were put into the precision category.

3.6 Discussion

The goal was to generate a comprehensive human grasp taxonomy for further analysis of human grasping movements. Since the area of human hand usage is very wide, the author defined which grasps are relevant. This definition excludes some grasps, but most of the grasps named in the literature are in accordance with this definition. Overall 147 grasp examples were found in literature and based on those 33 different grasp types could be extracted. The grasp types were then arranged in a self created taxonomy. The taxonomy is called comprehensive because it incorporates all major preceding publications. In that respect it is much more complete than any other presented taxonomy. Yet it suffers from the limitations it inherits from the publications it is based on.

The grasp types are arranged purely on the authors' intuition and are not based on real measurements. There is no guarantee that the listed grasps correspond to the ones used by humans. To the best knowledge of the author, there is no extensive study available which tries to classify human hand postures based on a measurement of real life hand usage. As the largest subset of grasp types was searched for, the presented taxonomy covers more hand postures than the grasp taxonomies presented in literature. If this is sufficient, or if there are major hand configurations missing cannot be determined. If such information would be available, it could be used to reduce the numbers of grasps and direct the effort onto the most important grasps. That would simplify the work in the following Sections as no effort is spend on grasps that are of no importance in real life.

Only very recently a preliminary study on the occurrence of different grasp types was published [98]. The finding is that a few grasp types constitute the vast amount of grasps needed. The study is limited to two subjects in unique environments. As the result is of a preliminary nature only and was published very recently, it is not taken into account in the following.

The only two grasp types that are disregarded, because the assumption is that they are very rarely used, are the "Distal Type" (grasp number 32 in Table 3.3) and the "Tripod Variation" (grasp number 33 in Table 3.3). Both grasps are very special, since they are used on a specific object and also in a specific task. That reduces the generality of such a grasp and therefore most likely their occurrence frequency. The "Distal Type", which is the grasp for chopsticks, was only introduced by Kamakura et al. [20].

The grasp types that were found will serve as a solid basis for further research. 31 grasp types will be considered in the measurement on human hand kinematics which is described in the next Chapter.

Chapter 4

Quantification of Anthropomorphic Hand Performance

The goal of this Chapter is to create a method to determine the level of anthropomorphism of prosthetic and robotic hands. Once the measure is defined, it is used to assess the score of two existing prosthetic and one robotic hand. This Chapter is based to a large part on [106], where the idea of quantification of anthropomorphic hand performance is presented. At the end of this Chapter, the system, based on a nonlinear dimensionality reduction algorithm, will be contrasted against PCA. The comparison shows astonishing results on the behavior of those two methods.

The remainder of this Chapter is structured as follows. Section 4.1 presents the general idea how the level of anthropomorphism of a given kinematic hand setup can be determined. A measure on how that can be done in a quantitative manner is presented in Section 4.2. To make the system work, a low dimensional space with very specific properties is needed. Section 4.3 is dedicated to finding such a space. Finally, in Section 4.4 existing hand designs will be evaluated.

4.1 System Description

Figure 4.1 and 4.2 visualize the basic idea [106]: the term *action manifold* is used to refer to the postures a hand can reach. This action manifold can represent all postures a hand can reach or a subset of those, generated for a specific purpose. For example, one may generate an action manifold that represents different types of tri-fingered grasps generated by a hand.

The dimensionality of the space in which this action manifold resides depends on how the hand postures are represented. If fingertip poses are measured (position + orientation) and represented with translational and rotational parameters (e.g. Euler angles),

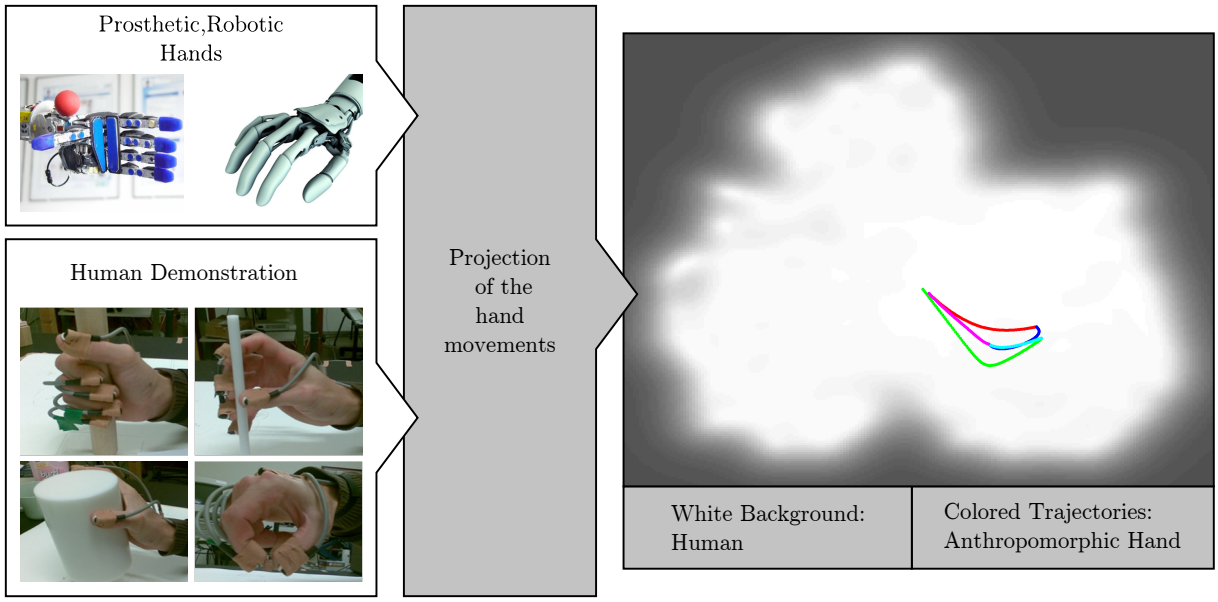

Figure 4.1: System Overview: The recorded human hand movements (grasps) are projected onto a two dimensional space using a nonlinear dimensionality reduction algorithm. The white area represents all demonstrated human hand movements. The movements of an artificial hand are then projected to that space and the overlap is used as the basis for comparison.

for a 5 fingered hand, the dimensionality of the representation space will be 30 (5 fingers x 6 dimensions per finger). Using different representations for the rotational parameters (quaternions, rotation matrices) will further increase the dimensionality of the representation space.

The idea is to start by generating an action manifold for a human hand and then to develop a method that allows a comparison between human hand and prosthetic/robotic hand action manifolds. For the visualization purposes we present the basic idea in Figure 4.2 - x_i, x_j show two axes of the, for example, 30 dimensional fingertip pose space mentioned above. "Robot 1", "Robot 2" and "Human" are the action manifolds spanned by three different hands. Depending on the kinematics of the hand, the action manifold may be different: for example, we observe that the action manifold of "Robot 1" is bigger compared to the other two hands. That could be due to the hand having many independent actuators and thus the intrinsic dimensionality of the action manifold is high. This leads to a higher number of available hand configurations. For the most extreme case of a one dimensional gripper, the area will collapse onto a line.

We can also observe that there is some overlap between the manifolds. In cases where the hands are kinematically identical, and assuming size normalization, these would overlap perfectly. This is also the basic idea pursued: the aim is to estimate the degree of overlap between human and artificial (prosthetic/robot) action manifolds, since this

overlap is closely related to the degree of similarity between the hands' capabilities.

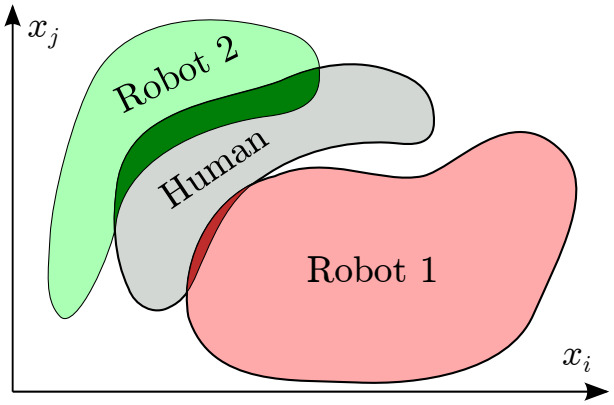

Figure 4.2: Hypothetical visualization of the high dimensional fingertip space $\mathbf{T}$. In that space each hand can reach a certain area/volume. The human hand is used as the golden standard. An artificial hand is considered anthropomorphic if the overlapping area/volume with the human hand is large.

The goal is thus to determine, from the manifold in the fingertip space, the level of anthropomorphism of a hand. More concretely, a large overlap between the robot manifold and the human hand action manifold indicates a high level of anthropomorphism. In that respect, in Figure 4.2, "Robot 2" would be superior to "Robot 1" whose manifold populates a large area, but resembles a less anthropomorphic behavior.

The manifold spanned by the human demonstration will heavily depend on which actions are used as exemplars: we can prioritize certain capabilities of the robot hand by deciding which actions/grasps are important. For example, if only very small objects are to be manipulated, there may be no need to include power grasps in the human datasets, because it would encourage hands with power grasp capabilities. However, the focus is on general-purpose hands, and therefore the human dataset consists of a wide range of grasps [87].

Once the data from different hands is available, a direct comparison in the fingertip space is difficult. Apart from the need to generate a high number of example points through sampling, the manifolds can have very complex shapes, requiring special metrics to be defined for the estimation of overlap. In addition, we need to make sure that each dimension is not weighted equally, e.g. the dimensions of the pinky finger and the thumb, since these fingers have a different impact on the grasping capabilities. Finally, the underlying manifolds cannot be visualized in an intuitive way.

To make the comparison and visualization feasible, the manifold spanned by the human hand motion is projected onto a lower dimensional space using a dimensionality reduction algorithm, described in Section 2.5.4. All possible fingertip configurations of an artificial hand are then projected onto this low-dimensional space.

Subsequently, the overlap is compared: a large overlap indicates that the hand is more similar to the human hand and thus more anthropomorphic.

As mentioned, one example of this mapping is shown in Figure 4.1 at the bottom. The white background represents all human hand movements projected to two dimensions and the colored trajectories are the projected movements of a prosthetic hand. The system consists of the following steps:

1) Human data generation: The first step is to generate a dataset of human grasping movements. These movements define the benchmark manifold to which the manifold of artificial hand movements will be compared to. Details on how this data was obtained is presented in Section 4.3.

2) Dimensionality reduction: A nonlinear dimensionality reduction method is used to project the high-dimensional manifold to a lower dimensional space suitable for visualization and comparison. More details on the algorithm are given in Section 2.5.4 and the properties of the latent space are described in Section 4.3.5.

3) Artificial hand dataset: Similar to the human dataset, a dataset of the movements of the artificial hand is generated based on the forward kinematics.

4) Projection: The artificial hand dataset is projected to the low dimensional space spanned by the human data. The projection of artificial hands is done in Section 4.4.

5) Overlap calculation: The overlap between the manifolds is measured in the lower-dimensional space. In order to quantify the overlap, an overlap measure is created, which is explained in Section 4.2.

The methodology differs from the approaches mentioned in Section 2.3.4 as it uses the end effector (fingertip) space instead of the joint space representation. In the former space, the position and orientation (pose) of the fingertips encode the configuration of the hand. The advantage of using the fingertip space over joint space is that this space is not embodiment specific as all five fingered hands share the same fingertip space. This more general parametrization also incorporates information on the underlying kinematic setup as, due to kinematic limitations, a hand cannot populate the complete space. This means that by specifying the points reachable in fingertip space (the action manifold) we also provide a notion of the kinematic structure of the hand.

4.2 Overlap Measure

Once the movements of an artificial hand are projected onto the human spanned latent space, the overlap between that space and the human spanned manifold has to be measured. Our approach is to discretize the latent space into a regular grid and count how

many cells are populated by a given hand design. For example, for a one DoF gripper the projection becomes a single line, whereas for a more complex hand with multiple actuators this can be a concentration of points with an arbitrary shape.

An important parameter for the calculation is the width of the cells as we regard all points within one cell as being equal. With equal we mean that if we vary the position within that margin, the resulting hand posture will only change by a small degree. As presented in Section 4.3.2, each subject performed the grasp types twice. The difference in the final grasp posture of the hand of trial one and trial two can be regarded as being irrelevant as both configurations resulted in a stable grasp. Points belonging to the actual grasping poses of trial one and two are projected onto the latent space and the distance between two corresponding points is averaged over all trials and subjects. This results in a maximum distance d_x and d_y in x and y direction respectively which can be regarded as being the same grasp. Those lengths will define the resolution of the grid in latent space. In our case we divided the latent space (described in more detail in Section 4.3.7) into 48 rectangles along dimension one and into 45 rectangles along dimension two. We did not include more rectangles, as in the regions not shown in the Figure the confidence was already very low (as indicated by the dark background in Figure 4.1).

The GP-LVM method models the mapping from the latent to high dimensional space using a Gaussian Process. This mapping provides us with a mean (prediction of the high dimensional location of the point) and a variance. The inverse of the variance, or confidence, is related to how certain the model is when reconstructing that point. The confidence is scaled into the interval $[0, 1]$, where the white area in the latent space plots corresponds to maximal confidence. A measure of the area of the human spanned latent space O_h can be calculated by summing the area of each cell $A_b = d_x \cdot d_y$ weighted by their corresponding confidence C_i.

$$O_h = \sum_{i=1}^{N_b} A_b \cdot C_i \tag{4.1}$$

$N_b = 48 \cdot 45 = 2160$ is the total number of rectangles needed to cover the area of the latent space where the confidence is nonzero.

The projection of the artificial hand movements discretized into V steps will result in a set of points $\mathbf{H} \in \mathbb{R}^{V \times 2}$ whose overlap O_r will be calculated. This is done by summing over all cells which are populated by at least one point $\mathbf{H}_v$.

$$O_r = \sum_{i=1}^{N_b} A_b \cdot \begin{cases} C_i & \exists \mathbf{H}_v \in b_i \\ 0 & \text{otherwise} \end{cases} \tag{4.2}$$

Finally O_r can be set into a relation to the area of human spanned space O_h and the

relative latent overlap O_{rel} can be calculated.

$$O_{rel} = \frac{O_r}{O_h} \cdot 100 \tag{4.3}$$

In the Figures where the movements of artificial hands are projected to the latent space, we also plot the cells that were populated by that hand. That gives an idea on how the system works and additionally helps to visualize the overlap.

The human movements have a tendency to be in a left-right direction as the starting position is on the far right side of the latent space. It would be preferable that the trajectories of an artificial hand are parallel to the humans. The presented measure does not take into account such alignments with the human trajectories. It solely measures static hand postures; the anthropomorphism of movements is not assessed. Nevertheless is it a prerequisite of anthropomorphic movements that the postures themselves are anthropomorphic. In that respect the measure assesses the basic requirement.

4.3 The Latent Space

This Section describes how the human dataset was obtained which was then processed and is used to define the *action manifold* of the human hand. Based on this dataset, a low dimensional (latent) space has to be found, which is optimal for the desired application of measuring the anthropomorphism of artificial hands. In order to do so, also background information on the Back Constraint. (BC) GP-LVM is needed, as well as how to best represent a 3D rotation to comply with the dimensionality reduction algorithm.

To create the low dimensional GP-LVM representations of the data, a matlab toolbox is used [85, 86].

Finally, four different metrics on the latent space quality are introduced and the best suited low dimensional representation is determined. That space is used for the remainder of this thesis to quantify artificial hand performance.

4.3.1 Data Acquisition

The data was generated with 5 subjects (3 male, 2 female), aged between 20 and 30 years. All subjects are right handed and have not reported any hand disabilities. The average hand length is 185.2 ± 13.3 mm and hand width is 81.1 ± 7.4 mm. The hand measurements were in accordance with the protocol provided in the literature [107]. A Polhemus Liberty system, recording at 240 Hz, with six magnetic sensors was used for recording the data. The spatial and angular resolution of each sensor is 0.8 mm and 0.15 degrees respectively. To represent rotations the system outputs quaternions, which

were kept throughout the whole experiment and data preparation. One sensor was applied to each fingertip, positioned on the fingernail and one was placed on the dorsum of the hand. See Figure 4.3(a) for an image of the markers applied to the hand. For the quality of the data it is of crucial importance that the relationship between the sensor and the fingertip, where it is applied, is constant. To guarantee a constant relationship between fingertip and the sensor, the tape to fixate the sensor was wrapped around the complete fingertip. Initial tests where the tape is only put onto the sides of the fingers, not covering the volar surface of the finger, proved unsuccessful. The sensors were able to move significantly in respect to the fingertip. To avoid that, the tape was wrapped around the complete fingertip to guarantee a good fixation of the sensor. It was accepted that the coefficient of friction, the sensibility and the range of motion of the DIP joints were reduced due to that fixation method. All that will lead to a change in the grasp kinematics, but that compromise had to be made.

The measurement protocol was the following:

1. Measurement of the subject's hand length, hand width, finger lengths and thickness of the fingertip [107].
2. Sensor calibration: The subjects were asked to place all fingers and the whole hand into a defined position. This allowed to determine the placement of the sensor with respect to the anatomical directions. See Figure 4.3(b) where the ring finger is being calibrated.
3. Measurement of grasping movements: Subjects were asked to perform the grasp types as listed in Table 3.3. The grasps "Distal Type" and the "Tripod Variation" were excluded due to their special nature. The trials started with the flat hand in the "starting position". Onto a start command the subject grasped the object with the demanded grasp type. The objects were placed on the object support (Figure 4.4(a)) and are shaped in such a way to facilitate the specific grasp type. The object was then lifted (Figure 4.4(b)) and put back onto its position. Finally, the hand was retreated back to the start position. Each grasp type was performed twice.

Then the data was processed including the following steps:

1. Calibration that aligns the coordinate systems of the sensors with the actual anatomical direction. Therefore the following transformation is performed frame by frame:

$$\mathbf{q}_{RN} = \mathbf{q}_{orig} \cdot \mathbf{q}_{calib}^{-1} \tag{4.4}$$

Where $\mathbf{q}_{RN}$ is the quaternion that is aligned with the anatomical direction, $\mathbf{q}_{orig}$ the quaternion that was measured during the trial and $\mathbf{q}_{calib}$ is the quaternion that

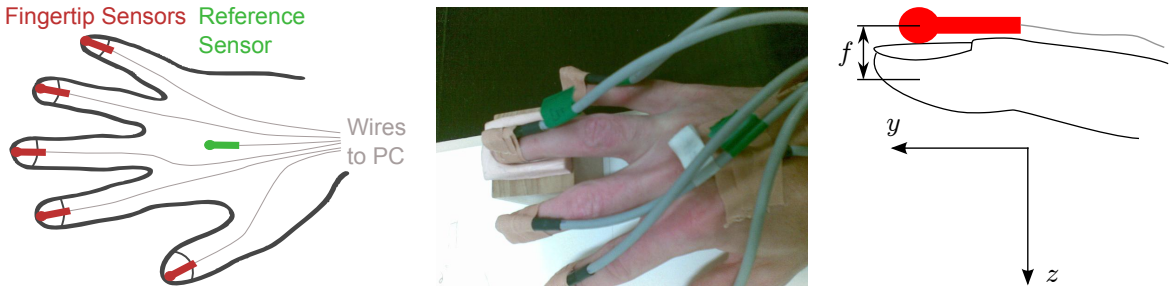

(a) Fixation of the sensors to the fingertips and the wrist.

(b) Calibration procedure of the finger. The fingers are put onto a support to define its position. The relationship between the finger and sensor are determined in that step.

(c) Coordinate system definition of the fingertip. The coordinate system has to be translated by f to be centered in the fingertip.

Figure 4.3: Setup of the fingertip sensors.

was measured during calibration (see Figure 4.3(b)). All five digits and the wrist sensor are calibrated.

2. Transformation of the fingertip data $\mathbf{q}_{RN}$ into the wrist coordinate system. The global movement of the hand depends strongly on the distance and orientation to the object. To provide some invariance to these aspects, the hand pose is defined in terms of the relative position and orientation of the fingertip sensors with respect to the wrist. The transformation to the wrist coordinate system is done by these steps:

$$\mathbf{\Delta} = \mathbf{p}_{finger} - \mathbf{p}_{wrist} \tag{4.5}$$

$$\mathbf{q}_{TF} = \mathbf{q}_{RNwrist}^{-1} \cdot \mathbf{q}_{RNfinger} \tag{4.6}$$

$$\mathbf{\Delta}_{TF} = \mathbf{q}_{RNwrist}^{-1} \cdot \mathbf{\Delta} \cdot \mathbf{q}_{RNwrist} \tag{4.7}$$

$\mathbf{p}_{finger}$ and $\mathbf{p}_{wrist}$ is the positional data from the Polhemus sensors. $\mathbf{q}_{TF}$ and $\mathbf{\Delta}_{TF}$ are the transformed orientation and position respectively.

3. Translation of the position of the fingertip origin to the center of the distal finger segment as shown in Figure 4.3(c). To this point the virtual position of the fingertip is in the center of the Polhemus sensor. The fingertip position has to be translated by f to be in the center of the distal finger segment.

$$\mathbf{\Delta}_{TF,TL} = \mathbf{\Delta}_{TF} + \mathbf{q}_{TF} \cdot \begin{pmatrix} 0 \\ 0 \\ f \end{pmatrix} \tag{4.8}$$

The offset f is the sum of the sensor diameter and the fingertip thickness divided

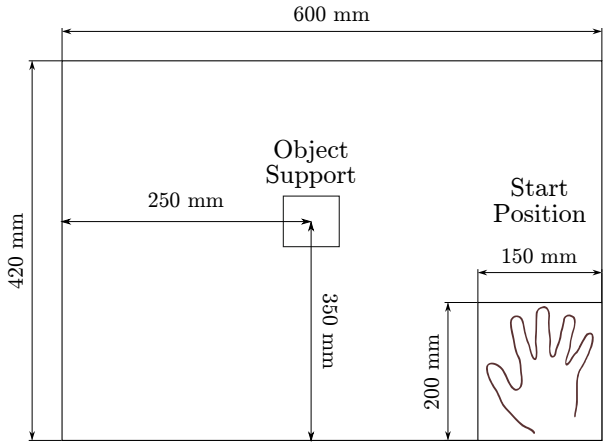

(a) Table setup of the experiments. The object to be grasped with a specific grasp type is placed onto the object support.

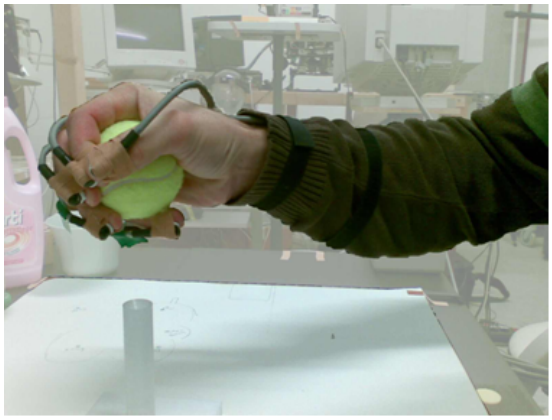

(b) The final grasp stage of grasp No. 11, "Power Sphere". The subject succeeded in grasping the object and lifted it from the supporting base.

Figure 4.4: Setup of the experiments.

by two translated into the z direction.

4.3.2 Data Set

Based on the measurement in Section 4.3.1, a high dimensional dataset is created which defines the human *action manifold*. The structure of the dataset is presented in Figure 4.5. The matrix has 4650 rows (5 subjects x 31 grasp types x 30 samples). In the vertical direction, the first subdivision is the subject. Within each subjects section there are the 31 grasp types present, which in turn are divided into the 30 individual samples. From each grasp trial 30 equally spaced samples are taken. The dimensionality of the dataset is 60 (5 fingers x 12 dimensions per finger), where the first division is by the finger and for each finger there are three parameters for position and nine parameters for rotations. The rotational component is nine dimensional as rotation matrices are used to encode 3D rotations.

Overall, this leads to a datamatrix of the size 4650×60. The dataset consists only of a concatenation of the trials performed by the multiple subjects. There is no additional information which labels the samples according to a grasp type or subject. Any structure found is based on the data itself.

As previously mentioned, each trial was performed twice, this allows for a creation of two datasets. The first trial will be used as the *test data*, whereas the second trial is used as *training set*. The size of the dataset is equal in both cases, but the scaling differs slightly. The scaling parameters of the training set are applied for the test set as well.

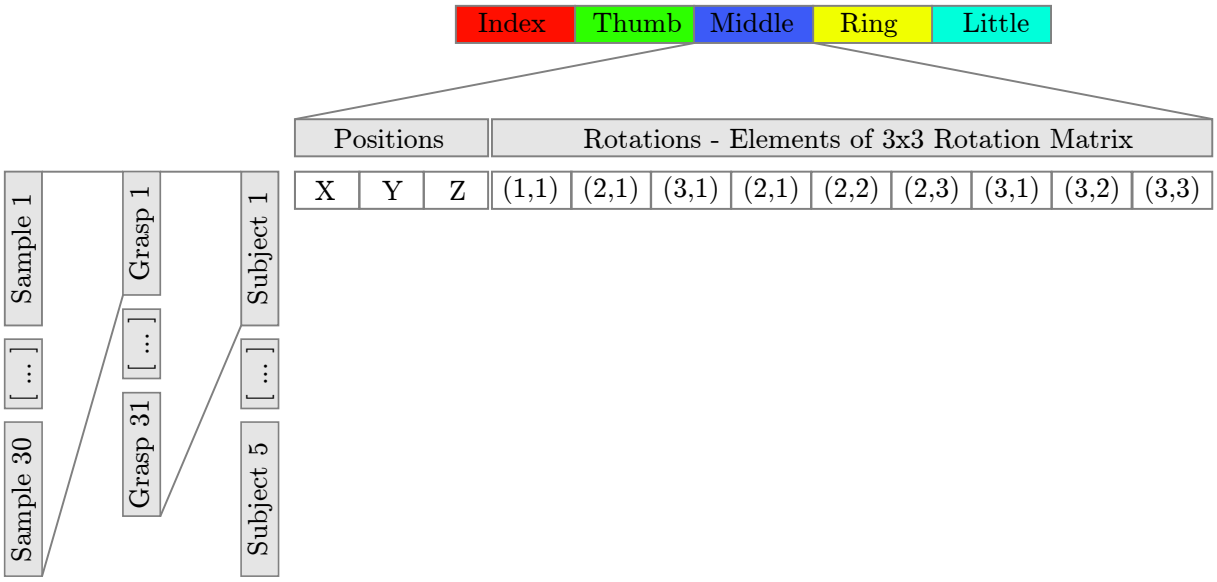

Figure 4.5: Structure of the human grasping dataset. Overall, the dimension of the datamatrix is 4650×60

4.3.3 Rotation Representation

The dimension of the data space is dependent on the representation of the orientations. There are different ways of encoding a 3D rotation, and each of them has different properties and numbers of parameters.

Euler angles are the most compact description of rotation in 3D space employing only three parameters. The big drawback of this method is the fact that the description with those 3 angles is not smooth, although the object moves smoothly in space. There are jumps in the data and additionally the method encounters the problem of singularities at certain rotations angles (gimbal lock) [108]. *Quaternions* use four parameters to define the orientation. Three parameters can be interpreted as a vector and the last parameter is the rotation about this vector. Besides some computational advantages, this method is still very compact, and it offers smooth transitions from one orientation to the other without singularities [108]. The main drawback of quaternions is that the Euclidean distance between them does not reflect their similarity. Due to their properties the signs of the components of the quaternion can be inverted without affecting the transformation matrix [109, p. 162]. Therefore, the quaternion $\mathbf{q} = (e_0, e_1, e_2, e_3)$ represents the same rotation as $\mathbf{q}' = -\mathbf{q} = (-e_0, -e_1, -e_2, -e_3)$. The euclidian distance between such a pair of quaternions is $\|\mathbf{q} - \mathbf{q}'\| = \|2\mathbf{q}\| = 2$, as quaternions are normalized $\|\mathbf{q}\| = 1$. Algorithms that compare 3D rotations based on the euclidian norm get trapped in that problem, treating similar rotations as being different. *Rotation matrices* use a 3×3 matrix to define the orientation. Those 9 parameters unambiguously define the orientation of an object at the cost of introducing many new dimensions to the dataset.

For the given application, the rotation matrix representation is the most suitable, as it unambiguously defines the 3D orientation of an object. We will disregard the other representations, even if their description would be more compact. The additional dimensions introduced by the rotation representation will not pose a large problem to the DR as the dimensions are perfectly coupled and can be therefore reduced without loss of information.

Scaling Methods

Each dimension of the human dataset has a different range. The reason for this being that some represent rotations, whereas others store positions. Additionally, different positional dimensions have a different movement spectrum. As the error function is spherical, each dimension is treated equally - thus dimensions with a large variance are assigned a higher relative importance. By scaling the data, the range of the columns is transformed to a common variance, thus avoiding the influence of different ranges. How the data is preprocessed before passing it to the GP-LVM algorithm is crucial for the results. All dimensions have to be weighted equally if they are scaled to a common range.

To determine the optimal scaling method, different methods to scale and weight dimensions were evaluated. The created datasets are listed below.

Handlength RM The positional variables are divided by the individual subjects' hand lengths.

Handlength RM Pos3 Rot9 That dataset additionally erases the individual influence of the hand size. In the next step, the positional variables are divided by three, and the orientational variables are divided by 9. The idea is to weight both positions and orientations equally, as rotations seem over-represented due to their larger number of dimensions.

Handlength RM Pos3 Rot9 Thumb3 Additionally to the "Handlength RM Pos3 Rot9" dataset, the dimensions belonging to the thumb were multiplied by three. The idea is to give the thumb a larger relative importance as it is the dominant finger in grasping.

4.3.4 Influence of the Kernel Width

In GP-LVM, we can use different parameters to influence the structure of the latent space. One of these parameters is the inverse width of the back constraints kernel, γ. As described in Section 2.5.4, the projection from high to low dimensional space is governed by back constraints. For the BCs the same kernel types can be used. In the case at hand, a RBF kernel is used. In Equation 2.8 we can observe that the ratio between the distance

between points $y_i - y_n$ and the inverse width $\frac{1}{\gamma}$ determines the influence of different high-dimensional points y_n on the low dimensional point x_i. The amount of contribution of each training set point y_n is determined by the kernel $k_{bc}(y_i, y_n)$ and the weight a_{jn}. As we use a RBF kernel (Equation 2.8) for the BC its width $1/\gamma$ can be set in order to define the distance up to which training points provide a significant contribution. To make a valid prediction of a new point, the model needs at least some points from the training set where the kernel is not close to zero.

Figure 4.6(a) represents a situation in which the kernel width is small compared to the interpoint distances. In this case, the support of any external point becomes negligible. New anthropomorphic data (small white circles) will not be supported by our latent representation in this case, thus

$$\frac{1}{\gamma} \ll y_i - y_n \Rightarrow a_{jn} e^{-\frac{\gamma}{2}(y_i - y_n)^T (y_i - y_n)} \approx 0, n \neq i \tag{4.9}$$

On the other side, a large kernel width makes all points in the original space to equally support any point in the latent space (Figure 4.6(c)), no matter if they are anthropomorphic (white circles) or not (crosses), thus:

$$\frac{1}{\gamma} \gg y_i - y_n \Rightarrow a_{jn} e^{-\frac{\gamma}{2}(y_i - y_n)^T (y_i - y_n)} \approx 1, \forall n \tag{4.10}$$

Our goal is to use such a value of γ, that only those points that correspond to anthropomorphic postures are taken into account, Figure 4.6(b).

As we cannot directly determine how well the kernel width represents the manifold, we project the two datasets to the latent space and assess their shape. The goal is to determine a value where a random hand model has very low coverage, whereas the test set (which is close to the training data) still covers large proportions of the latent space.

4.3.5 Metrics on Latent Space Quality

This Section explains four metrics which are used in order to assess the quality of the latent space models. Some of the methods make use of the overlap measure introduced previously in Section 4.2.

Reconstruction Error

In order to evaluate the quality of the learned mappings we use the score of the reconstruction error of the training data [66]. The reconstruction error shows how much the mapping connecting the observed and the latent representation distorts the data. It takes a point from the high dimensional space and pushes that point through the latent space and back

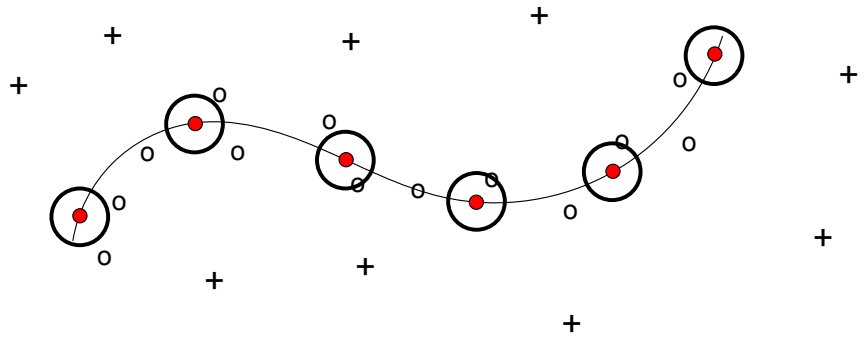

(a) Too small kernel width. There are many regions on the manifold which are not represented properly by training data.

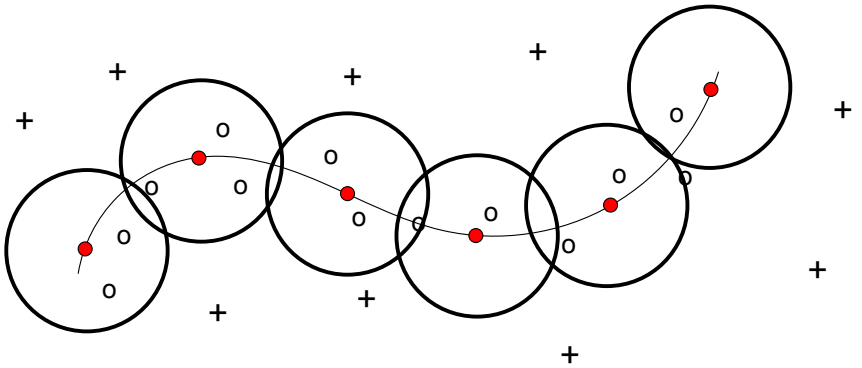

(b) Correct kernel width. The manifold is represented correctly, so that the test set can be supported by data, whereas the more distant points of the random hand are not within the supported region.

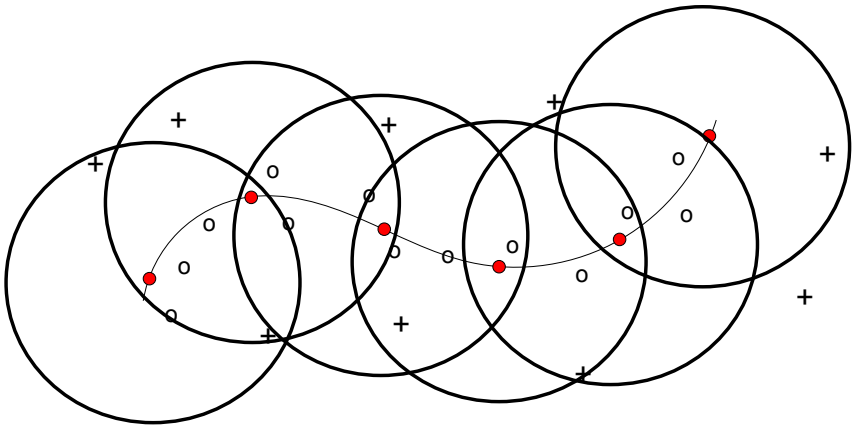

(c) Too wide kernel. The kernel width is large, so that even the very distant points of the random hand model are within the supported region.

Figure 4.6: Different kernel width and their influence on the discrimination between the training set (tiny circles) and the random hand set (black crosses). The manifold (black line) is sampled by datapoints (red dots) and their corresponding kernel width (black circles).

to the original space. The difference between those two points is then calculated. That is performed for the training points, which tests how well the model adapts to those points. Additionally it is performed for the test set, where it allows to assess the performance for points which are new, but similar to the training data. Since no information about the classes of the grasp types is processed, it does not test the generalization ability of the model. The reconstruction error is not sensible to a difference of the test and training set for a given grasp type and subject. It is possible that two trajectories of the same grasp are located in totally different areas in latent space, but the reconstruction error is still small.

To calculate the reconstruction error the following steps are performed:

1. Scale the dataset
2. Project points to latent space
3. Projects latent points back to data space
4. Unscale the data
5. Calculate reconstruction errors between the original dataset and the dataset obtained in point 4.

Positional Error: The difference between each fingertip is calculated. The algorithm calculates the average distance between the original and the reconstructed fingertip position of all samples in the dataset.

Rotational Error: The difference between two quaternions is calculated using the cosines law where the two quaternions $\mathbf{q}_1$ and $\mathbf{q}_2$ are regarded as 4D vectors.

$$\delta = \arccos(\mathbf{q}_1 \cdot \mathbf{q}_2) \tag{4.11}$$

The result δ is the angle between the original fingertip orientation and the reconstructed fingertip orientation.

The calculations are repeated for all samples in the data set and the average positional and rotational errors are calculated. As the rotational representation is a rotation matrix, it is transformed to quaternion and Equation 4.11 is utilized.

Discriminative Power

A grasp model for each grasp type based on Gaussian Mixture Regression (GMR) [110,111] is created. This procedure fits a mixture of Gaussians into each set of sequences, augmented with the time dimension. For each timestep (not limited to the original number of samples) a mean and variance of the low dimensional pose representation can be obtained. The output are trajectories in low dimensional space that characterize each of the grasps

[112]. Figure 4.7 shows some of the GMR trajectories for the GP-LVM 2D that is used for the rest of the thesis. Each grasp model is based on 5 trajectories, as performed by the subjects. The dark line in the right column corresponds to the mean trajectory and the light area marks the variance the model has on certain points of the trajectory. One can clearly observe that different trajectories have a different signature in the latent space.

Therefore one can compute the probability of a new grasp sequence having been generated by a particular GMR model. By comparing those probabilities it can be estimated which is the most likely grasp class that generated that sequence, and compare it with the real grasp that was actually executed [112]. The result is a classification rate of the test set where a high value indicates a good grasp separation while keeping the subjects' trajectories close.

Random Model

The resulting latent space should have the ability to discriminate between an anthropomorphic hand and one that is not. Thus, when the movements of a non-anthropomorphic hand are projected to the latent space, the points should not overlap large areas of the latent space. Otherwise a large overlap could be obtained, grading such a hand as human-like – which the hand is not. That should occur even in the case of a high dimensional hand with a large number of Degrees of Freedom (DoF). Potentially, such a hand creates a large action manifold in the fingertip space. Still, it is very unlikely that such a manifold is in similar regions as the human one. For example, if we think of a 30 dimensional space (which is the lowest possible dimension as each fingertip has 6 DoF), then dividing each dimension into only two halves will create approximately one billion of sectors. The high dimension of the data space makes such an alignment just utterly unlikely.

To test this ability we create random hand models and project their movements. The random models are created using random Denavit-Hartenberg parameters with 3 DoF for each finger. Additionally, the position and orientation of the fingers' base are random and the relative orientation of the fingertip coordinate frame to the kinematic chain is random. Joint angles are taken at random from the 15 dimensional space, where each joint has a 0 to 2π range. Overall 20000 random samples from the joint space are taken and their corresponding fingertip poses are calculated. The hand models are created by a Matlab robotic toolbox [113] which allows to do forward kinematics to calculate the fingertip poses.

Two such random hand models are shown in Figure 4.8; by simple inspection it becomes clear that this hand setup is not anthropomorphic. We do not present other hand model images as none of them have human-like features.

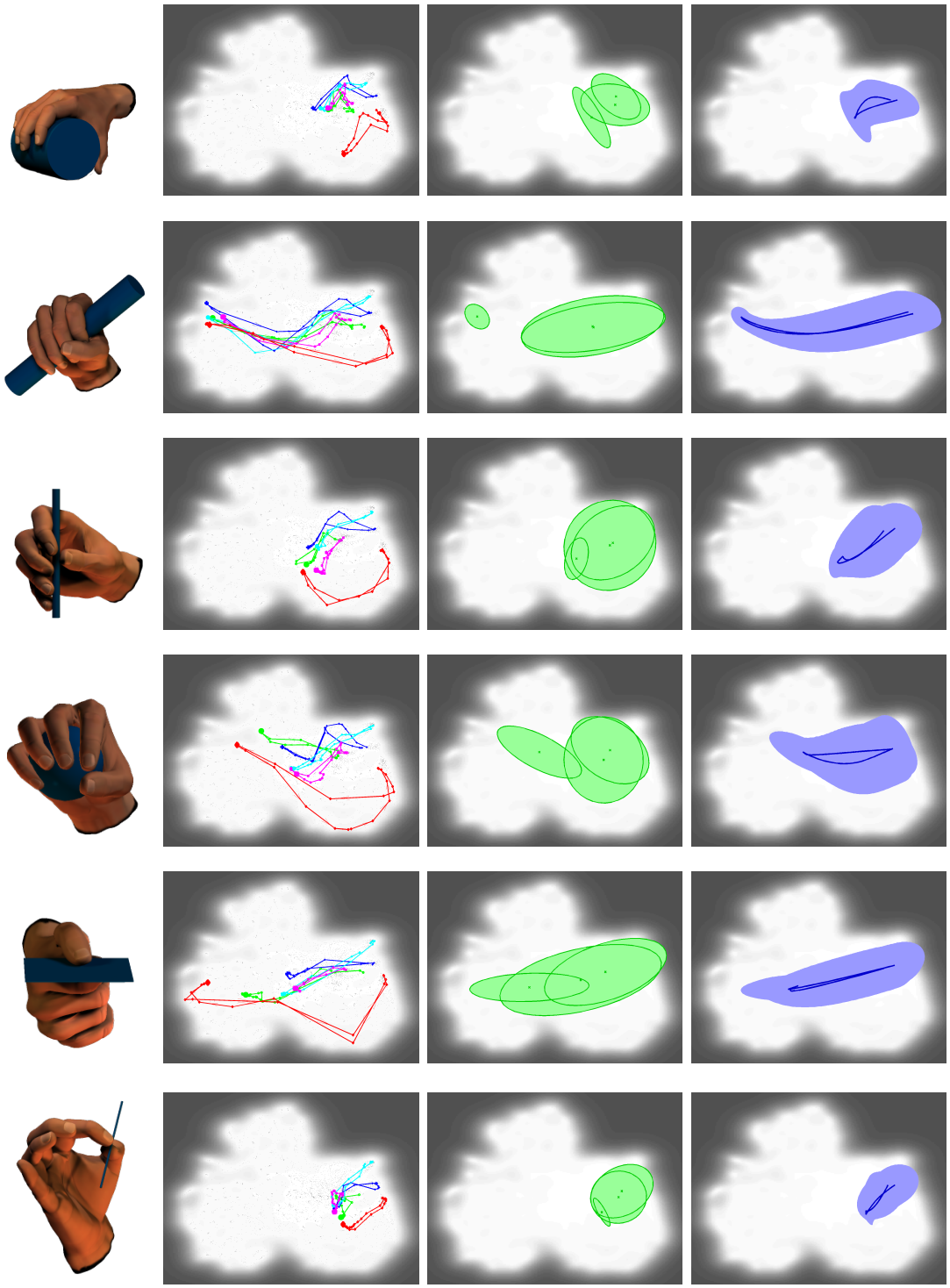

Figure 4.7: Visualization of the GMM/GMR processing pipeline for some grasps. Different signatures in the latent space are visible for different grasp types. From left to right: Picture of the grasp, projection of the five trajectories of the subjects, three gaussians fitted to the data, gaussian mixture regression. In the right column the dark line corresponds to the mean trajectory, whereas the light area represents the variance. From top to bottom the following grasp types are plotted: Large Diameter, Small Diameter, Prismatic 4 Finger, Power Sphere, Lateral, Tip Pinch.

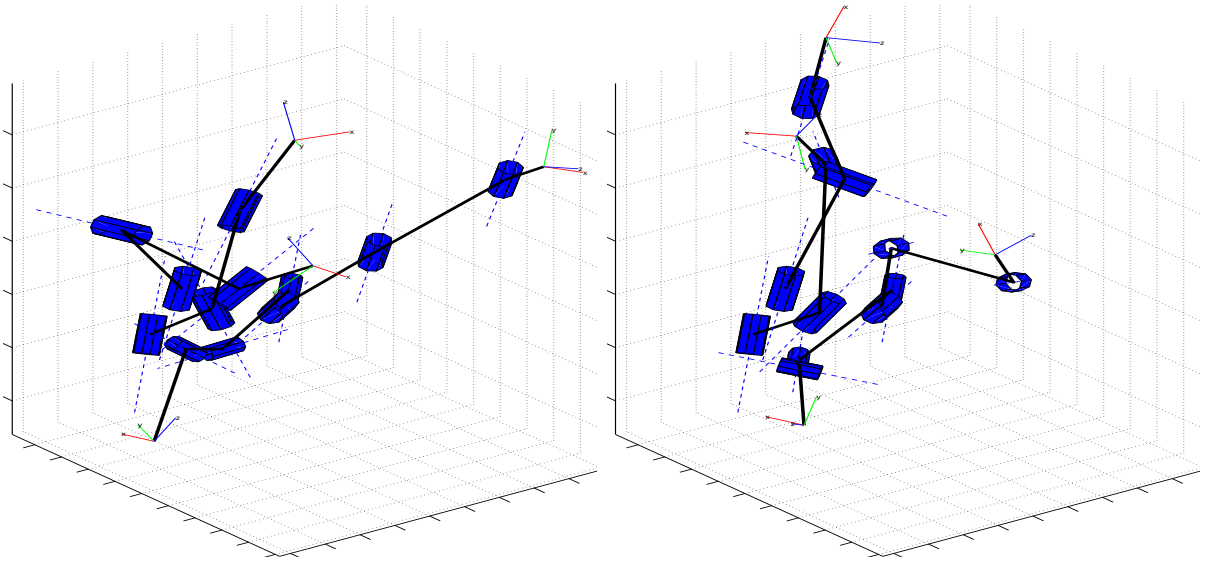

Figure 4.8: Two hand models based on random DH-parameters. Five kinematic chains represent the five digits of the hand. Both models do not show human like features.

Test Set

The random hand model test verifies if the model is selective, meaning that unanthropomorphic hands cannot cover large proportions of the latent space. The additional requirement is, that given points that are similar to the training set, the whole latent space can be filled. If both conditions are fulfilled, the system is able to distinguish between points that are human-like and that are not.

To test this, the test set is projected to the latent space. From a functional perspective the test data is equal to the training data as in both cases the subjects succeeded in grasping the object with the demanded grasp type. The only variation between the sets is the variation introduced by the subject's variance. The result from a good latent space model is that the test set covers major proportions of the latent space.

4.3.6 Model Comparison

As preliminary results showed, GP-LVM has superior performance over other DR methods like Isomap, LLE and PCA [66, 112]. Therefore, those algorithms are not taken into consideration in this comparison and the focus was onto GP-LVM. All datasets (Section 4.3.3) use rotation matrices, as only they have the desired properties of an unambiguous definition of the fingertip orientation. Overall, a variety of different models is created. The scaling of the data differs and the parameters of the model creation are subject to variation. Consequently, this leads to a large number of models, all with different properties. The goal is to find a model which is able to distinguish between anthropomorphic (large

first trial coverage) and non-anthropomorphic (very little random hand coverage, both described in Section 4.3.5) hands. Those two measures are the most important ones. The reconstruction error and the discriminative power are of less importance, but still the final model has to offer a decent performance in those two fields as well. Those two measures make sure that the dimensionality reduction per se works and delivers good results.

The BC projection to the latent space is governed by a RBF kernel. For such a kernel the inverse width is the most important parameter that can be set in order to define the behavior of the projection. The idea is to find an intermediate value of the kernel length which allows a discrimination between anthropomorphic hands and the random hand model. Section 4.3.4 discusses this in more detail. The length was incrementally varied over a large range, until a good length was determined.

Table 4.1 shows the results of the created models. To make the metrics with their different ranges comparable, the following method is applied. Each metric (column in Table 4.1) is scaled in such a way that the worst result has a value of 0 and the best result a value of 1. The in between results were scaled linearly. It was not always the case that the best value corresponds to the highest value. For the reconstruction errors and the projection of the random hand a value of zero would be optimal. To raise the relative importance of the projections of the test data and the random model, those results are multiplied by three. Finally, the score is the sum of the individual results.

There are clear trends visible. First, the initialization method has an minor influence – results where only the initialization varies have the same results. Second, the dataset with handlength scaling has by far the best results on the reconstruction error calculation. The error is dependent on the scaling method but not the kernel length. Even though a larger kernel value is a larger constraint on the latent space, it does not alter the performance on the reconstruction error. Third, the discriminate power has the highest values for the second scaling method (positions divided by 3 and orientations divided by 9). The best results are obtained with a variety of different kernel widths, where no sensitivity to the inverse width is present. Finally, the coverage shows the expected characteristic. A small inverse width has good results on the test set (all points can be projected properly), whereas a large inverse width has good results on the random hand model (all hand configurations collapse to a single point in latent space). Between those two extremes the ideal case is located, having a decent performance on both measures.

4.3.7 The Selected Model

From the competing models the model employing handlength scaling with a kernel width of 1 and an initialization with PCA is superior. Compared to the other models, it has a very good result on the reconstruction error. As demanded, the overlap of the random

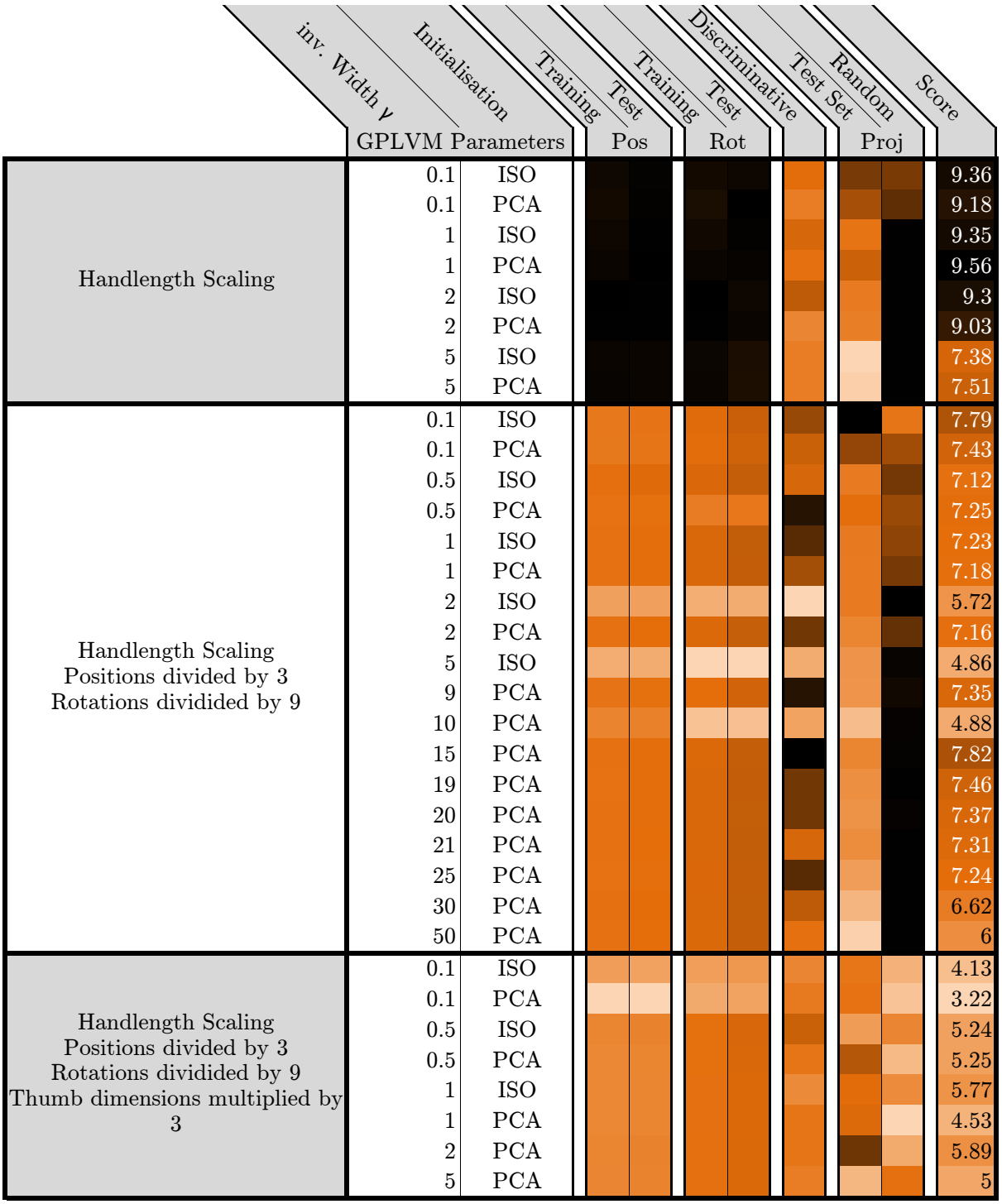

	inv. Width γ	Initialisation	Training	Test	Training	Test	Discriminative	Test Set	Random		Score
	GPLVM Parameters		Pos		Rot				Proj		
Handlength Scaling	0.1	ISO									9.36
	0.1	PCA									9.18
	1	ISO									9.35
	1	PCA									9.56
	2	ISO									9.3
	2	PCA									9.03
	5	ISO									7.38
	5	PCA									7.51
Handlength Scaling Positions divided by 3 Rotations dividided by 9	0.1	ISO									7.79
	0.1	PCA									7.43
	0.5	ISO									7.12
	0.5	PCA									7.25
	1	ISO									7.23
	1	PCA									7.18
	2	ISO									5.72
	2	PCA									7.16
	5	ISO									4.86
	9	PCA									7.35
	10	PCA									4.88
	15	PCA									7.82
	19	PCA									7.46
	20	PCA									7.37
	21	PCA									7.31
	25	PCA									7.24
	30	PCA									6.62
	50	PCA									6
Handlength Scaling Positions divided by 3 Rotations dividided by 9 Thumb dimensions multiplied by 3	0.1	ISO									4.13
	0.1	PCA									3.22
	0.5	ISO									5.24
	0.5	PCA									5.25
	1	ISO									5.77
	1	PCA									4.53
	2	PCA									5.89
	5	PCA									5

Table 4.1: Results of different metrics for the latent space models. The variation is the applied scaling, the kernel width and the initialization of the latent space. Black indicates best performance in a column, whereas white represents the opposite. The columns of the Projections (Proj) are multiplied with 3, as those are the measures with the highest importance. The score column is the sum over all individual scores. Abbreviations: Pos: positional reconstruction error; Rot: orientational reconstruction error; Proj: Latent space overlap O_{rel}

hand model is low and the overlap of the test set is still high. The discrimination between grasp types, as tested with the GMM/GMR models is average.

To gain intuition on the topology of the space, Figure 4.9 presents five grasp trajectories as performed by the five subjects. Depending on the grasp type, the final grasp posture is at different locations in the latent space. From the initial starting position on the right side, the subjects proceed to the final grasping point (in the circles) and then retreat back to the start position. What is not shown here is that similar grasp types will also be close in latent space [59], and in general follow the human notion on similarity. Additionally, it is observed that the further left in the latent space, the fingers tend to be more flexed. That is only natural, as the starting posture is the flat hand and as the fingers flex, the difference to that original posture increases. The discrimination between grasp types is not as good as in [112], where the classification rate is higher. Due to the different applications this compromise had to be made.

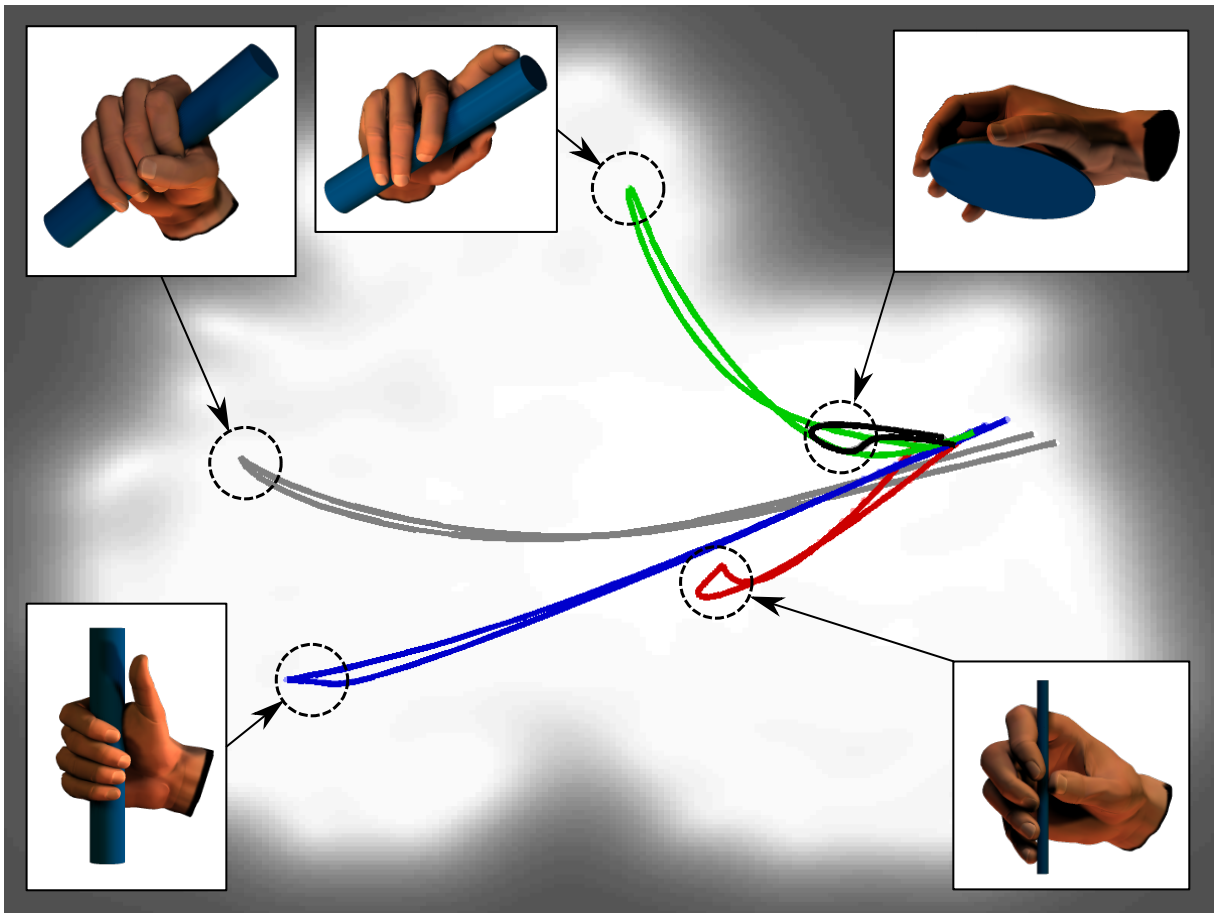

Figure 4.9: Latent space representation of the grasping data. The trajectories correspond to the average trajectory of 5 subjects performing the shown grasps. Each grasp type is located at a distinct area in latent space. Only a few major grasp types are presented in the Figure.

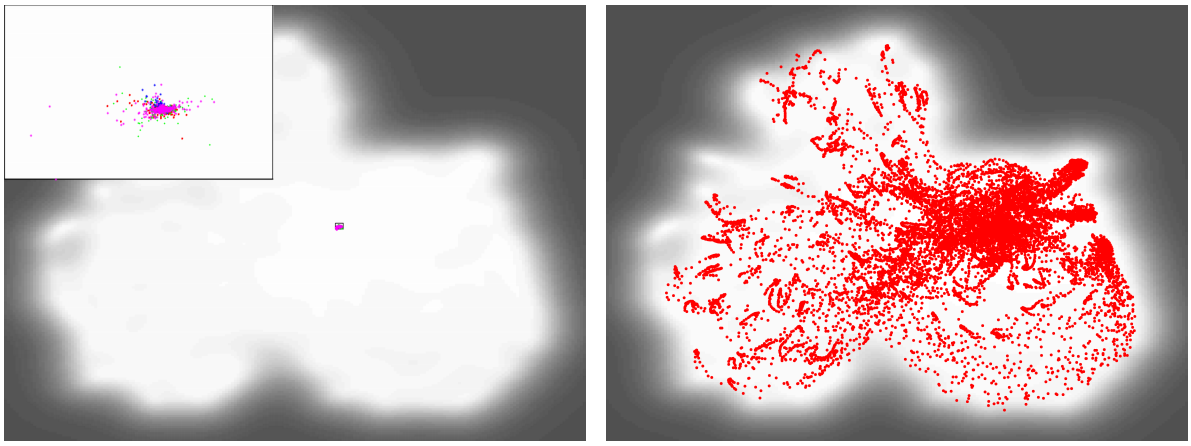

(a) Projection of four random hand models to the latent space. The left top picture is a magnification of the latent projection points. In that subfigure different colors indicate different hands.

(b) Projection of the test set to the latent space, the points cover most of the white area.

Figure 4.10: Projections to determine the latent space quality. For the random hand model a small coverage is desired, whereas for the test set the opposite is the case.

The projection of the movements of four random hand models is presented in Figure 4.10(a). As demanded, the points cover only a very restricted region in the middle of the space. On the contrary, the points from the training set cover most of the latent space. That can be seen in Figure 4.10(b). Given the correct points, which are close to the human grasping manifold, the system projects points to regions that differ to the random hand projection. Yet, due to the width of the kernel there is a "halo" around the points which increases the area O_h and thus the training set covers 52.5 % of the latent space as it misses the cloudy areas. As the size of the human space is constant for all hands, this will not affect the following analysis.

All grasp trajectories share the same start and end position. That is the flat hand posture, where the hand is put flat onto the table. Therefore, all grasp trajectories are forced to start and end at the same location. That fact can be seen in Figure 4.9, where all lines start and end in a similar location in the right part of the latent space. Consequently, the first and last few samples of all grasps are very similar as the hand always has to close the fingers to a certain degree to create the grasping posture. There is no grasp where the fingers have to extend in order to move to a grasp. That forces the latent space to have a certain shape. From the starting point on the right side of the latent space, all trajectories have to move a short path in parallel, which is the common flexion of the hand. That in turn forces the grasps to be closer than necessary as they all have to be somewhere on the left of the starting point. Thus the trajectories only spread over a quarter of a circle, where the starting location is the center. That is a weakness of the measurement setup; a better approach might be to use a different hand posture as start/end configuration. One

possibility might be to place the hand onto a spherical support with a diameter of about 10 - 20 cm. That would roughly represent the posture of the relaxed hand. In that case the common hand posture would be situated closer to a mean hand posture. Hence, some grasps would require an extension of the hand, where others demand a flexion. Thus a more star-like shape might be possible, where the initial position is at the center. Finally that would lead to better grasp separation.

4.4 Projection of Existing Hands

The first application of the introduced overlap measure is to determine the score of existing hands. Therefore two prosthetic hands with a low number of DoF and a highly complex robotic hand are tested. The hand models are created using a robotic matlab toolbox [113] and the kinematic structure is defined via DH parameters. At the end of each hand Section, a short discussion regarding the data generation and how the results can be interpreted is given. Additionally, the system is compared against the linear method PCA, which is the most commonly used method for dimensionality reduction. This comparison yields some surprising results on the different of those two methods.

4.4.1 SensorHand

The Otto Bock SensorHand [23] is a prosthetic hand (see Figure 2.7(a) and Section 2.3.1) with three actuated fingers which are all driven by the same motor. The mechanical structure is covered by a glove, which is responsible for protecting the mechanics of the hand and creating a more human-like appearance. The glove also emulates the ring and the little finger, resulting in a 5-digit design. There is a metal bar within the glove which couples fingers four and five to the movements of the middle finger. As they are solely connected via the glove, the movement amplitude decreases from middle to little finger. The forward kinematics of the hand takes that into account by reducing the maximal finger flexion of the ring and little finger. The finger angles β_i, where $i = 1$ is the thumb, and $i = 5$ is the little finger, are depending on the driving variable c, where $c = 43°$ is hand closed and $c = 0°$ is hand opened. Overall 100 equally spaced samples of c are taken from that range. The corresponding finger flexion angles β_i are as follows.

$$\begin{aligned} \beta_{1,2,3} &= c \\ \beta_4 &= 0.9 \cdot c \\ \beta_5 &= 0.8 \cdot c \end{aligned} \tag{4.12}$$

Fingertip poses are computed based on these angles. Their projection during of one cycle of the transition from open to closed hand, which is all the hand is capable of, is

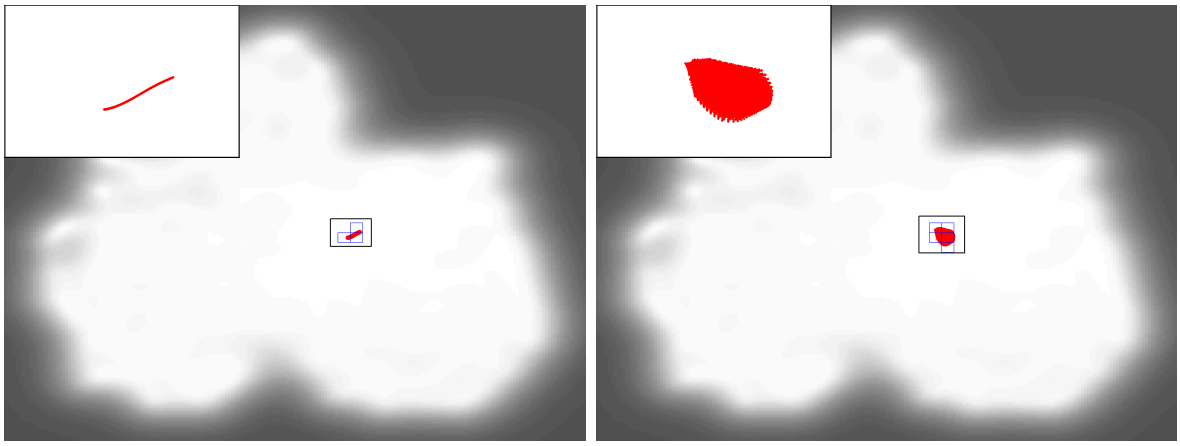

(a) Projection of the fingertip movements of the Otto Bock SensorHand to the latent space. The red points represent the trajectory of one open-close cycle. The trajectory covers 0.24 % of the human manifold.

(b) Projection of the fingertip movements of the 5 DoF "Otto Bock SensorHand" onto the latent space. The trajectory covers 0.4 % of the human manifold.

Figure 4.11: Projection of the Otto Bock SensorHand.

shown in Figure 4.11(a). The hand is able to cover 0.24 % of the human manifold. Still, the trajectory is different to the projection of a random hand (Figure 4.10(a)).

Overall the hand has some major differences to the human hand. The position of the thumb is not anatomically correct; it is basically rotated 180 degrees, so that it perfectly opposes the index and middle finger. Even though the position of the thumb fingertip is potentially correct, the orientation is not. The human simply cannot position the fingertip in the way the SensorHand does. Additionally, all finger MCP joints share the same rotation axis. A more natural way would be to orient the axes in such a way that the fingers are slightly abducted when the MCP joint is extended [9]. All those non-anthropomorphic features combined with the one dimensional movement seem to be the reason why the latent space trajectory of the hand is relatively short.

As hand models are used, the properties of a hand setup can be changed and the effect on the latent space overlap can be analyzed. The 5 joints which are coupled in the SensorHand (the CMC of the thumb and the MCP joints of the fingers) are actuated independently, conferring five DoF to the hand. The range of motion is the same as previously, and 9 equally spaced flexion values are taken from each joint. Overall, this creates $9^5 = 59049$ different hand postures which are projected to the latent space. The projection (Figure 4.11(b)) shows that increasing the dimensionality of the hand does not change the latent space overlap much. The much more complex hand covers only 0.4 % of the human manifold, which is a slight increase over the original SensorHand. For that hand, adding independent actuators proved to be a bad choice for increasing the hand anthropomorphism.

4.4.2 Michelangelo Hand

The next generation of prosthetic hands by Otto Bock is the so called Michelangelo hand [26], presented in Section 2.3.1. As the hand is still in development, the exact control scheme of the hand is not yet finalized. Therefore, the current hand prototype with the following hand postures is used:

- Hand open for tripod pinch (OT)
- Hand open for lateral pinch (OL)
- Neutral position (NP)
- Tripod pinch (TP)
- Lateral pinch (LP)

The following movement trajectories connecting positions are incorporated into the hand model.

- OT $\rightarrow$ TP
- OL $\rightarrow$ LP
- NP $\rightarrow$ OT
- NP $\rightarrow$ OL
- NP $\rightarrow$ TP

Each trajectory is sampled with 100 points and the corresponding fingertip poses are projected onto the latent space. Figure 4.12(a) shows the projection of those movements, where the colors indicate different trajectories. Compared to the SensorHand, it can be observed that the trajectories are much longer. Therefore they are able to cover a larger area of 2.8 % of the human manifold. That is a seven times larger overlap than the SensorHand. Even though the hand has very few DoF, its overlap with the human manifold is significantly larger as the general setup is closer to the human hand.

The tripod pinch (TP) and lateral pinch (LP) are located on the left side whereas the hand is opened on the right side of the latent space. In between lies the neutral position (NP) with trajectories connecting it to OT, OL and TP. Compared to the human grasp trajectories of Figure 4.9, the movements of the Michelangelo hand show a left-right dominance as well. The starting position is also on the right side, whereas the grasp positions are on the left. That is a sign that not only is the hand capable of covering larger areas in the human manifold, but also that the movements itself are more human-like.

The positions of the tripod pinch and the lateral pinch are relatively close in latent space. The reason seems to be that the system is weighting every finger roughly the same.

As the poses of four of the five digits are nearly identical (in the lateral pinch the fingers flex a little bit more), it is plausible that the projections in the latent space are similar.

As described above, the Michelangelo hand is controlled by choosing different trajectories, along which the hand is controlled as being one-dimensional. That step is necessary as the controller (as described in Section 2.3.3) of the prosthetic hand lacks a proper way to control the full two DoF of the hand. In the remainder of the thesis, the Michelangelo hand is used as the starting point for further hand optimizations. As the goal is to determine the mechanical potential of the hand, not the potential influenced by a certain control scheme, the full two dimensional hand is taken into account. Therefore all possible digit flexion and thumb abduction values are calculated and projected. The resulting overlap can be seen in Figure 4.12(b), where the resulting overlap is 3.9 %. That number will serve as the baseline for all further analysis.

As already done with the SensorHand, the complexity of the hand is increased by assigning the hand 5 DoF – the flexion of each digit is actuated independently. As the thumb has an additional DoF (abduction/adduction) this value has to be specified as well. It is set into the intermediate rest position. Changing the value of this joint does not affect significantly the results. The range of motion from each digit is sampled with 9 angles, resulting in the same number of points as in the SensorHand case. The resulting overlap is 7.9 %, which is considerably more than the 2.8 % the original hand has. In that case it seems that introducing additional DoFs is a suitable way to equip the hand with more anthropomorphic capabilities. In the projection of the 5 DoF Michelangelo in Figure 4.12(c), it becomes visible that the extreme position in the right-left direction corresponds to the open and the grasp position respectively. All movements of the original Michelangelo lie beneath the line connecting those two positions and have very roughly a triangle shape. The movements of the 5 DoF hand overlap an additional space above that triangle. The top point in the projection in Figure 4.12(c) corresponds to a hand position where the index finger is extended but the other fingers are flexed and the thumb is in moderate flexion. The ability to individually flex fingers seems to be important to reach new areas in the latent space. That is a difference to the SensorHand where the introduction of finger individuation does not influence substantially the latent space overlap.

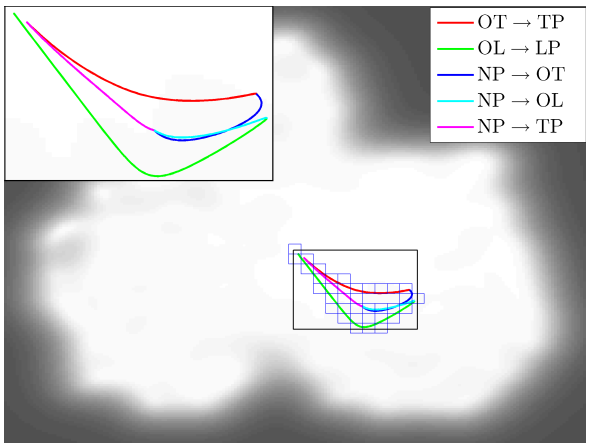

(a) Projection of the fingertip movements of the Otto Bock Michelangelo Hand to the latent space. The hand is able to cover 2.8 % of the human manifold.

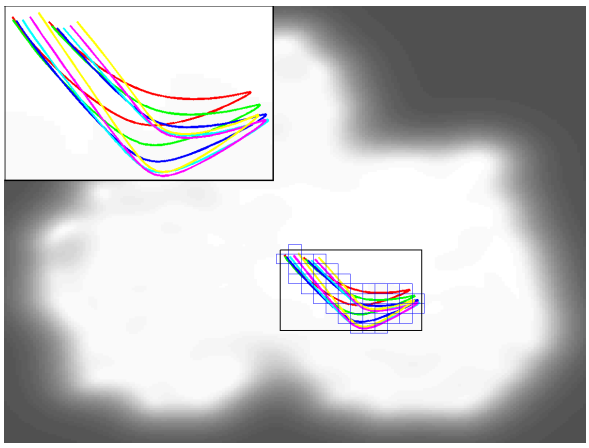

(b) Full two dimensional Michelangelo hand. In that case the thumb drive is driven independently to the fingers. The colors correspond to different abduction values of the thumb. The overlap is 3.9 %.

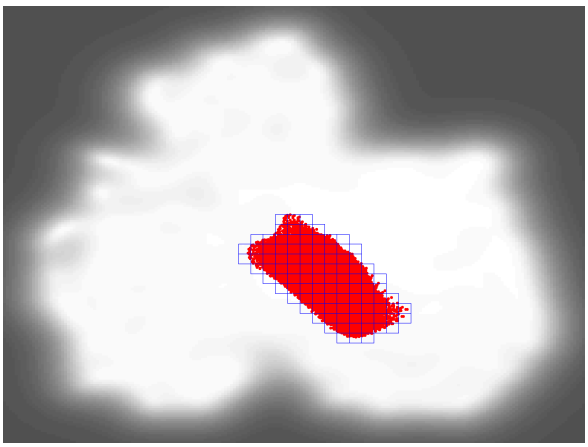

(c) Projection of the virtual 5 DoF Michelangelo hand to the latent space. The red points represent the area the hand can reach and it results in a total overlap of 7.9 %.

Figure 4.12: Different Michelangelo Models and their overlap of the latent space.

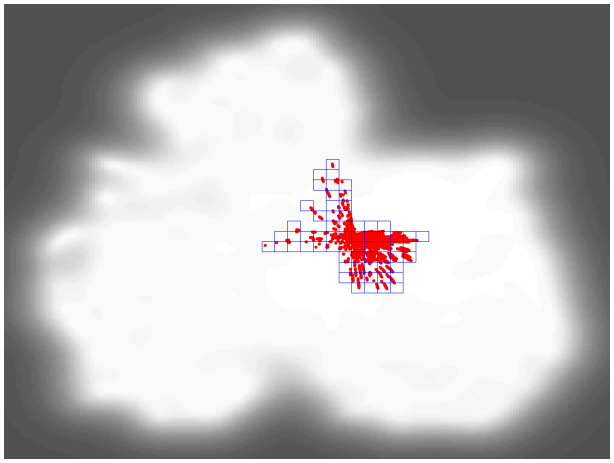

Figure 4.13: Projection of the FRH-4 hand. It covers 5.2 % of the human manifold

4.4.3 FRH-4 Hand

As an example of a hand with many degrees of freedom, we use the FRH-4 hand [31] built for a mobile assisting robot ARMAR. The hand is presented in Section 2.3.2.

Each of the eight DoF has a range of 90 degrees. To calculate all hand configurations, four samples are taken from each of the joint workspaces. Each joint can be flexed by {0, 30, 60, 90} degrees and due to the high dimensionality of the hand this leads to a total number of $4^8 = 65536$ hand configurations. Further increasing the number of samples would require prohibitively large computational times.

The kinematic structure makes it difficult to define where the hand length can be measured (which is important for scaling the positions prior to projection to the latent space). Therefore, a parameter sweep was performed through all possible hand lengths, and the length with the maximal overlap was determined. This length is assumed to be the correct hand length and the results corresponding to that length are given. For the two prosthetic hands that step is not necessary, as information on the hand size available. The resulting hand length of the FRH-4 hand is 25 cm, which is slightly larger than the maximal human hand length of about 21.15 cm. [107]. The width of the FRH-4 hand is 9.3 cm [31], which is comparable to the hand width of a large human hand [107]. The calculated hand length seems to be slightly too large, given the hand width, but due to the different kinematic setup to the human hand, that difference seems acceptable.

The projection of the hand with the determined hand length of 25 cm is shown in Figure 4.13. The overlap is 5.2 %. Compared to the large number of actuators this is a relatively low value, given that the Michelangelo hand with only 2 DoF can already cover 2.8 % of the human manifold. As described above, the hand has some features which are not anthropomorphic, which explains the reduced overlap.

Figure 4.13 shows that the outermost points seem to be slightly isolated from the

rest. That is due to the rather coarse sampling of the joint space which has only a few points at the intersection to the action manifold of the human. If the number of points is increased even further, more points would be located there, being able to further increase the overlap. To test how much the sampling influences the coverage, the method to obtain the joint values was changed. Instead of a systematic variation of the joint angles, the joint space is sampled with 60000 random points. The overlap is calculated of five such sets. The result is an overlap of 9.2 ± 0.25 %. The different sampling method increased the overlap, but it is still small when compared to the human hand. For the SensorHand and the Michelangelo Hand this resampling was not necessary as their joint space could be sampled densely enough. In that case the distance between neighboring points in the low dimensional space is small as compared to the side length of the rectangle.

4.4.4 Human Hand Model

To determine the level of overlap of a (human) hand controlled by two linear dimensions, a human hand model is created. The joint values of the hand are given by a linear combination of the first two PCs. The basic idea is similar to [35, 63].

The first two PC according to [13] are implemented into a human hand model. The model consists of 21 DoF, each finger has four joints and the thumb is assigned five joint axes. The hand is shown in Figure 4.14(a). The control space of the hand is two dimensional - the first two PCs as defined in [13]. Due to differences in the kinematic structure the PCs for the thumb cannot be implemented directly. The joint values are measured differently and cannot be transferred directly to the hand model. The coefficients were changed by hand to better fit the model. Additionally, in [13], the abduction of the MCP joints of the fingers is measured as the angle between two neighboring fingers. Therefore, only three values define the abduction of the four fingers. To comply with the hand model, the abduction of the middle finger was set to zero. The initial hand pose corresponds to the mean posture as defined by [13] and the range of motion was adapted, so that the hand moves from an extended position to the flexed position.

The projection of the fingertip postures is shown in Figure 4.14(b); the overlap is 3.4 %. That is a relatively low number which can be explained by the implementation of the PCs. First, the definition of some of the joint angles had major differences. That is in particular the case for the thumb where the coefficients had to be changed to a large degree. Second the dominant directions found by PCA seem not to be consistent to the most important directions of GP-LVM. Both methods seem to look at different aspects in the data. Furthermore, PCA is a linear method, so it cannot comply with the nonlinear GP-LVM.

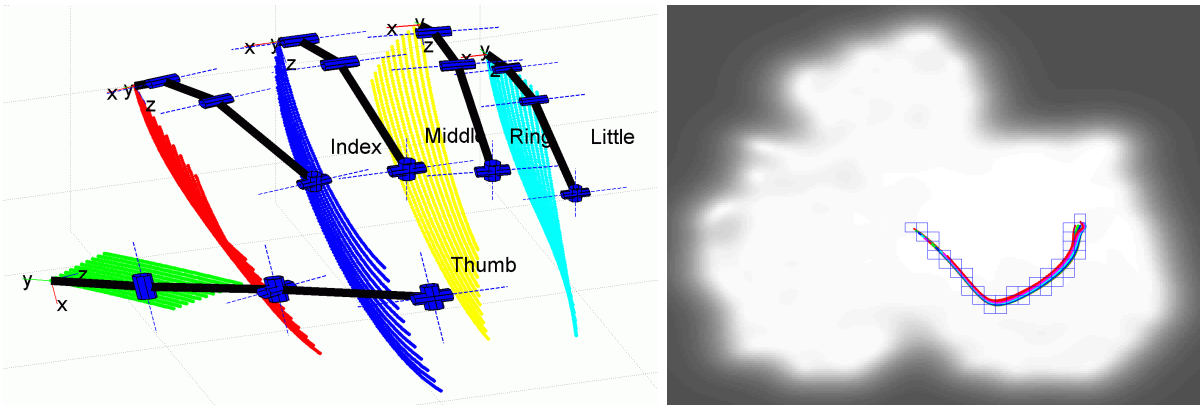

(a) Human hand model driven by the first two PCs. The colored point clouds represent the fingertip positions.

(b) Projection of the human hand model. It covers 3.4 % of the human manifold.

Figure 4.14: The human hand model controlled via two PCs and its projection.

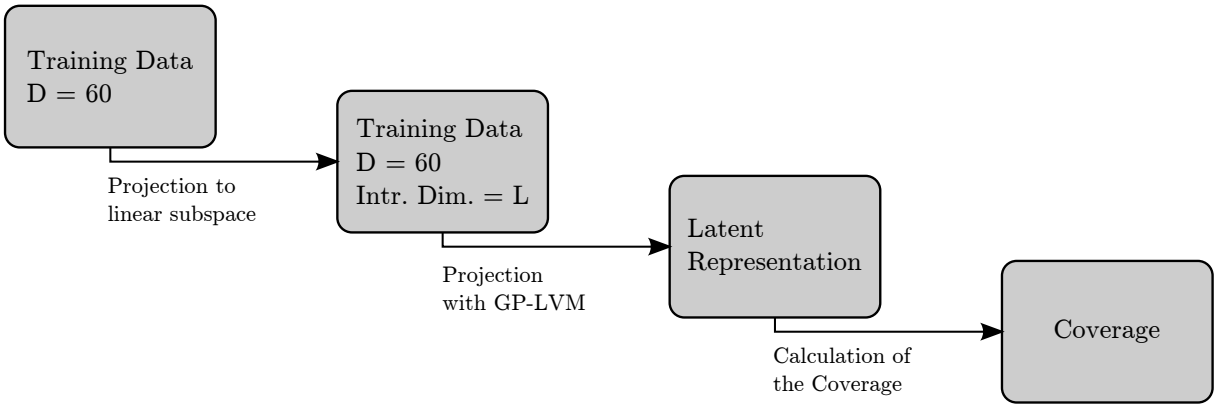

Figure 4.15: Restriction of the training dataset to a linear subspace which is defined by the first L PCs. This restricted dataset is then projected to the latent space and its coverage calculated. D is the dimension of the Fingertip space $\mathbf{T}$.

4.4.5 Principal Components of the Space

In literature, the standard approach to do dimensionality reduction in grasping is to use the linear method Principal Component Analysis (PCA). The goal of this section is to compare PCA with GP-LVM, the method which the coverage measure is based upon.

In order to do so, the following strategy is used, as presented in Figure 4.15. PCA is applied on the training data, which resides in the high dimensional fingertip space $\mathbf{T}$. The PCs, which are vectors in the high dimensional space, point into the directions with decreasing amplitude of the variance. The training dataset is then projected onto the first L PCs, therefore restricting the points to a linear subspace in the fingertip space. The basis vectors of the space correspond the Principal Components (PCs). The next step is to project that dataset with reduced intrinsic dimensionality onto the latent space with GP-LVM. Finally, the coverage is calculated.

The dimensionality of the linear subspace is varied from 1 to the full 60 dimensions. Some of the corresponding latent spaces are shown in Figure 4.16. The plots show how with increasing L, the latent coverage develops. For $L = 1$ the latent signature is a line. Interestingly, the line does not pass the whole low dimensional space, but has a rather curved shape. The second dimension does add some width to the line, but the bigger contribution is that it elongates the signature even more. The full length of the latent space is now covered. Only the next few dimensions do spread the points further, beginning to fully cover the space. In the five dimensional case ($L = 5$) the signature is already very close to the projection of the training data ($L = 60$).

The coverage corresponding to the latent space projection is shown in Figure 4.17(a). The behavior of the curve is unexpected. For the first five dimensions the score increases. The gain for each new dimension increases, where the largest gain is from dimension 4 to 5, with 17 %. For $L = 1 \dots 5$ it follows a quadratic increase. At $L = 5$ the behavior changes abruptly and flattens out. The overlap with a five dimensional space is already nearly 50 %, which is close to the 54.5% overlap of the full space. Interestingly though, the coverage slightly rises above the level of the full dimensional space for $L \approx 10 \dots 30$. That may be due to that the intermediate description being somewhat different to the original dataset, and therefore the points spread more. But the effect is not very strong, the fluctuation is in the magnitude of a few percent.

The shape of the overlap curve is fundamentally different to the behavior of the variance (Figure 4.17(b)) and the reconstruction error (Figure 4.17(c)) curve. In both latter cases the gain for each new dimension progressively decreases. That means that the first few dimensions are of large importance and higher dimensions do not contribute much. In particular for the cumulative variance, the first two PCs dominate as they contribute over 70 % of the variance. On the contrary, the overlap curve needs five dimensions for a full description. Having less than this number of dimensions results in an incomplete description, thus missing important details of the data. That suggests that the nonlinear projection of GP-LVM is not only sensible for the first five dimensions of the linear subspace, it seems that those dimensions are needed in order to make valid projections. Once a certain level of detail is reached, adding additional details to the description is too fine to be identified by GP-LVM.

The finding highlights the fundamental differences between a linear and a nonlinear method. GP-LVM projects the data onto a two dimensional embedding which is used to quantify the degree of similarity achieved via PCA. When a linear space is used, five dimensions are needed to achieve a result similar to the two dimensional GP-LVM.

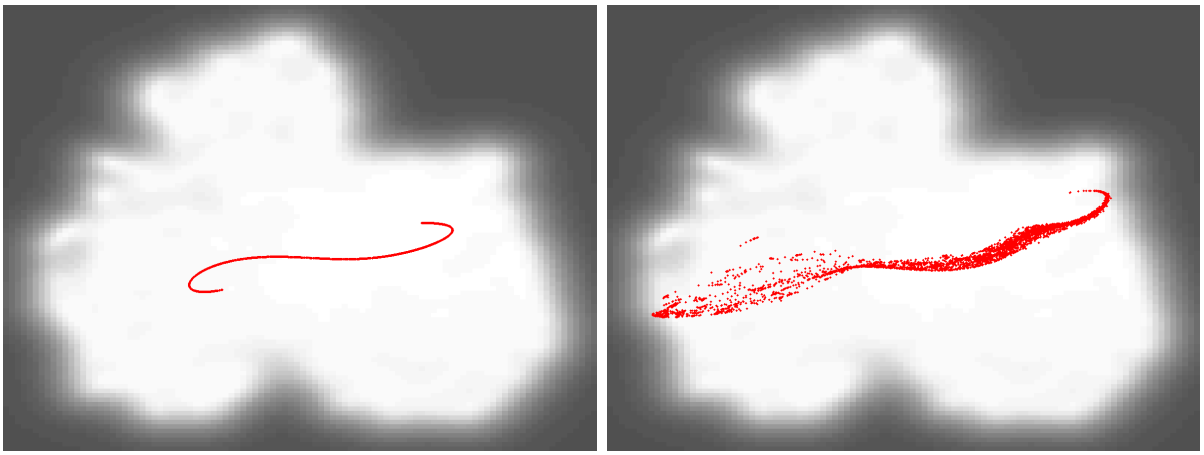

(a) $L = 1$ (b) $L = 2$

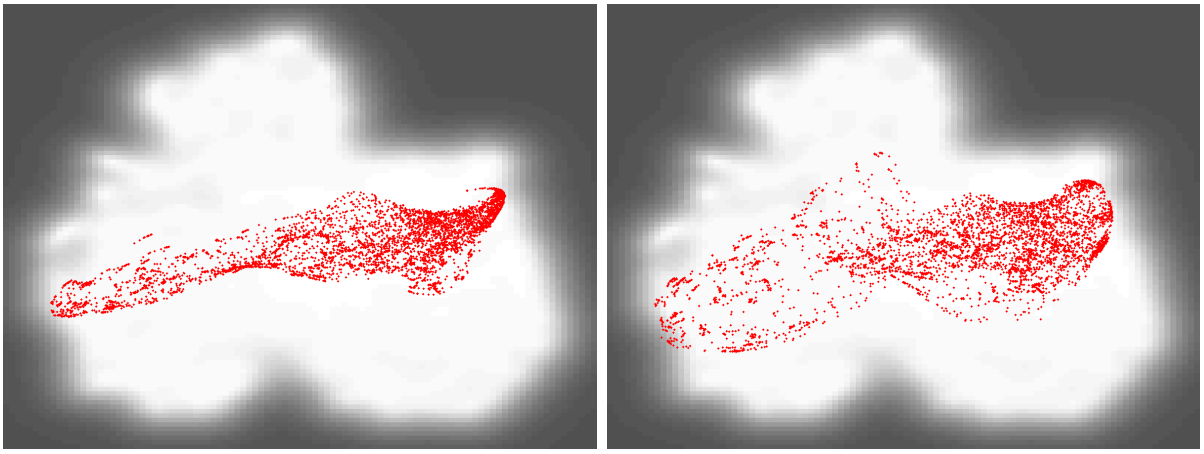

(c) $L = 3$ (d) $L = 4$

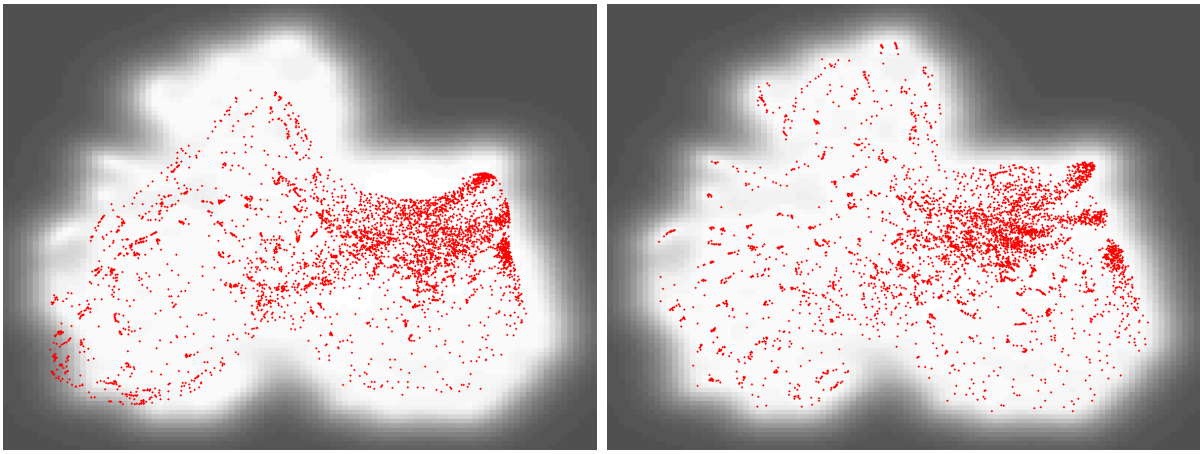

(e) $L = 5$ (f) $L = 60$; Projection of the training data.

Figure 4.16: Projection of linear subspaces calculated with PCA. The first five dimensions add significant coverage.

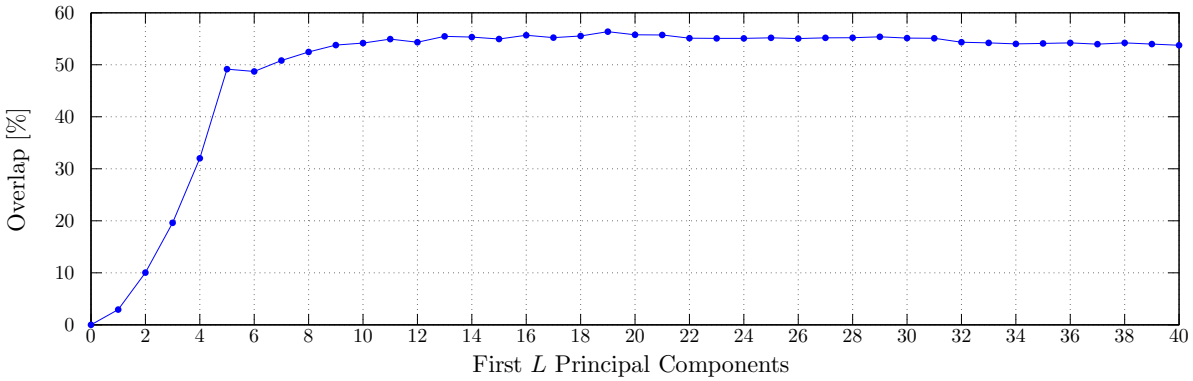

(a) Coverage of the latent space as function of the number of PCs, which are the basis vectors of the linear subspace.

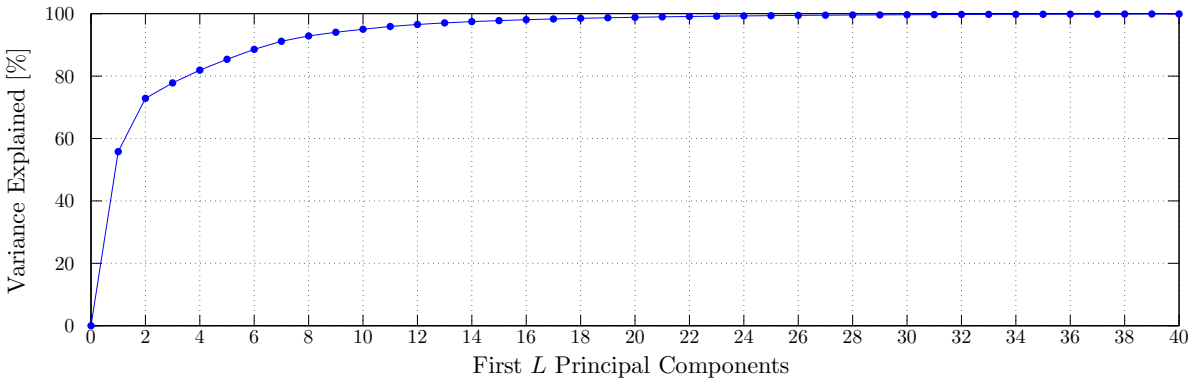

(b) Cumulative variance as function of the number of PCs.

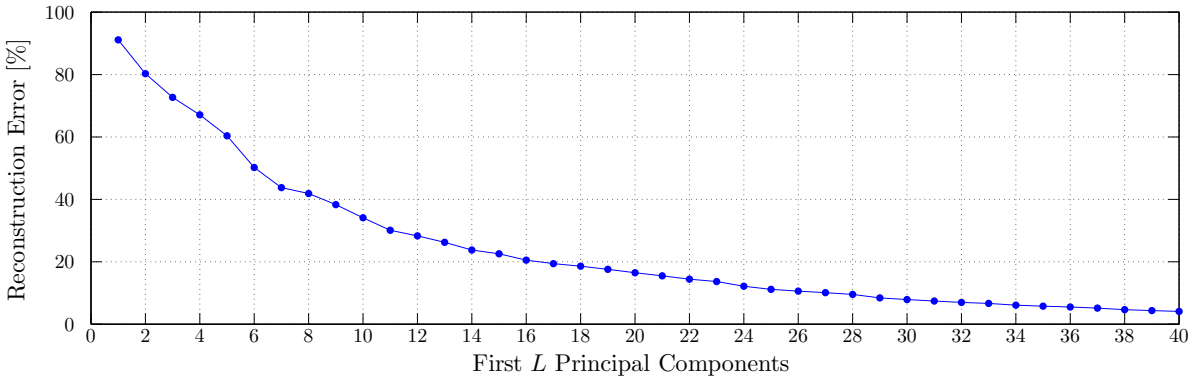

(c) Reconstruction Error as function of the number of PCs. The biggest reconstruction error still being below 100 % is by coincidence.

Figure 4.17: Comparison of the coverages and the cumulative Variances with increasing number of Principal Components. As the last 20 Principal Components are very static, they are not plotted.

4.5 Discussion

The presented method is an attempt to quantify the capabilities of an anthropomorphic hand prior to realization. One big advantage of the system is that the proposed measure can be applied to a broad range of different hands. The only condition is to use a five-fingered hand. The input to the measure is a kinematic hand model, which defines all fingertip postures it can reach - its *action manifold*. In the thesis this set was obtained using a kinematic hand model implemented via the robotics toolbox [113]. The fingertip postures are obtained by forward kinematics. The type of couplings between fingers and how the DoF move the joints can be of arbitrary type. There is no need to have linear couplings for example. They can be based on nonlinear functions or be hard coded. That manifold is compared to the human one, arguing that a large overlap results in an anthropomorphic hand design. To make the comparison feasible, both manifolds are projected to a common two dimensional space where such a comparison is possible.

The proposed overlap metric solely looks for the similarity in the fingertip postures, not for functional requirements. Consequently, a hand with hand shapes similar to the human will be given a high score. It could be that the fingers never touch each other, what actually is important for some grasps. Still, it is a prerequisite for anthropomorphic hand function that the fingertip postures are similar. At the current state, the results from the tested hands look promising and follow the intuition of the author. Yet, those results have not been tested in reality to confirm the results. Additionally, the measure only processes snapshots of grasp postures, without processing time and dynamics of a grasp. In order to grasp properly, not only the final grasp posture is important, but also the opening and closing of the hand. At the moment a large score does not guarantee proper grasp trajectories. One possible way to overcome this limitation is to add a layer that processes the open-close trajectories of an artificial hand. If those are parallel to the human grasp trajectories the score should be higher than in the case of perpendicular trajectories.

In the current implementation, all digits have the same importance, irrespective of the fingers involved in a specific grasp. If a finger is not involved in one grasp, it can be arbitrarily positioned without affecting the quality of the grasp. One example is the "adduction grasp", where an object is put between the index and middle finger. Some subjects closed the remaining fingers, whereas others extended them. That results in a large difference in the grasp dataset, even if the grasps are very similar from a functional perspective. At the moment that problem persists within the system. Therefore it might be beneficial to add a layer that processes the information on which fingers are in contact with the object. Such a layer could define which fingers are of relevance for specific grasps and exclude others. Additional work is needed in order to find a feasible solution for this

question. Another way would be to restrict the grasping dataset to grasps which employ all five fingers, but that excludes many grasp types.

As the method only depends on kinematic hand models, it is very simple to modify the hand and calculate the overlap of the new hand. That allows for a fast iteration over new hand designs, thus accelerating the design process. Otherwise one would have to realize hand prototypes, which is time consuming and expensive. To create a fully actuated hand prototype, which is important for testing, one has to implement all mechanical structures. With the proposed method, the decision on actuation is independent of the decision of the kinematics. Otherwise, the design process might be guided too much by the choice on the actuation and not by the functional requirements of the hand. Consequently, a superior kinematic design might not be taken into account, as it is assumed to be too difficult to build.

The method is very general and not restricted to grasping. In principle, the hands are contrasted against the training set which the latent space is based on. The goal of this thesis is to develop the method itself and to create hands that are general purpose grippers. Therefore, a dataset consisting of a large variety of one handed static grasp types of the human is used. That is only a sub set of all possible movements. Other movements are intrinsic manipulation, two handed manipulation, gestures and many more. If, for example, the focus of a new hand model is not to grasp but to be able to perform the sign language, a different training set is needed. In that case the dataset would have to consist of such hand movements. A hand which is able to cover a large proportion of the hand signs will most likely have a different kinematic structure than a hand suitable for grasping. It covers different aspects of the human hand capabilities.

Chapter 5

Optimizing Kinematic Hand Setups

The previous Chapter presented the method to evaluate the level of anthropomorphism of artificial hands and results on existing prosthetic and robotic hands. In this Chapter the idea is pushed further and new hand models are developed. The goal of those hands is to maximize the overlap, while keeping the mechanical complexity and the number of DoF small. To achieve the goal of increased overlap, different approaches are used. In the first step, kinematic parameters of selected hand models are varied in order to maximize O_{rel}. Further, new design elements and DoF are introduced. The impact of those on the overlap is determined. Finally, those two approaches are integrated, resulting in hand designs that to some extend outperform the previous designs.

This Chapter is structured as follows. In Section 5.1 a sensitivity study is conducted to gain knowledge on the behavior of kinematic parameters. The next step, as presented in Section 5.2, is to optimize design elements with respect to the overlap measure. In Section 5.3 the results are merged, resulting in new hand designs that even exceed the optimized ones. Finally, in Section 5.4 the overlap measure and the new hand models will be discussed.

5.1 Sensitivity Study

For the optimization one has to select a set of parameters that are subject to optimization. The selection of correct parameters is crucial, as otherwise the increase in the overlap will not be as large as it could potentially be. Up to this point there is no knowledge on how design parameters (segment lengths, joint orientations and positions, etc.) influence the overlap. Therefore this sensitivity study is conducted – the goal is to determine which parameters have a large influence on the overlap. Such parameters yield the biggest potential when being optimized. In principle it would be possible to optimize all parameters simultaneously, but that would lead to a very complex optimization problem that is not

the focus of the thesis. Additionally, such an optimization changes the complete appearance of a hand. Specific design choices might introduce constraints on the hand that allow only a variation of certain parameters.

The hand model is defined by a set of kinematic parameters, where $\mathbf{w} \in \mathbb{R}^K$ corresponds to the unchanged parameters of the hand. To calculate the sensitivity of a single kinematic parameter of such a hand model, the following procedure is performed.

The overlap O_{rel} for a defined parameter variation is calculated. The difference between two neighboring values is determined and averaged over all samples. Thus, the sensitivity S_k of the k-th parameter is calculated as

$$S_k = \frac{1}{12} \sum_{i=1}^{12} |O_{rel}(\mathbf{w} + \mathbf{v}_{k,i+1}) - O_{rel}(\mathbf{w} + \mathbf{v}_{k,i})| \tag{5.1}$$

The kinematic parameters $\mathbf{w}$ contain a mixture of variables that define a position and a rotation. Therefore a differentiation between positions and rotations is necessary. It has to be determined if this parameter is of rotational (flexion offset of joint, rotation of the finger base) or translational (segment length, position of the finger base) type. Depending on the case, $\mathbf{v}_{k,i}$ has different values:

$$\mathbf{v}_{k,i} = \mathbf{e}_k \cdot \begin{cases} \mathbf{v}_{pos,i} & \text{positional parameter} \\ \mathbf{v}_{rot,i} & \text{rotational parameter} \end{cases} \tag{5.2}$$

The steps in the variation of $v_{k,i}$ are chosen to be 1/100 of a characteristic value. For positions that is 20 cm, which is roughly the size of the hand and for rotations that is 90 degrees which corresponds to the average joint range of motion. If the k-th kinematic parameter is of translational type, then the following parameter set is used: $\mathbf{v}_{pos} = (-1.2, -1, \ldots, 1.2)^T \in \mathbb{R}^{13}$. If the k-th kinematic parameter is of rotational type (flexion offset of the DH parameter, base rotation), then a different parameter set is used: $\mathbf{v}_{rot} = (-5.4, -4.5, \ldots, 5.4)^T \in \mathbb{R}^{13}$. Positions are measured in cm, whereas rotations are measured in degrees.

The following parameters of the hand models are analyzed.

- Rotation about $\{x, y, z\}$ of the finger base
- $\{x, y, z\}$ translation of the finger base
- The Denavit Hartenberg parameters $\{\alpha, a, \theta_0 + \theta, d\}$ of the links, where θ_0 defines the offset of the joint.

A typical curve of the overlap as function of some parameter values $\mathbf{v}_{pos}$ and $\mathbf{v}_{rot}$ is presented in Figure 5.1. It can be observed that the different parameter variations show

different trends in their coverage O_{rel}. Some parameters do not influence the overlap, whereas others have large potential to influence the overlap.

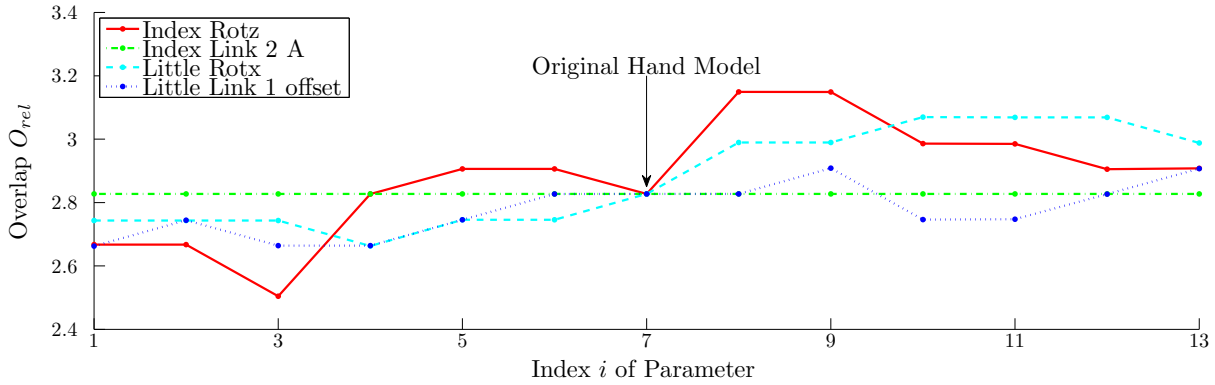

Figure 5.1: Influence of some randomly picked design parameters on the overlap. Depending on the parameter, the overlap behaves different. For some it is constant throughout the variation, whereas for others the overlap changes substantially. At $i = 7$ the parameter variation is zero, thus this is the overlap of the unchanged Hand. In that case the parameters belong to the Michelangelo hand and the legend indicates which parameters were subject to variation.

The sensitivity study is conducted for the three hands presented in Section 4.4.

5.1.1 SensorHand

The overall coverage of the SensorHand is low, as it covers only a small area. Therefore the parameters $\mathbf{v}_{pos}$ and $\mathbf{v}_{rot}$ had to be doubled, in order to see a significant influence on the overlap. The sensitivity analysis with those parameters is presented in Figure 5.2. The values for link 3 of the thumb are white as this digit only has two joints. Due to the small coverage there are only a few parameters that show differences and those are very small when compared to other hands. The most prominent parameter is the z-rotation of the thumb. How this parameter influences the thumb orientation is presented in Figure 5.3. The rotation follows the intuition on how the thumb could be rotated in order to increase the anthropomorphism. The original orientation of the thumb is not human-like as it perfectly opposes the index finger with a joint axis parallel to the index finger axis. The other parameters that have nonzero sensitivity are values that change the index finger rotation about the x-axis and values that influence the index finger flexion.

5.1.2 Michelangelo

The next analysis is conducted for the Michelangelo hand and the results on that hand are presented in Figure 5.4. Overall, the plot does not show individual parameters that

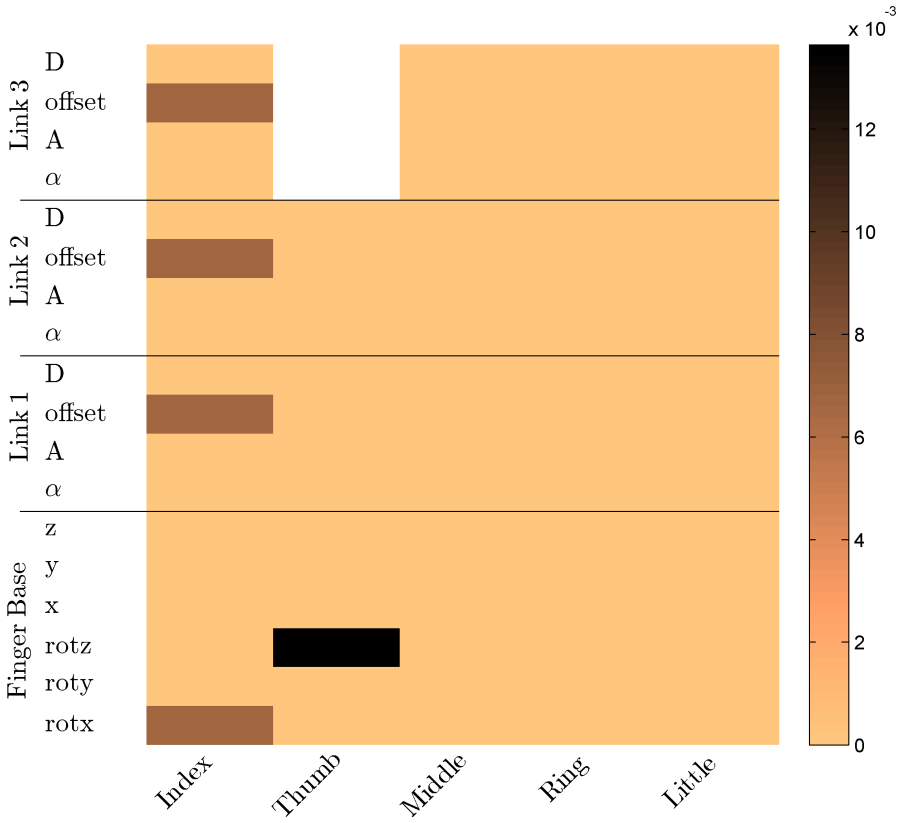

Figure 5.2: Sensitivity values for the SensorHand. Black indicates a high sensitivity value, whereas a lighter color represents the opposite. The field for link 3 of the thumb is missing as the thumb is modeled as a two link chain.

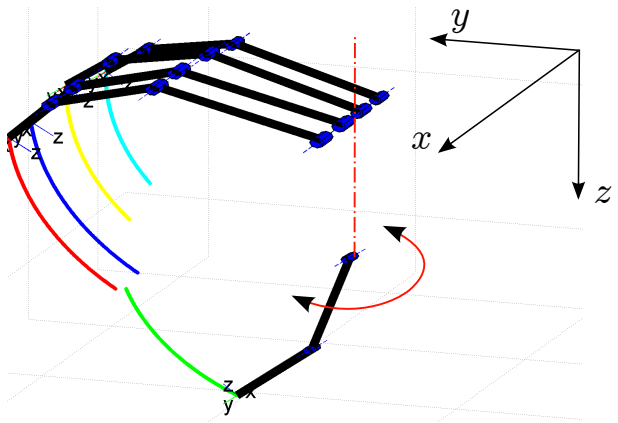

Figure 5.3: Variation of the z-rotation of the thumb base. The arrow indicates the rotation, whereas the dashed-dotted line represents the rotation axis, which is parallel to the z-axis.

are outstanding. Many parameters, distributed over various fingers and joints show high values. Compared to the SensorHand, the coverage is much larger. Therefore a small difference in the hand kinematics will result in a different latent space signature. Even a subtle difference can result in a change of the number of boxes that are filled by one design. That is significantly different to the SensorHand, where the unaltered hand only covers three boxes. In that case the difference in grasp kinematics has to be quite substantial to influence the overlap O_{rel}.

To further analyze the results, the mean sensitivity per finger is calculated and presented in Figure 5.5. The fingers with the largest influence on the overlap are the index and the thumb, followed by the little and the ring finger. The middle finger is the finger with the least impact. It shows which fingers one should focus on to in order to increase the capabilities of the hand.

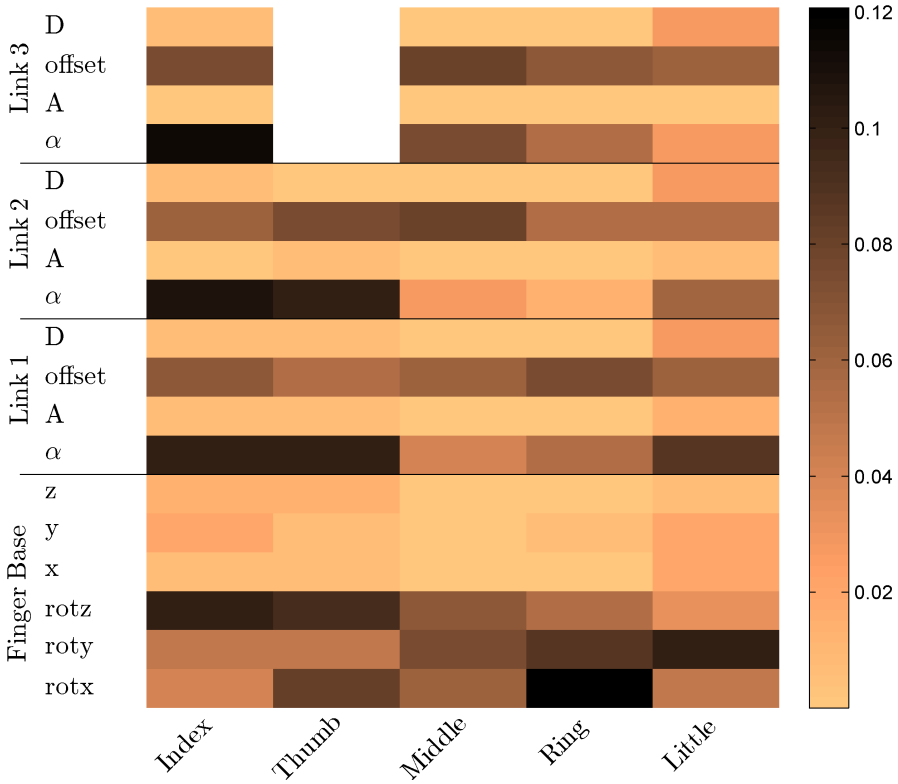

Figure 5.4: Sensitivity values of Michelangelo. Black indicates a high sensitivity value, whereas a lighter color represents the opposite. The third link of the thumb is missing as it is modeled as a two link structure.

5.1.3 FR-H 4 Hand

To be able to calculate the coverage of the FRH-4 hand, the number of samples taken from the eight dimensional joint pace are reduced to three as otherwise the calculation

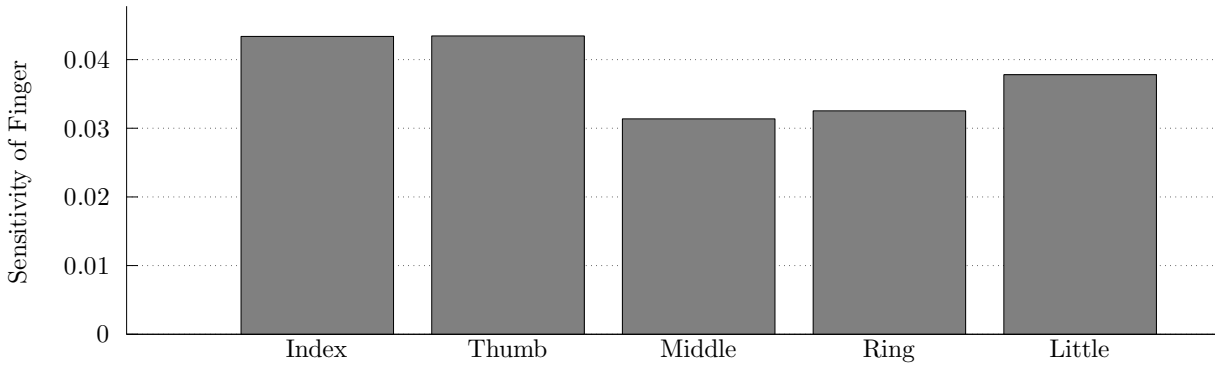

Figure 5.5: Mean Sensitivity per Finger of the Michelangelo hand

time would be prohibitively long. Consequently the joint space is sampled by $3^8 = 6561$ points. The result is presented in Figure 5.6. The plot shows that the parameters of the thumb have the largest sensitivity values. Similar to the SensorHand, the thumb is very different to the human as its joint axes are perfectly anti-parallel. Additionally, the flexion of the index and middle finger show a large sensibility. That can be achieved either by rotating the base orientation (x-rotation) or through a offset in the finger joints. As the joint axes are perfectly aligned to the coordinate axes the effect on the fingertip orientation is equivalent.

5.1.4 Discussion

The sensitivity study is the starting point for the optimizations that follow. It gives an idea on parameters that should be optimized in order to achieve the largest increase of the coverage.

The most important result is that parameters that influence positional variables (segment length, DH parameters A and D) have a low sensitivity value and therefore no large influence on the overlap. On the contrary, rotational variables (orientation of the finger base, DH parameters α and offset) show a much higher influence on the overlap. A reason to this discrepancy might be that the positions are affected by different hand sizes and that influence was not eliminated completely by scaling. The overall variation in the positions might be larger and this increases the variance in those dimensions. Consequently, the projection in these directions are less sensitive and therefore changing such a parameter does not affect the coverage by much. The result is important as this indicates that the optimization of hands should focus on parameters that are connected to orientations as only they have a large impact on the overlap.

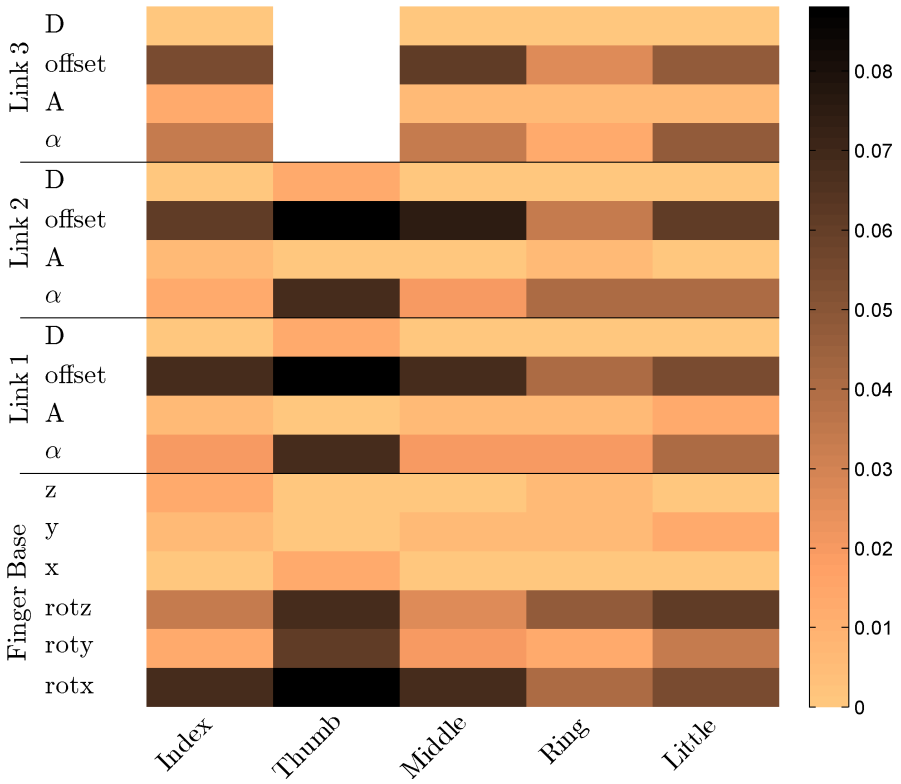

Figure 5.6: Sensitivity values of the FR-H 4 Hand. Black indicates a high sensitivity value, whereas a lighter color represents the opposite. The field for link 3 of the thumb is missing as the thumb has only two joints

5.2 Optimization of Kinematic Parameters

Within this section kinematic parameters of hands will be optimized. As it is impossible to optimize all kinematic parameters of a hand simultaneously, a good initial value for the optimization is needed. The SensorHand and Michelangelo hand will serve as starting point, where various parameters are optimized with respect to the overlap measure. The focus is on the Michelangelo hand as it offers the best initial value. The overlap is already high, but the hand is still simple as it only has two DoF.

To optimize a given kinematic hand setup, a function $f_{hand} : \mathbb{R}^K \rightarrow \mathbb{R}$ is created. The input parameter is $\mathbf{w} \in \mathbb{R}^K$, where K is the number of parameters to be optimized. The function returns the overlap O_{rel}. In order to calculate O_{rel}, the function creates a hand model that is based on the models presented in Section 4.4. A variation of the hand is created which is governed by the input parameters. The next step is to calculate the fingertip poses and finally to calculate the overlap, which is returned by the function. That can be formulated as

$$O_{rel} = f_{hand}(\mathbf{w}). \tag{5.3}$$

The function f_{hand} has to be adapted for each optimization, to incorporate the correct model and to modify the correct kinematic parameters. Consequently, the parameter set which maximizes the coverage O_{rel} is sought.

$$\{\mathbf{w}_{max}\} = \text{argmax}_{\mathbf{w}} f_{hand}(\mathbf{w}) \tag{5.4}$$

Due to the boxcounting, as described in Section 4.2, method O_{rel} varies non-smoothly. Gradient based optimization techniques cannot be used as they will get stuck on such a plateau. To overcome this problem a probabilistic approach is used – simulated annealing [114] is applied to find an optimal solution. The simulated annealing function provided by Matlab is used. Each optimization is run 10 times in order to determine the distribution of the results. If not terminated earlier by the quality criterion, the optimization was terminated at 4000 iterations. Test runs have shown that an increase in the number of iterations does not produce significantly better results. Usually, the algorithm terminates at the maximal number of iterations.

An overview of all hand models created, analyzed and optimized in this thesis is given in Figure 5.7. Roughly, the figure reads from top to bottom - the first step is to project existing hands and determine their overlap. That is done in the first row. The next step is to virtually assign more DoF to the hand, as done in the second line. Of particular interest is the Michelangelo 2D hand, as this determines the mechanical capabilities of the hand. The 1D hand is trajectory controlled - various trajectories in the 2D space

are hard coded to allow a one dimensional control of the hand. As the focus is onto the mechanical limitations of the system, the 2D hand is of larger relevance and will serve as the starting point for improvements of the Michelangelo hand. All those steps are presented previously, in Section 4.4.

Based on those hands, some kinematic parameters are optimized to generate even better hand models. Those are located in the next line and labeled red. The first optimization is to change the thumb of the SensorHand. This is the most most un-anthropomorphic feature of the hand and the sensitivity study also reveals the largest potential for the thumb. A substantial increase is archived, without affecting the dimensionality of the control space. The next step is a large scale optimization of 42 parameters of a human hand model. That proves to be difficult terrain, without a consistency between the 10 optimizations. Finally, the Michelangelo hand serves as the best initial value available and most of the improved hand models are based on it.

Marked blue, the Michelangelo hand is further adapted by introducing new design elements. That is done without optimization, as that proved to be a very time consuming process. By combination of the results a significant improve in the overlap can be achieved. The best result is obtained with a five dimensional adaption of the Michelangelo hand, which covers 27 % of the latent space. Given that the training set itself has a coverage of 54.5 %, that is a major achievement.

5.2.1 SensorHand Thumb

The first optimization concerns the thumb of the SensorHand (Section 2.3.1). The sensitivity study, as well as the intuition by the author indicate that the thumb is the most un-anthropomorphic feature of this hand. Therefore optimizing parameters that influence the thumb are assumed to have the highest potential to increase the score of the hand.

The first approach is to optimize the position, orientation and scaling factor of the thumb. Position and orientation define the pose of the thumb base in space, whereas the scaling factor influences the length of the segments. The initial values are the values defined by the real SensorHand. For the rotation the limits are set at $\pm\pi$ added to the initial value. The limits for the positions are different for each dimension, as in certain directions more variation is meaningful. The scaling factor is set to be between 0 and 2. Overall the limits are set broadly – allowing for a large degree of variation. The optimization is run 10 times, and the distribution of the results can be seen in Figure 5.8. The color code presents the overlap of the individual result, whereas on the left four hands corresponding to one parameter set are shown. The results have an overlap around 1.1 %, a significant increase to the original hand with 0.24 %. On first sight, the distribution of the results show a major variation. On a closer look, two different regions can be identified.

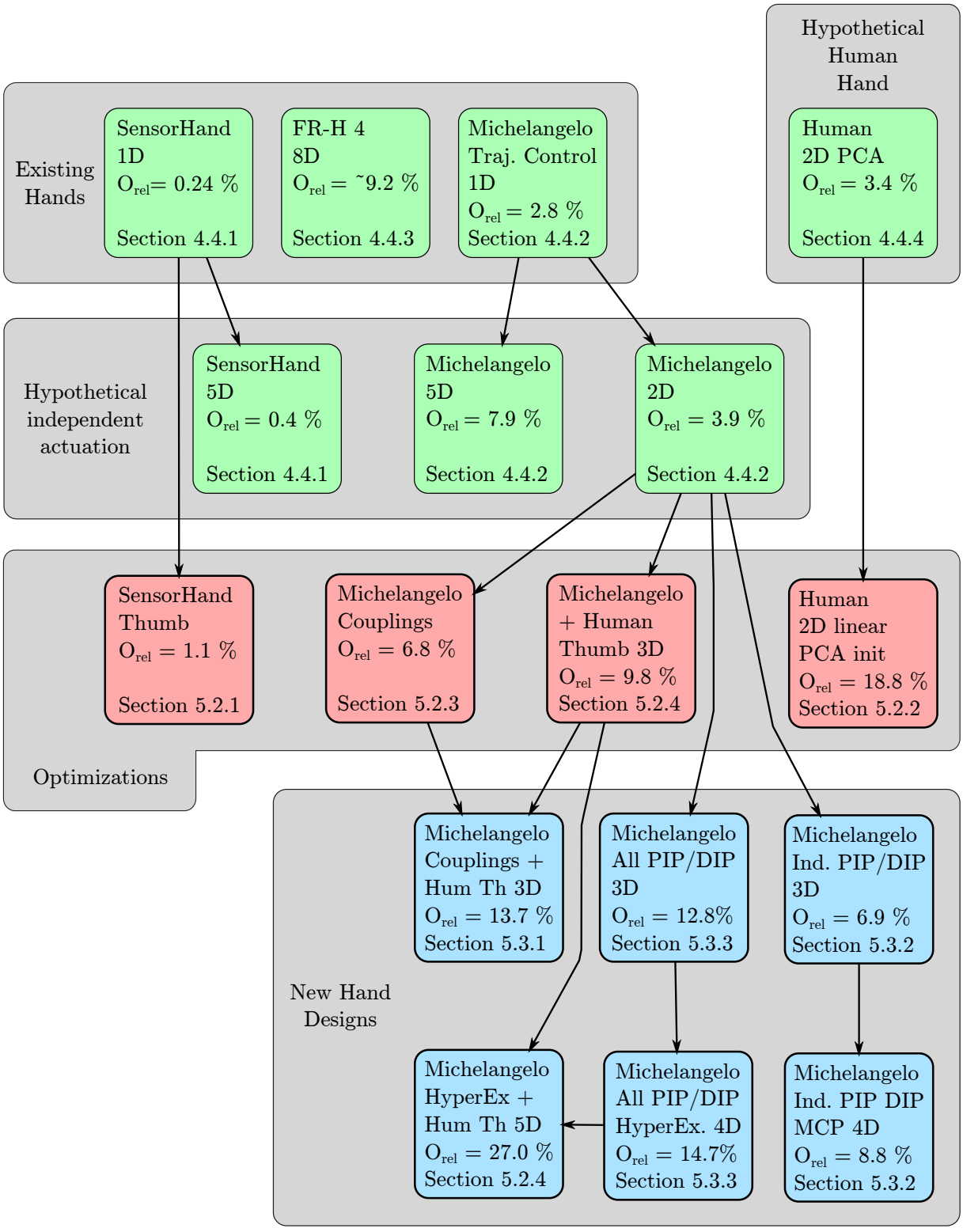

Figure 5.7: Overview of the tested hands. The green background represents results that are not subject to optimization and are therefore described in the previous Chapter. Hands with red background are subject to optimization. Blue indicates new hand designs, derived without optimization. The connections indicate which hand was altered in order to create the new hand design.

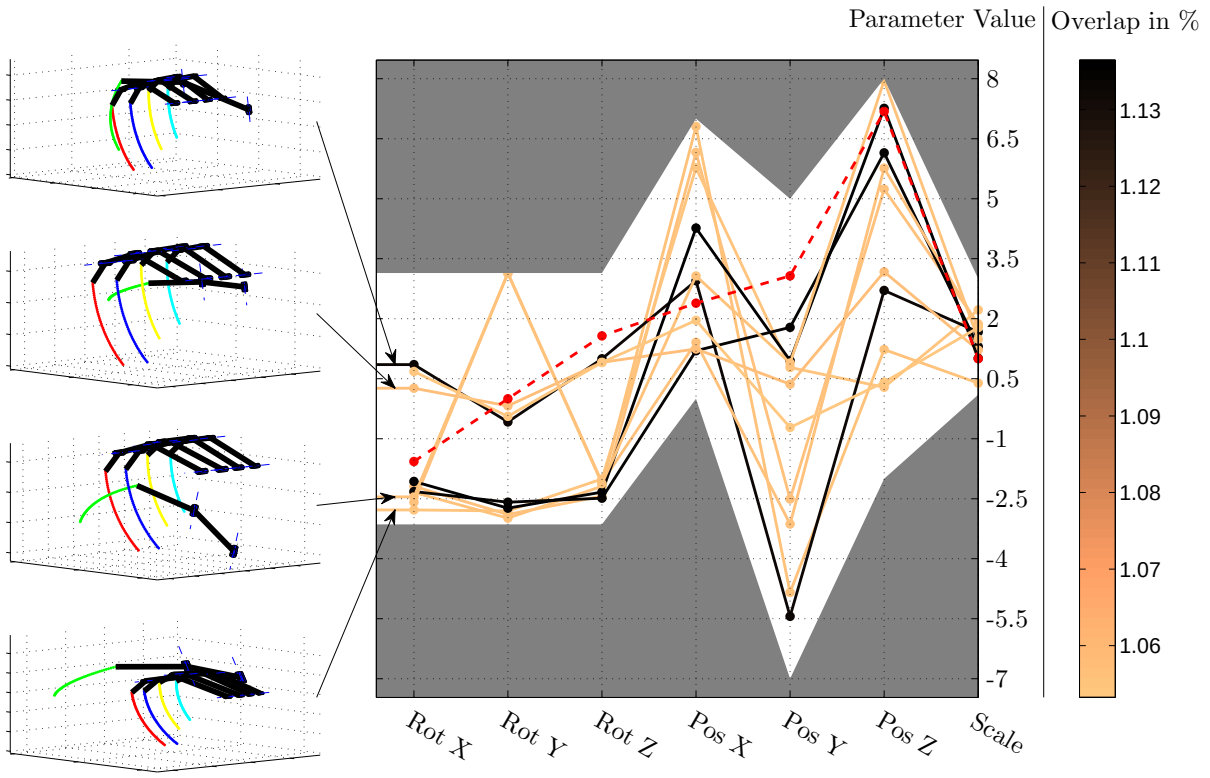

Figure 5.8: Results of the Thumb base optimization for the SensorHand. The first three parameters are the rotations, the next three the positions and the last is the size. The grey area represents the limits set for the parameters. The red dashed line shows the initial values. The color code of the results expresses the overlap O_{rel}, which varies from around 1.1 %, a substantial improvement to the original coverage of 0.24 %. The unit of the rotations is radiant, whereas the positions are measured in cm.

The results of the rotations are quite consistent, basically falling into two parameter sets. Only one result does not fall into one of those. In contrast, the positions and the scaling vary to a large degree. The results are distributed over the complete range, not being restricted to certain parameter combinations.

Due to the problems reported in the first optimization run, a second optimization is conducted. The optimization is restricted to the three rotational parameters. The limits are the same as previously and the optimization is run 10 times. The result of this optimization is presented in Figure 5.9. Similar to the previous run, two parameter sets are possible. One is about {36,0,40}°and the other is ca. {-144,-144,-144}°. Those are also the same results as reported in the first optimization run. Again, the images on the left show four hands that correspond to four parameter sets. The top hand corresponds to the "upper" solution, whereas the three hands below correspond to the "lower" solution. Even though the parameters are very different, the orientation of the thumb looks similar. That is possible as the description with three rotational angles is not unique. To further assess the difference between the solutions, the angle between two such orientations is calculated. Similar to Section 4.3.5 the difference between two quaternions is calculated via the dot product. The results reveal that the orientations are consistent within a small range. The maximal angular difference between two solutions is 21 degrees, with an average difference of about 10 degrees.

The results of the two optimization runs fit well to the sensitivity analysis. It also supports the assumption, that in the current implementation the system is only sensible to orientations. That statement is based on two facts. First, the results of the orientations are much more consistent when compared to the positions. If the overlap is not influenced by the positions, one can basically pick all parameter values without a penalty from the overlap. Second, the overlap values are the same in both optimizations. In the two cases the best overlap is about 1.13 %. If the positions influence O_{rel}, then the first optimization should have a larger value.

Overall, the optimization results in a significant improvement to the overlap. From the unchanged SensorHand with 0.24 %, the optimization was able to raise the level up to about 1.1 %. That is an improvement of more than four times without affecting the dimensionality of the hand!

5.2.2 Linear Human Hand Model

The previous result on the SensorHand shows that in a simple case, where only a few parameters are optimized, the optimization works as intended. It delivers meaningful and consistent results. Therefore the next step is to go full scale and optimize many parameters simultaneously. The directional goal is to optimize most kinematic parameters of a hand

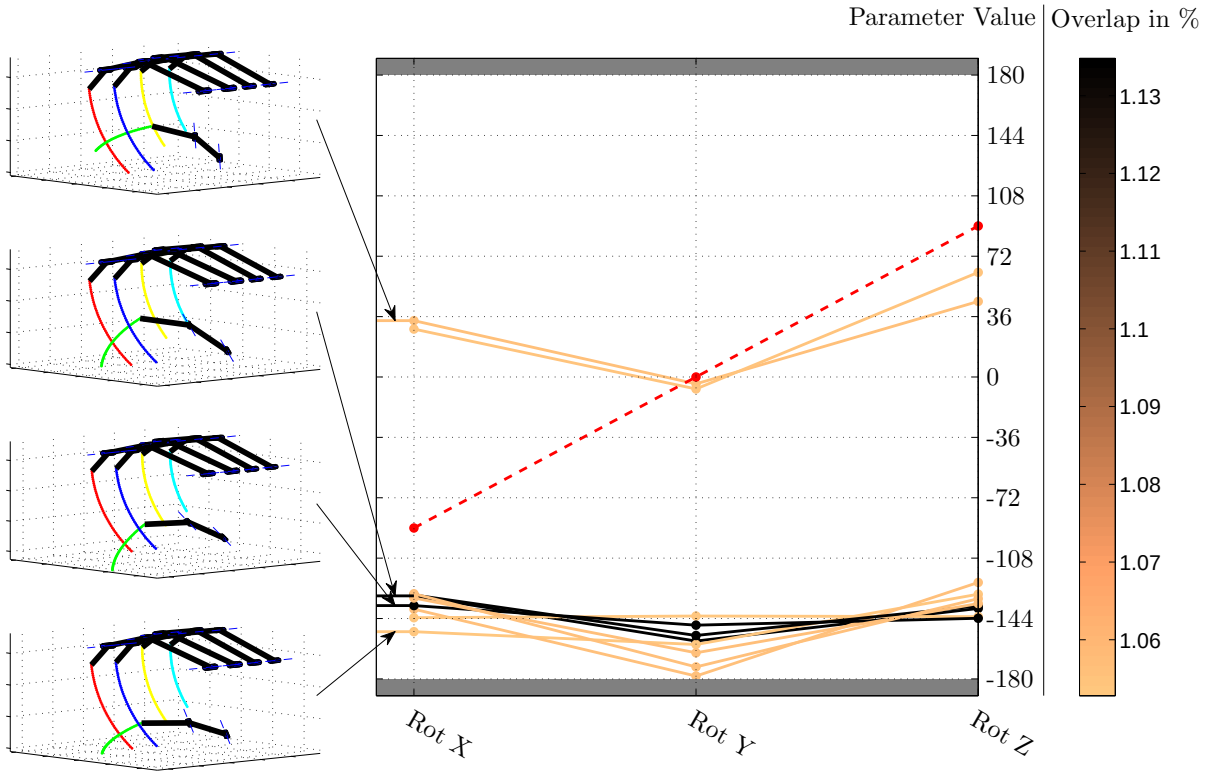

Figure 5.9: Results of the orientation optimization of the SensorHand thumb. The grey area represents the limits set for the parameters which are set to ± 180 degrees. The red dashed line shows the initial values. The color code of the results expresses the coverage, which varies from 1.06 % to 1.13 %, a substantial improvement to the original coverage of 0.24 %. On the left some hands are presented as corresponding to a parameter set.

model to determine an optimal model without much input from the user. Finally that would deliver a hand that maximizes the overlap measure, without being influenced by human choices on how such a hand should look like.

A human hand model is created, which is based on the model presented in Section 4.4.4. The feasible hand configurations are defined by a linear combination of the first two PCs. Finally the first two PC are varied in order to maximize the overlap. The Principal Component of the model will act as the initial values. The upper and lower limit is ± 0.2 added to the initial value. As the hand has 21 dimensions, each PC consists of 21 values. Thus the optimization problem consists of an optimization of $2 \cdot 21 = 42$ parameters. In that case the orthogonality is rejected, not requiring the two basis vectors to be orthogonal. Otherwise that constraint would reduce the number of parameters by one.

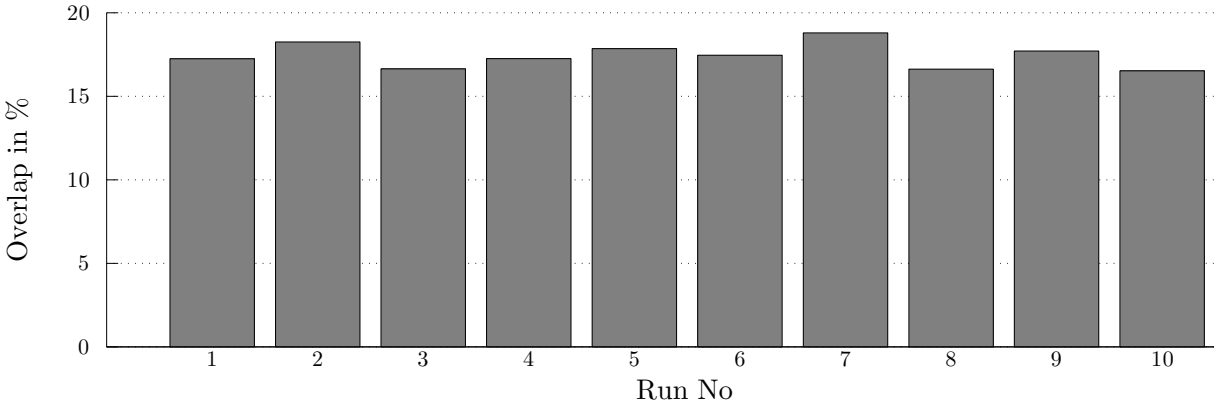

Figure 5.10: Coverages of the 10 runs of the 2D human hand model

The achieved overlaps can be seen in Figure 5.10, which shows that the overlap is around 17 %, with a maximum of 18.8 %. Compared to the variation of the SensorHand, these results vary to a larger degree, overall with an amplitude of 2.3 %. To further assess this, Figure 5.11 shows the PCs. Within that figure some values are consistent, but there is no real consensus between the solutions. Hands which belong to four of such parameter sets are presented in Figure 5.12. All fingertip workspaces look different, some of them cannot be regarded as being anthropomorphic.

The overlap of the PCA controlled hand is 3.4 %. The results archive overlaps of up to 18.8 %, a substantial improvement compared to the original hand. That can be due to two reasons. First, the PCs are based on a different dataset compared to the overlap measure. Even tough the first two components seem to be quite consistent throughout (see Section 2.5.1) publications, a variation is possible. Second, this is also a way to show the difference between those two dimensionality reduction algorithms. GP-LVM, being a nonlinear method, will deliver different results as compared to PCA. The directions

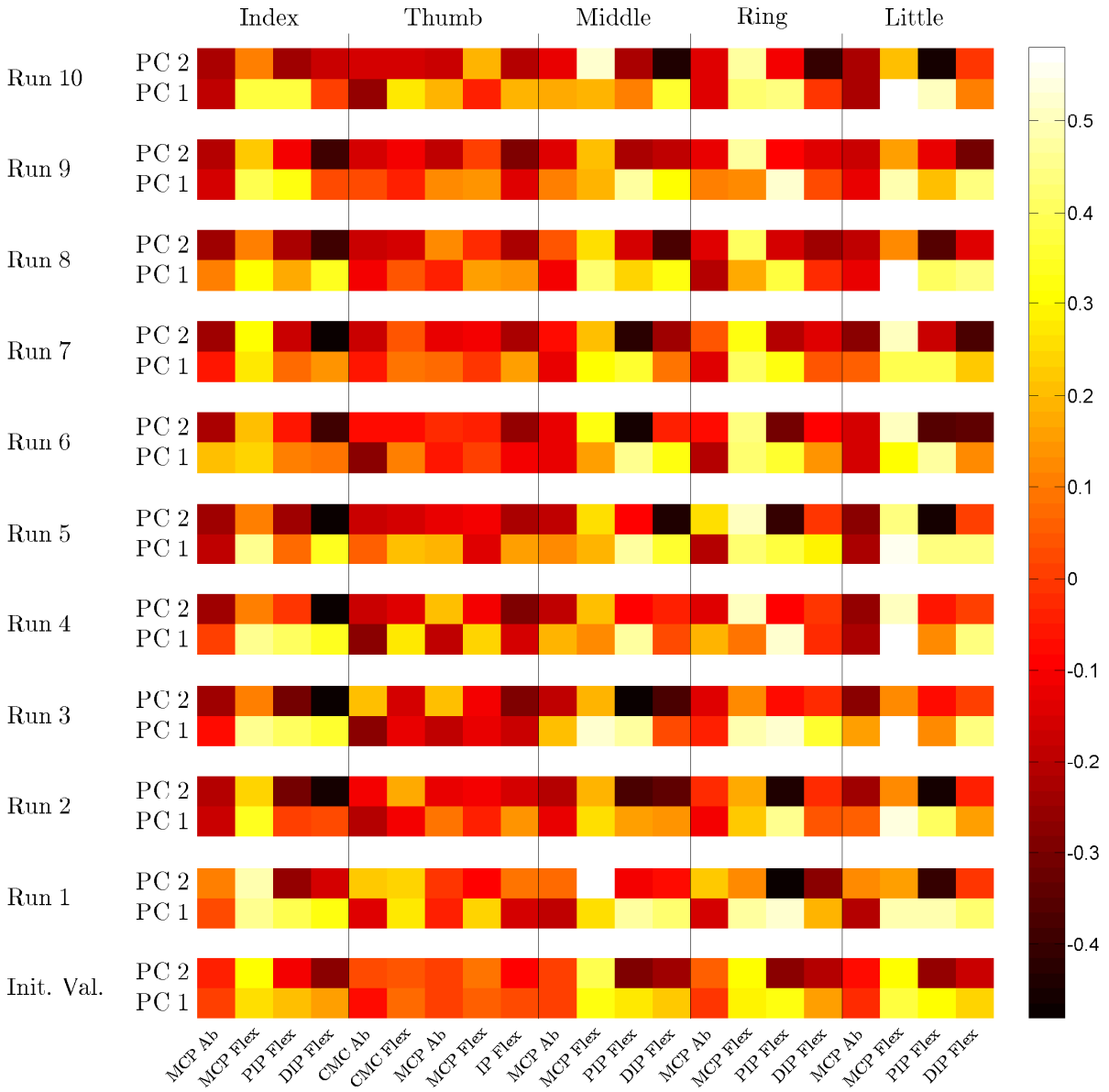

Figure 5.11: Visualization of the 10 optimizations of the hand controlled via two PCs. Each run optimizes 42 parameters, which correspond to the first two principal components of the 21 DoF hand. The colors indicate the values for the components.

defined by PCA do not correspond to the directions that maximize the overlap. That difference is also highlighted in Section 4.4.5.

Additionally, the results show that the optimization falls into multiple local minima, each of them with a different actuation pattern of the hand. That demonstrates that this optimization formulation is too unconstrained, not being able to deliver consistent, reasonable results. Consequently, a large scale approach cannot be done with the current implementation. Consequently, the next optimization should be simpler, optimizing only a handful of parameters simultaneously.

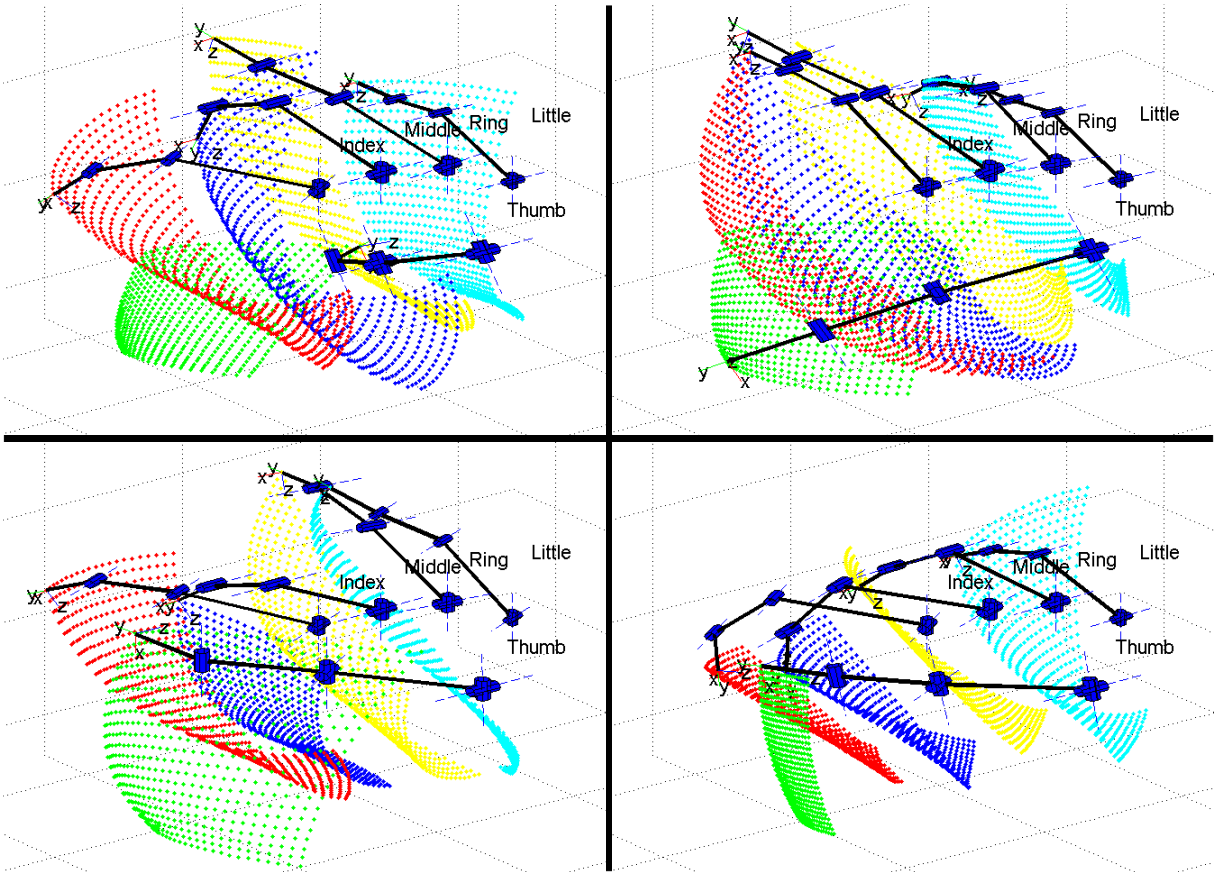

Figure 5.12: Four results of the linear hand model optimization. The points represent the fingertip locations the hand can reach, each color belongs to one finger.

5.2.3 Michelangelo Couplings

The optimization of the human hand model in the previous Section reveals that it is impossible to optimize many kinematic parameters simultaneously, with the current implementation of the system. Therefore finding an optimal hand with only a few iterations is not possible. The goal of the thesis is to find new hand models that have only a few actuators, but resemble the human hand more closely. That goal cannot be reached by large scale optimizations of many parameters, so a different approach has to be taken. A good initial hand model is needed, which new hand designs will be derived. Of the hands tested in Section 4.4, the Michelangelo hand is the most adequate. The Michelangelo 2D hand is employed, not using the restricted trajectory control. With its two actuators the hand is still easy to control, but the coverage is good with a value of 3.9 %. In order to improve the overlap measure, this hand model will be changed iteratively.

The first optimization that is based on the Michelangelo hand introduces articulated finger PIP and DIP joints. Per finger, those two interphalangeal joints are connected to the MCP joint, moving in a coordinated manner. Per finger, one coupling factor determines

the degree of co-articulation between the interphalangeal joints and the MCP joint. The coupling factor was limited to be in a $\{0 \dots 2\}$ range. A coupling factor of 0 corresponds to stiff fingers, whereas a factor of two relates to a finger where the flexion of the PIP and DIP joints are twice the value of the MCP joint. The factor of 0 is also taken as the initial value for the optimization as this is the value used in the original Michelangelo hand. Due to the different kinematic structure of the thumb it cannot be included into the optimization. Therefore four parameters, belonging to the four fingers, are subject to optimization. As presented in Section 4.4.2, that hand overlaps 3.9 % of the latent space. That value serves as benchmark for the optimization.

The result can be seen in Figure 5.13. The maximal coverage is 6.8 % which is a large increase. Except for one outlier, the results reveal two possible coupling configurations. One configuration is a progressive increase in the coupling factor. Such a coupling scheme results in a hand with the flexion of the fingers progressively increasing towards the little finger. The hand plot at the bottom left corresponds to such a hand. Thus the index finger is relatively stiff, with a coupling factor of about 0.4. The factor steadily increases towards the little finger, where it is about 2. The other configuration is a coupling factor of approx. 1 for all fingers. That means, that all interphalangeal joints are flexed in direct coordination with the MCP joints. Two such hand models are presented in the middle of Figure 5.13. As all fingers are flexed, such a hand is good for full hand power grasps, like the "Large Diameter", "Small Diameter" and "Medium Wrap". The other solution favors grasps like the "Tripod", where the thumb opposes only the index and possibly the middle finger.

5.2.4 Michelangelo with Human Thumb 3D

The goal of this optimization run is to replace the thumb with an improved version, where the orientation of the flexion and abduction axes resembles a more natural rotation. Therefore the thumb is replaced with a thumb that is inspired by the human hand model. This thumb has two DoF (flexion, abduction) at the CMC joint and one DoF (flexion) at the MCP and IP (flexion) joint. The fifth parameter (the abduction in the MCP joint of the hand model thumb), was not taken into account, as the goal was to keep the hand model as simple as possible. The idea beeing that by a proper orientation of the thumb base, most of the human thumb functionality can be attained.

The kinematic structure of this thumb is different to the original setup, therefore the flexion of the thumb cannot be linked to the main drive any more. Consequently, the thumb needs two joint values – flexion and abduction of the CMC joint. Combined with the parameter for the main drive, which defines the finger flexion, this creates a 3D hand model. The joint values of the main drive are sampled with 50 points. For the thumb

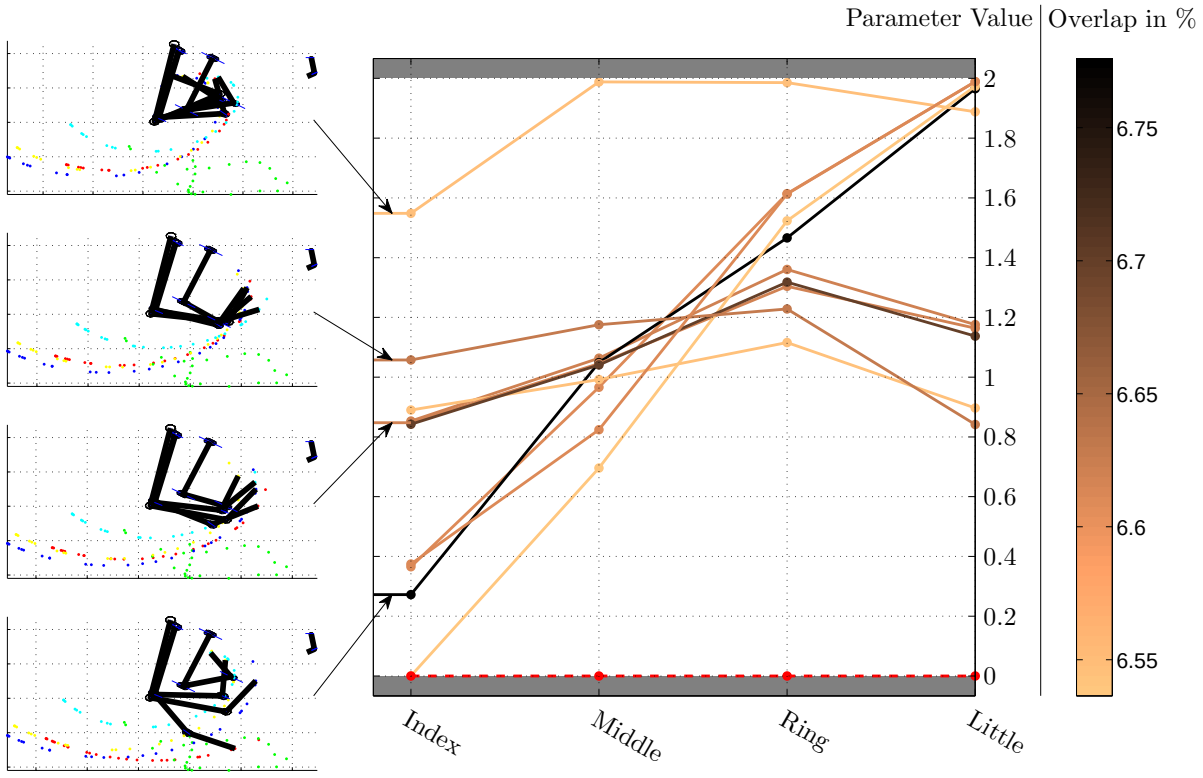

Figure 5.13: Results of the couplings parameter optimization of the Michelangelo hand. One parameter couples the PIP and DIP joint of one finger to its MCP joint. The lower bound and the initial value were set to 0 and the upper bound was set to 2. The maximal coverage is 6.8 % which is a large increase to the 3.9 % the hand has without couplings. The left hand plots show the hand models corresponding to the indicated parameter sets.

flexion 7 samples are taken from a $\{0 \dots 90\}$ degree range and for the thumb abduction 9 samples are taken from a $\{-15 \dots 25\}$ degree interval. The length of the thumb is determined by the parameters provided by [44]. Based on the index and middle finger length of the Michelangelo hand, a corresponding length of the thumb is calculated.

Similar to Section 5.2.1 the orientation of the thumb base is subject to optimization. The base can be rotated about x,y and z axis. In the initial position of the thumb the flexion axis is parallel to the y-axis and the thumb points outwards in a 45 degree angle relative to the palm plane. The limits for the base parameters are set to $-\frac{\pi}{2}$ and $\frac{\pi}{2}$. In addition to those three base rotation values, the shape of the stiff thumb is optimized. Those three parameters influence the flexion of the CMC, MCP and IP joint. The limits are 0 and 90 degrees.

The results are presented in Figure 5.14. Except one outlier, the results of the rotations are very consistent. The flexion values of the thumb are consistent as well, favoring a thumb that is relatively straight. The overlap is increased by a large degree, with a range of the overlap between 8.7 % and 9.8 %. The best result is shown in Figure 5.15.

The plots of the hands show a stunning behavior. Interestingly, the thumb is orientated very much outwards. In Figure 5.15(a) the thumb points to the right. At the presented position, the thumb is in maximal extension. That is unnaturally extended and the thumb even points above the x-y plane, which corresponds to the palm of the hand. In maximal flexion, which is indicated by the green points that correspond to the thumb fingertip locations, the thumb still is not touching the other fingers. The intuition is that in maximal flexion the trajectories of thumb and fingers should intersect. Why such a thumb orientation is selected cannot be determined. One explanation might be that in most grasps an object is held between the fingers and the thumb. Therefore there is a distance between those fingertips, which is also the case for this hand model.

On the contrary, the orientation of the CMC joint axes look very natural and correspond to the human intuition. They are similar to the position determined in the SensorHand thumb optimization in Figure 5.9. The angular difference between the best result of each optimization is 21 degrees. Given that the hand models are different and the optimization includes also other parameters, the difference is small. It seems that there is one optimal value for the orientation of the thumb CMC flexion axis.

5.3 Validation of Design Elements

The previous section presented how kinematic parameters of hand models can be optimized. The optimizations proved to be difficult and time consuming, therefore an alternative approach is taken in this Section. New design elements and DoF will be introduced, and their influence on the coverage is determined. This does not deliver the best possible parameter set, but determines the quality of the conceived design.

5.3.1 Michelangelo Couplings with Human Thumb 3D

In the Sections 5.2.3 and 5.2.4 two different parts of the Michelangelo hand were modified to increase the latent space overlap. The first optimization couples the PIP and DIP joints to the MCP joints. That adaption increases the latent space coverage from 3.9 % (the 2 dimensional Michelangelo) to 6.8 %. The second optimization replaces the thumb. A more human-like thumb is added, where the base rotation of the thumb and the zero flexion is subject to optimization. In that case the coverage increases from 3.9 % to 9.9 %. As both results optimized different parts of the hand, the results were composed creating a new hand model. The best results from both cases are taken, conferring a 3D hand model. The main drive flexes the fingers and two actuators control the thumb of the hand. Figure 5.16 shows the projection of the fingertip movements to the latent space. The result is that the hand is able to overlap 13.9 %, a large increase to the individual optimization

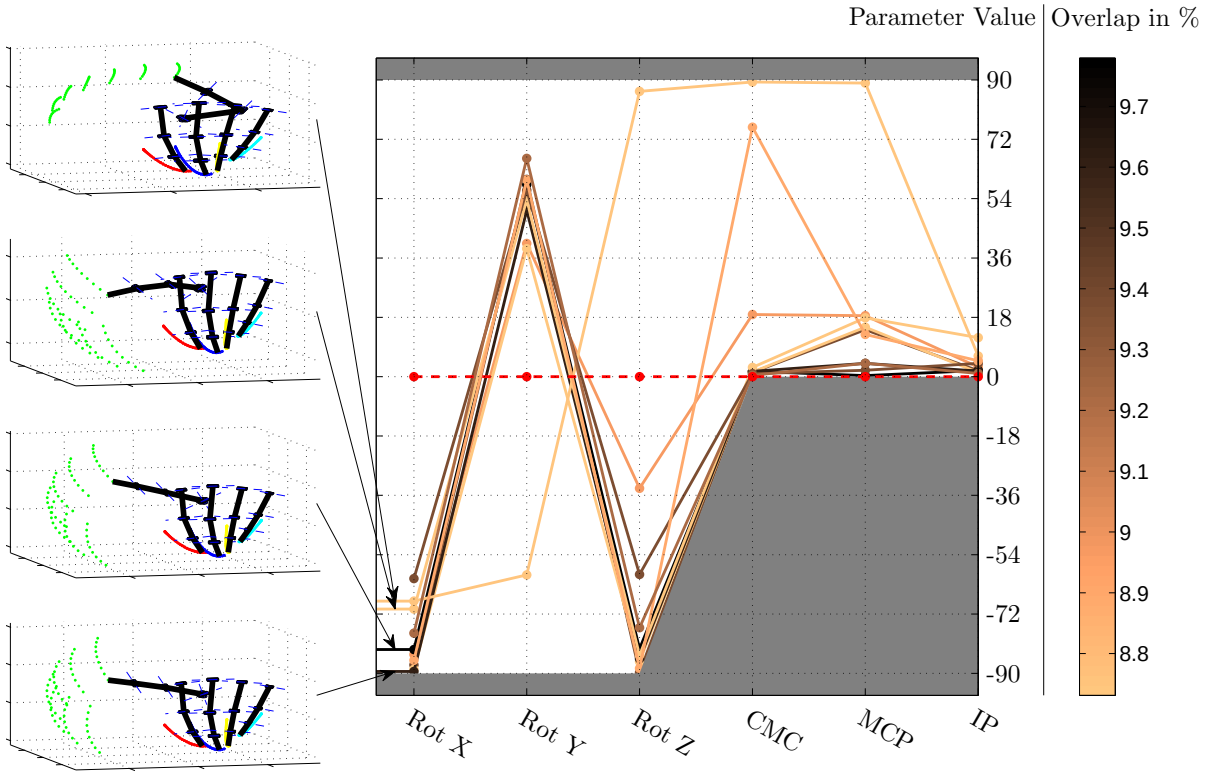

Figure 5.14: Optimization results of the Michelangelo hand with human thumb 3D. The base of the thumb was subject to optimization. The upper and lower bound for the parameters is indicated by the grey area. The initial value (red dashed line) was at zero degrees. The maximal coverage is 9.8 %. The left hand plots show the hand model corresponding to the indicated parameter sets.

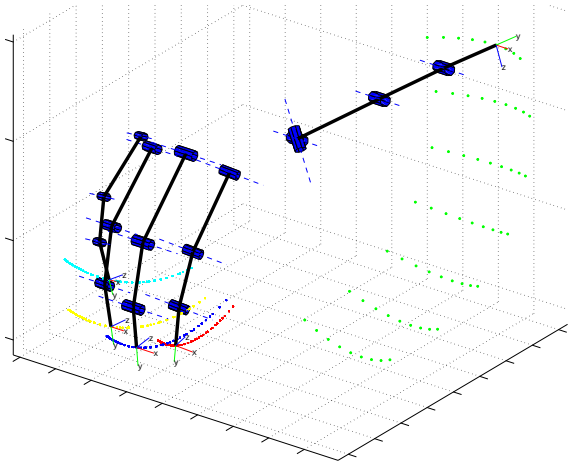

(a) 3D plot of the best result. The orientations of the thumb CMC flexion and abduction axes are human-like. On the contrary, the flexion values of the thumb are not anthropomorphic as the thumb is unnaturally extended.

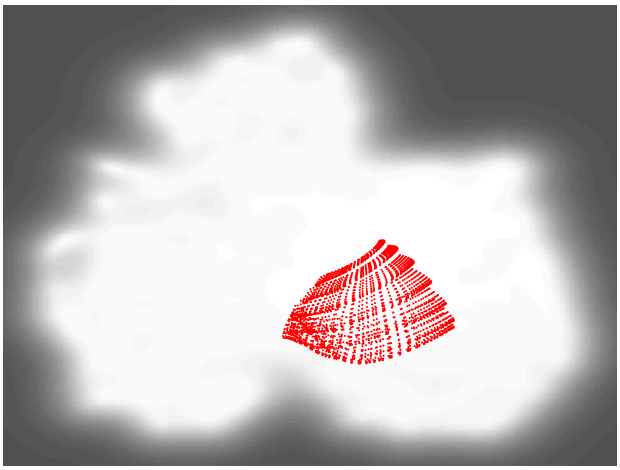

(b) Latent signature of the best result. The maximal overlap is 9.8 %.

Figure 5.15: Best Result of the Michelangelo hand with human thumb

results. The color code shows the different thumb abduction positions. It also shows that for each color most of the area is covered. This indicates that the abduction of the thumb does not contribute strongly to the overlap. With one thumb abduction position a larger proportion can be covered as well.

When Figure 5.15(b) and Figure 5.16 are compared, it becomes evident what the additional capability of finger flexion adds to the space. Without the ability to flex the fingers, the space to the left is not covered. The right side is similar for both cases. That corresponds well to the finding, that the further left the point is located in the latent space, the more the fingers are flexed. Still there is significant space to the left and right of the points, which corresponds to a more flexed and extended hand.

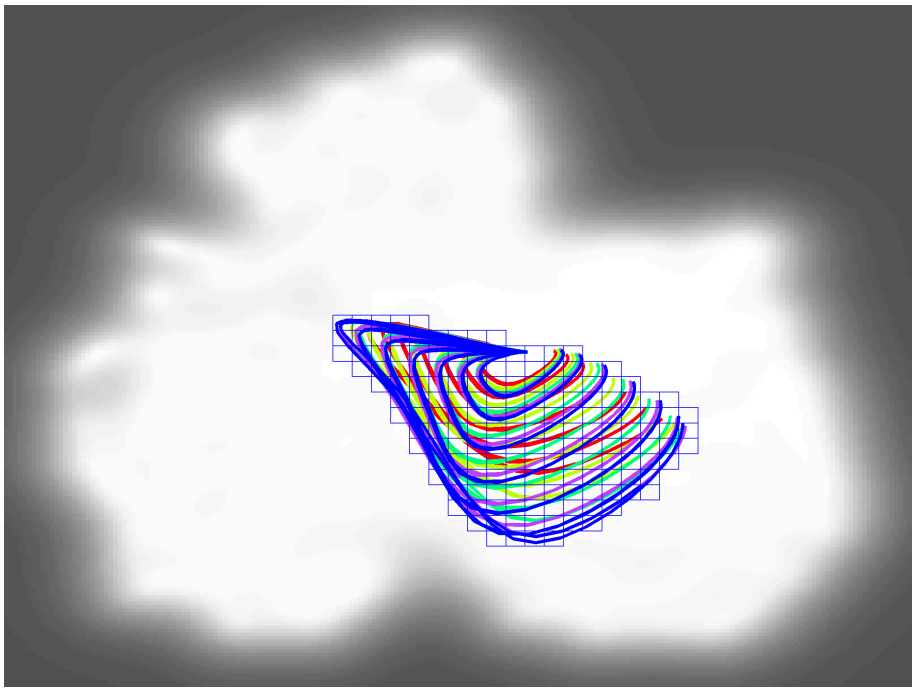

Figure 5.16: Latent space overlap of the Michelangelo Hand with PIP and DIP joints coupled to the MCP joint. Additionally the new two dimensional thumb is added to the hand model. The resulting coverage is 13.9 %.

5.3.2 Michelangelo with Independent Index

The hand feature which is the most demanded by prosthetic users is the ability to point with the index finger and to have individually controlled digits [5]. Therefore this Section analyzes how an independently controlled index finger influences the overlap. Such a finger allows to point and is at least one individuated digit.

The first approach is to replace the stiff finger of the Michelangelo hand with a finger that has one intrinsic DoF. As basis the two dimensional Michelangelo hand (Fig-

ure 4.12(b)) is taken. The additional motor drives the PIP and DIP joint of the index finger. The two joints are coupled 1:1 and the range of motion is between 0 and 90 degrees, conferring a three dimensional hand model. The projection of the hand movements is presented in Figure 5.17(a) and the corresponding overlap is 6.9 %. That is an increase of 3 % to the original hand. The colors in the figure represent the flexion values of the PIP/DIP joints. The red lines, which correspond to fully extended PIP/DIP joints, cover the largest area. With increasing flexion value, the covered area becomes smaller and moves closer to the random hand position. That is an indication that the most important additional feature is to be able to fully extend the finger, not to further flex it. The blue area corresponds to fully flexed joints and the size of the spot is small.

As an independent index might be important for grasping, the idea is pursued further and the coupling of the index MCP joint to the main drive is is removed. The index MCP joint is driven by an additional actuator. The range of motion is between 0 and 90 degrees. Combined with the independent PIP/DIP drive, this hand model is four dimensional. The projection is shown in Figure 5.17(b) and the overlap $O_{rel} = 8.8$ %. The colors in the figure correspond to the flexion values of the MCP joint.

Given that for both changes one additional actuator is introduced, the gain from the alterations is rather small. With three dimensions, other hands (eg. the one in Section 5.3.1) are able to overlap up to 13.9 % of the space. At first glance the view of the prosthetic users opposes the results who give an individual index finger a very high priority. Still, the overlap measure on such a hand is small. Here it is important to keep in mind that the coverage measure is based on the grasp taxonomy. Within that classification only one handed grasping movements are taken into consideration. For example pointing and pushing movements are not within the scope. For such movements an independent index might be of much value, but this is not tested here.

5.3.3 Michelangelo Underactuated Finger Joints

The designs in this section try to determine how underactuation of the finger joints can potentially increase the anthropomorphism of the Michelangelo 2D hand. Underactuation cannot be measured directly with the system, as it needs an an object that interacts with the hand. The objects resistant force is the reason why the finger wrap around the object and they stop moving when the object is touched. In the simulation there are no objects involved, consequently underactuation cannot be implemented directly. To estimate the capabilities of an underactuated hand a different approach is taken.

The goal is to determine the score of a hand with underactuated fingers. In specific, the movement of PIP/DIP are supposed to be coupled to the individual MCP joint. Depending on the object size, the fingers can be extended or flexed in the grasp position.

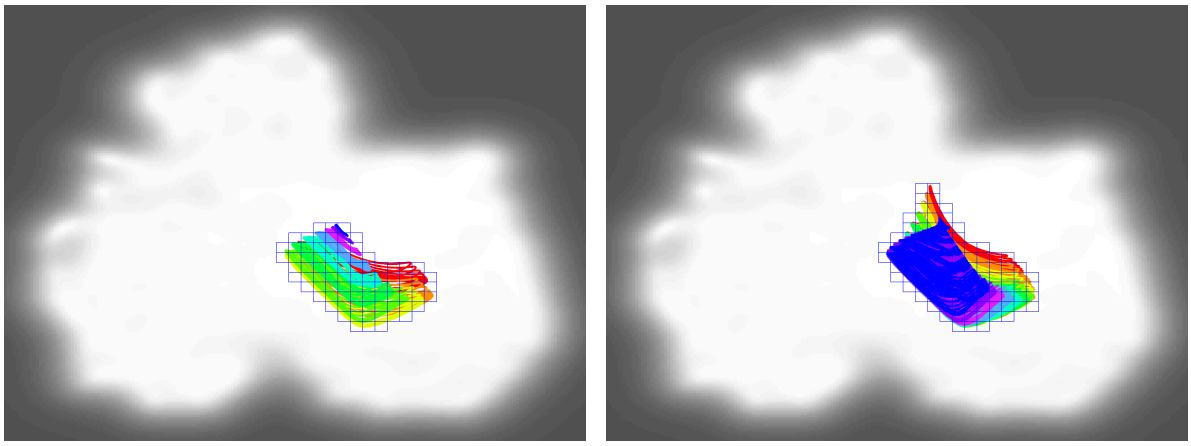

(a) Index finger of the Michelangelo hand replaced with an index finger that has one intrinsic DoF. It allows to flex the PIP and DIP joint in a coordinated manner. The corresponding overlap O_{rel} is 6.9 %. Red corresponds to a flexion value of 0, whereas blue indicates a PIP/DIP flexion of 90 degrees.

(b) Additionally to a) the MCP joint of the index finger is assumed to be actuated independently. Therefore this hand model has 4 DoF. The corresponding overlap O_{rel} is 8.8 %. Each color corresponds to one MCP value.

Figure 5.17: Hand models that assess the importance of an independent index finger.

To simulate that behavior an additional DoF is introduced which flexes the PIP/DIP joints in a coupled fashion. The joint value is the same for all eight joints and has a range from 0 to 90 degrees. In total, 4590 points are taken to sample the joint space. The corresponding projection is shown in Figure 5.18(a) and the overlap is 12.8 %. The points have a large left-right spread, being closer to the edges of the space. Therefore, compared to the other hand models, the overlap is relatively high. The only model exceeding the overlap value is the model with optimized finger couplings and thumb position from Section 5.3.1.

Depending on the flexion value, a different area is covered. Full extension corresponds to the red points on the right side, whereas full flexion is the blue area. The intermediate flexion values of about 30 - 40 degrees have the largest areas. The fingers of the Michelangelo have a designed preshaped flexion of about 20 - 30 degrees, which fits well to the optimal value determined here. Accordingly, the flexion of the fingers should be slightly increased to maximize the achieved overlap.

To further improve the hand, a passive hyperextension of the DIP joints is introduced. For many precision grasps that capability allows to better align the fingertips with the thumb. For example, to be executed correctly, the "palmar pinch" is dependent on that feature. Also, the five digit "prismatic 4 finger" grasp is facilitated by that ability. Therefore a fourth DoF is introduced which allows for a coupled hyperextension of all four DIP joints of the fingers. The range of motion is $\{-30 \dots 0\}$ degrees. The projection of that hand is shown in Figure 5.18(b) and the overlap is 14.7 %. The forth DoF further explores

the latent space by 1.9 %. Again, the color code represents the new feature - in that case the hyperextension of the DIP joints. For each hyperextension value, the points basically cover the same space as previously. That explains why the increase in the coverage is small. It seems that this feature is of minor importance for the grasping capabilities.

Both results give a rough estimation of the real capabilities of the underactuated hand. At this stage it is not possible to determine if the real hand shapes would be simpler or more complex than the model. If it was simpler, meaning that the PIP and DIP joints are coupled directly to the MCP values, that hand model would be similar to the one in Section 5.3.1. In that case the underactuated hand overlap is reduced, being closer to 6.8 %. On the other hand, if the hand has to conform itself to many different object sizes and shapes, the hand shapes could be more complex. In particular the coupling between fingers would be broken, conferring the hand model higher complexity. If that is the case the overlap would even exceed 14.7 %.

The latent space signatures in in Figure 5.18 show, that in both cases there is a trajectory moving to the random hand position. Starting from the left top of the point cloud, it moves horizontally to the right until it reaches the random hand location. In Figure 5.18(a), most of the blue points correspond to that trajectory. That point represents the random hand model, therefore postures that fall onto that spot are non anthropomorphic. To determine which flexion angles contribute to the coverage, the maximal flexion value for both models is both varied and the overlap is calculated. Figure 5.19 shows the dependency of the maximal flexion value for both hand models. At around 80 degrees the curves flatten out. That means that adding a larger flexion capability to the hand does not add extra functionality to the hand. It only increases the complexity of the hand, as a larger range of motion adds extra mechanical challenges. According to this plot it is sufficient to flex the fingers up to a maximum of ca. 80 degrees.

5.3.4 Michelangelo with Human Thumb and Underactuation

This hand combines the best results that have been achieved in the previous Sections. It takes the best result from the optimization which is the changed thumb with an overlap of 9.8 %. Additionally the best hand so far from this Section, which is the hand with underactuation abilities, is taken. This hand has a common flexion of the PIP and DIP joints and the hyperextension of the DIP joint which results in an overlap of 14.7 %. Those two results are combined to a new hand with a total of five DoF. Those are:

1. Combined flexion of all four finger MCP joints according to the main drive coupling
2. Combined flexion of all four finger PIP/DIP joints up to 90 degrees
3. Hyperextension of the finger DIP joints up to 30 degrees

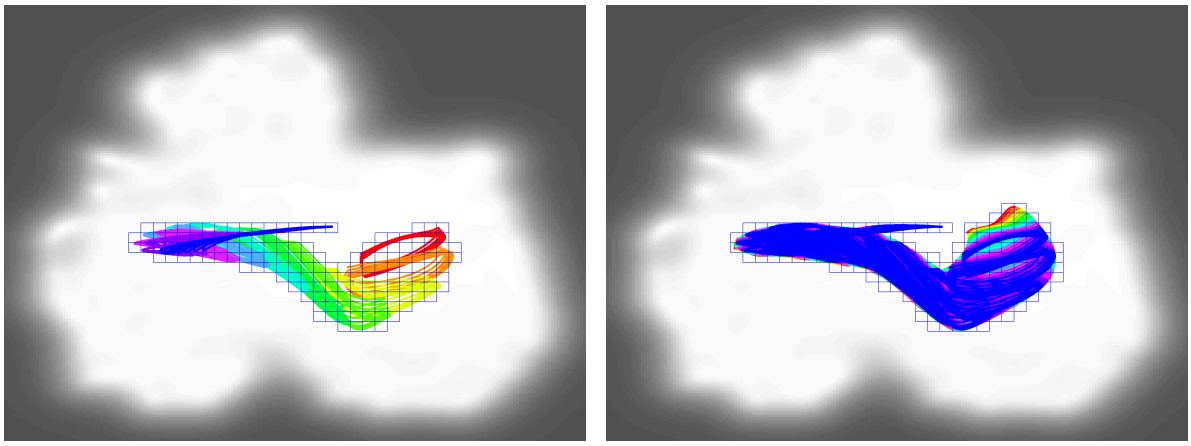

(a) Independent movement of the PIP/DIP joints of the four fingers. That additional DoF emulates a hand with passive adaption capabilities. The coverage is 12.8 %. The colors indicate the 10 degree steps of the flexion angles of the PIP and DIP joints.

(b) Additional to a) a forth DoF is adjoined to the hand model. That is the ability to hyperextend the DIP joints with up to 30 degrees. The hand achieves an overlap of 14.7 %. The colored trajectories correspond to different levels of hyperextension.

Figure 5.18: Michelangelo hand model with underactuation capabilities.

4. Flexion of the thumb CMC joint
5. Abduction of the thumb CMC joint

The joint space is sampled with 124950 points and the corresponding latent space signature is presented in Figure 5.20. The hand offers the best performance seen so far, it is able to populate 27.0 % of the latent space.

The blue points correspond to the thumb in maximal flexion, whereas the red points represent maximal extension of the thumb. One has to keep in mind, that the thumb corresponds to the one found in Section 5.2.4. That specific thumb has the property that even the flexed positions correspond to a thumb flexion where the thumb points

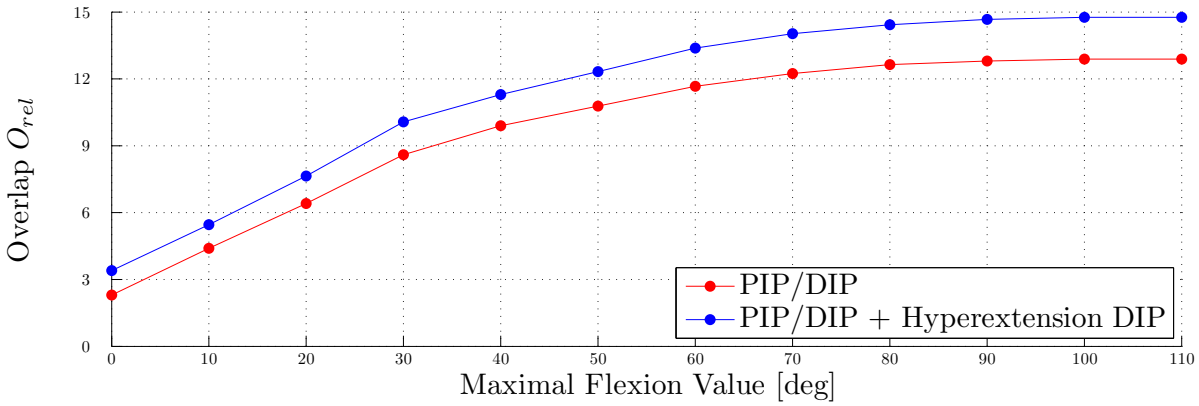

Figure 5.19: Overlap O_{rel} as function of the maximal flexion value. It is shown for both hands that mimic underactuation.

outwards. As the largest point cloud corresponds to the maximal flexion angle, it was further increased to determine the gain that can be achieved. The additional overlap that is gained from a maximal flexion angle of 150 degrees (that corresponds to a more natural thumb) is about 0.1 %. The points move very fast towards the random hand location, without exploring new areas in the latent space.

The large overlap value demonstrates that the constitution of the two hands makes sense, as the gain over the individual hands is large. This comes at the cost of additional dimensions of the control space of the hand. As the introduction of the hyperextension of the DIP joints only increased the coverage by 1.9 %, it can be assumed that if that ability is removed from the hand, the coverage will only decrease by that small amount. A run, with removed hyperextension capability supported the assumption. The 4D hand, is able to overlap 24.9 % of the space. The loss is 2.1 % compared to the five dimensional hand model. That gives a possibility for a slight reduction in complexity without affecting the large potential of the hand.

It seems, that the underactuated hand is responsible for the left/right elongations, whereas the the thumb influences the vertical stretch. What is still missing is the start position - the hand cannot be shaped totally flat, as would be required to move even farther to the right.

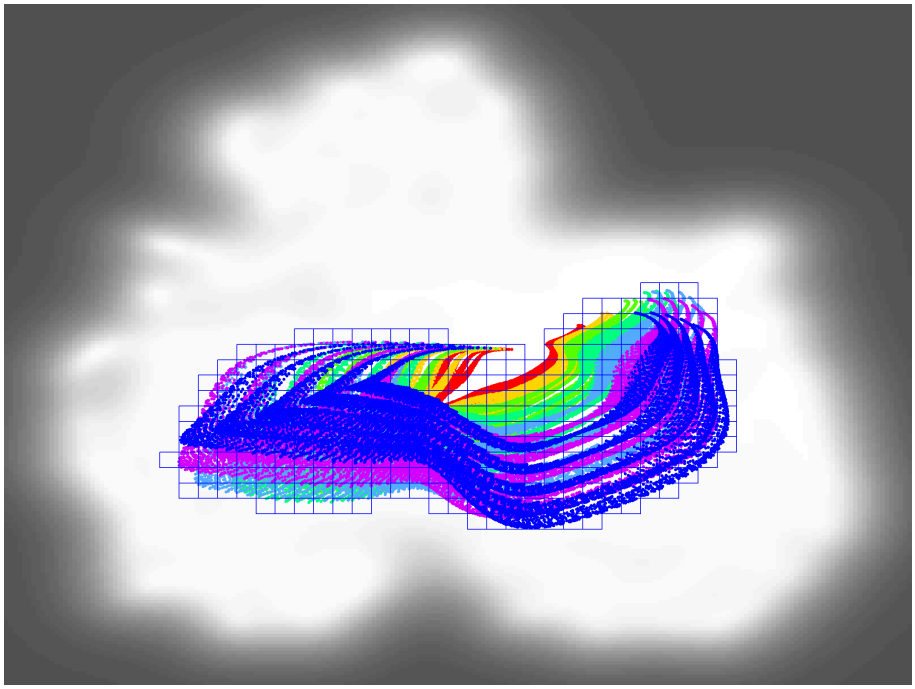

Figure 5.20: Hand that combines the result of the underactuated fingers with a human thumb. The model has five DoF and a resulting coverage of 27.0 %. The colors correspond to different thumb flexion values.

5.4 Discussion

The process of optimizing kinematic hand setups proved difficult. First, the parameters that are subject to optimization have to be defined with care. A poor definition of the parameters ends in local minima and no consistency between different runs of the same optimization problem. Similarly, if too many parameters are optimized in parallel, many local solutions will be found. That prohibits finding an optimal hand in only a few iteration steps, given the current implementation. Additionally, such an optimization is time consuming, taking about 24 hours on a computer with Intel® Core™ i7 CPU and 8 GB of RAM. Therefore corrections in the optimization problem and iterations over new hands take time. Still, this approach is much faster than the classical approach of building prototypes.

During the optimizations the limits for the parameters were set very wide, thus not restricting the parameters to meaningful regions. The optimized parameters show a behavior that they follow the intuition of the author and tend not to run into the defined limits.

As already indicated by the sensitivity study in Section 5.1, the orientations dominate the optimization and have a sharp maximum. For future applications, the goal should be to shape the system in such a way, that both orientations and positions influence the overlap. That will increase the overall quality of the results as some properties of the hand model can only be measured by the positions.

The results show, that an additional DoF, that affects all fingers has a larger impact on the coverage compared to movements of single fingers. For example the introduction of a coupled DoF that flexes the PIP/DIP joints of the fingers resulted in a larger coverage than an index finger that has an additional DoF. There are two possible explanations for this. First, having an additional parameter that moves many fingers, results in a change in many dimensions of the dataspace, thus increasing the action manifold. A larger volume most likely will result in a larger overlap. Second, the hands are all still simple in design. Therefore it might be the case that a variation in the full hand flexion facilitates more grasps than an independently controlled index finger. In the latter case only a few precision grasps are made possible. Up until now no hands have been realized, thus it is not possible to rule out one of these possibilities. It needs extensive testing with real prototypes to answer this issue.

Some hands show a tendency that their latent points come close to the position of the random hand. That is the location where all non-anthropomorphic hand configurations collapse onto. Therefore this location represents a large variety of hand configurations, which do not resemble the human grasping movements. At the moment the system does not process this information at all. A more thorough analysis on the points that fall onto

that region might hold additional insights on the behavior of the hand. For example, if half of the hand configurations fall onto that spot, it could be argued, that the hand has many capabilities that can be removed without affecting the anthropomorphism of the hand. That could lead to a simpler hand design with the same capabilities. It might even be of benefit to add a penalty for points that are close to the random hand location, thus actively pushing the points away from that location during the optimization.

Except for the measurement of the human kinematics, there are no objects present in the simulations. The advantage of that is, that the output is not specific to a certain class of objects. Still, due to the absence of objects, underactuation cannot be implemented directly. To work, underactuation needs an object which exerts force onto the digits. A workaround is to introduce additional virtual DoF, that simulate the different finger postures that are possible due to wrapping around objects. Such an approach is taken in Section 5.3.3, where underactuated fingers are analyzed.

Concerning the results of the optimizations and the creation of new hand designs, it has been shown that the introduction of more DoF are no guarantee to increase the anthropomorphism of hands. The FR-4 hand, with its 8 actuators covers nearly 10 % of the latent space. Such an overlap value can be even exceeded by a hand with three actuators. For example the hand described in Section 5.3.3 is able to cover 12.8 %. A smart coupling of more than one joint to one actuator and a proper orientation of the axes made such a result possible.

Overall it has been shown that the system works as intended, simplifying and accelerating the design process of new prosthetic and robotic hands. New hands were created virtually and evaluated with respect to the overlap measure. Within half a year, where the system has been used to find new hand designs, multiple new hand models could be created. The theoretical findings still should be validated using a real prototype.

Chapter 6

Conclusion

Creating new – improved – artificial hands is a difficult process. Commonly, the hand is based on the ideas of the engineers designing it. Depending on the experience and skill of the engineer, the resulting hand will be of different quality. In order to determine the quality of a design, it needs to be built and tested in real life experiments. Such a process is both expensive and time consuming. This thesis deals with the problem and develops a method to determine the quality of anthropomorphic hands prior to realization.

The first step towards the goal is to define human hand usage. The human hand serves as the golden standard in grasping, being the most versatile hand we know of. Therefore a comprehensive grasp taxonomy is created, based on an extensive literature survey of existing grasp classifications. A definition clarifies which grasps are relevant for the study – the focus is on one handed static grasps. The comprehensive taxonomy consists of 33 different grasp types, incorporating all relevant grasps from previous studies. Of that set 31 grasp types were used to define the human hand capabilities. The perfect artificial hand will be able to perform all those grasps.

The main contribution of the thesis is a system which allows to compare the capabilities of a kinematic hand setup with the grasping movements of the human. A large overlap of the movements indicates that the hand is anthropomorphic, whereas a small overlap indicates the opposite. The presented method is the first approach to quantify the anthropomorphism of prosthetic and robotic hands prior to realization. Therefore this tool has a large potential in speeding up the design process, as a new hand design can be evaluated at an earlier stage. The large advantage of the system lies in the fact, that it allows for a large range of hands to be tested; the only limitation is that the hand has to be five-fingered. Apart from this, the hand can have arbitrary complexity, with all kinds of coupling definitions. They can be hard coded or be based on nonlinear functions. The toolbox *Grade Your Own Hand* [105] has been made public, which allows the community to test their hands and compare it against other designs.

The applicability of the system is shown in different ways. *First*, it is used to determine the anthropomorphism of two existing prosthetic and one robotic hand. It shows that a large number of actuators does not imply large anthropomorphism. *Second*, based on the overlap measure, kinematic parameters were optimized, resulting in hand designs that are optimal with respect to this measure. The results look good, following the human intuition on improved versatility. *Finally*, all prior results are combined, creating new hand designs that yield a large potential dexterity with only a few actuators.

Overall, it was shown that an increase in the degree of anthropomorphism can be achieved by a smart definition of the hand kinematics. It is not a prerequisite for such a hand that it has many Degrees of Freedom. That can be seen by comparing different hands with the same number of actuators; for example if the five dimensional SensorHand is compared to the 5D Michelangelo hand. In both cases the same joints are actuated, but due to differences in the kinematic chains of the fingers the overlap is significantly different. The SensorHand, where all joint axes are parallel and the thumb is perfectly opposing the the fingers, has an overlap of 0.4 %. In contrast, the Michelangelo hand, which features a much more human like orientation of the joints, is able to populate 7.9 % of the space. That demonstrates, that even though the control space is similar, the results are significantly different.

Hands, that were created using the system, have not been realized and tested in a real application. Therefore the results presented in the thesis all have a certain degree of uncertainty. In the future, some hand designs should be actually built and their performance compared with the results from the overlap measure. Only then a conclusive statement concerning the validity of the results can be given.

The presented methodology is not limited to five-fingered general purpose hands. The underlying human dataset defines the movement against which the artificial hands are contrasted. Therefore exchanging that dataset exchanges the paradigm of a perfect hand. For example, if precision grasps are the main focus, a new dataset could be created consisting of a range of precision grasps.

6.1 Outlook

There are various things that can be done in order to continue with the research.

The results are only as good as the input. In that case that is the *Comprehensive Grasp Taxonomy*, which defines what movement the artificial designs are supposed to mimic. The classification is based on a literature survey, yet it is not based on observing humans in everyday life situations. Therefore the possibility exists that some grasp types were never taken into consideration, whereas others could be neglected.

To overcome the limitations, a completely different approach is necessary. One would have to use a data driven approach, where many subjects are recorded performing all kinds of different hand movements. To record the hand postures the instrumentation should be as non-invasive as possible, thus reducing the influence on the results. Another important constraint is that the dataset should represent all hand movements, not being restricted to a special application. Such a dataset can be the basis for a variety of analysis. One approach would be to perform a cluster analysis to determine the hand postures which represent the majority of movements. That grasp list would consist of snapshots of hand configurations without taking time into account. A more elaborate approach would be to extract not only a snap shot, but model the grasp as a parametric model. Such a grasp type would be a function of the object size. Therefore the problems introduced by different object sizes could be removed. In the comprehensive grasp taxonomy that problem is present, as some grasps differ only by the object size. Such grasp types could be merged to one model.

The presented *overlap measure* is the first step to access the degree of similarity between human and robot hand. Yet, there is some potential for improvement. At the moment the system processes snapshots of hand configurations without taking time and dynamics into account. Not only the hand configurations should be human-like, but also the movements of an artificial hand should resemble the human. Therefore it is desirable that the trajectories of human and machine are parallel in the latent space. Such a trajectory should be given a higher score, as compared to a perpendicular trajectory. More work is needed in order to implement such measures to the system as well.

Finally, it should be investigated if the general approach can be extended to other areas where two high dimensional entities have to be compared. One possible application might be to compare full body movements of human and robot. The same principles can be applied in that case, where a large overlap indicates that the robotic kinematic structure is similar to the human. That can be used to gain similar insights on the overall level of anthropomorphism of an robot, similar to the results obtained on hands in this thesis.

Glossary

ACT	Anatomically Correct Testbed
BC	Back Constraint: A extension to GP-LVM which allows a fast projection from data to latent space [85].
CMC	Carpo-Metacarpal
CT	Computed Tomography
DIP	Distal Interphalangeal
DH	Denavit Hartenberg: A formalism to describe a kinematic chain [41].
DoF	Degree of Freedom: Minimal number of parameters necessary to specify the configuration of a system.
DR	Dimensionality Reduction: The process of projecting data to a lower dimensional embedding which maintains most of the structure of the space.
GP-LVM	Gaussian Process Latent Variable Model: A probabilistic nonlinear dimensionality reduction algorithm, first proposed by [86].
Intrinsic Movement	The object is being manipulated without a global movement of the arm.
IP	Interphalangeal
LLE	Locally Linear Embedding: A local, nonlinear dimensionality reduction algorithm [76, 78].
MCP	Metacarpal
MDS	Multi Dimensional Scaling: A global, nonlinear dimensionality reduction algorithm [76].
PC	Principal Component: One basis vector as determined by PCA.
PCA	Principal Component Analysis: A linear dimensionality reduction algorithm [67].

PIP	Proximal Interphalangeal
Pose	Position and Orientation combined to one vector.
Posture	Configuration of the hand.
RBF	Radial Basis Function : A type of kernel for GP-LVM
VF	Virtual Finger: One or more fingers work together as one function unit, the virtual finger.

List of Figures

2.1 The human forearm anatomy 5
2.2 Bones of the human hand 6
2.3 Range of motion of the Metacarpal joint 7
2.4 Differences of the grasp stability when the thumb is employed 8
2.5 Opposition types 10
2.6 Sequence of hand grasps 11
2.7 Prosthetic hands by *Otto Bock* 13
2.8 *Touch Bionics I-Limb™ ultra* hand 14
2.9 The *Shadow Dexterous Hand C6* 14
2.10 FRH-4 Hand 15
2.11 Denavit Hartenberg coordinate frame definition 20
2.12 Comparison of the first two Principal Components 26

3.1 Taxonomy of Schlesinger 33
3.2 Grasp types listed by Coones and Chao 33
3.3 The "Power Grip" category from Kamakura et al. 35
3.4 The "Intermediate Grip" category from Kamakura et al. 36
3.5 The "Precision Grip" category from Kamakura et al. 37
3.6 Kamakura's "Grip involving no thumb" 38
3.7 Eight basic hand positions according to Lister 38
3.8 Elliott and Conolly's hand postures 39
3.9 Grasps named by Lyons [94] 40
3.10 Grasp types defined by Kroemer 41
3.11 Grasp types referenced by Cutkosky 42
3.12 Grasp Types as defined by Kang and Ikeuchi 43
3.13 Six hand postures by Light et al. 44
3.14 Grasp types defined by Exner 45

3.15 Power grasps as defined by Edwards et al. 46
3.16 Combination of Power and Precision grasps as defined by Edwards et al. . 47
3.17 Precision grasps as defined by Edwards et al. 47
3.18 Miscellaneous and Nonprehensile grasps according to Edwards et al. 48
3.19 Kapandji's grasp types 49

4.1 Overview over the system to quantify the hand anthropomorphism 59
4.2 Hypothetical visualization of the fingertip space 60
4.3 Setup of the fingertip sensors. 65
4.4 Setup of the experiments. 66
4.5 Human Grasping Dataset 67
4.6 Kernel width explanation 70
4.7 GMM/GMR processing pipeline. 73
4.8 Two random hand models. 74
4.9 Grasp trajectories in the latent space. 77
4.10 Projections to determine the latent space quality. 78
4.11 Projection of the Otto Bock SensorHand 80
4.12 Different Michelangelo Models and their overlap of the latent space 83
4.13 Projection of the FRH-4 hand 84
4.14 The human hand model controlled via two PCs and its projection 86
4.15 System description to restrict the training set to a linear subspace 86
4.16 Projection of PCA spaces 88
4.17 Comparison of PCA results over the dimension 89

5.1 Influence of parameters on the overlap 94
5.2 Sensitivity values for the SensorHand 95
5.3 Variation of the z-rotation of the thumb 95
5.4 Sensitivity values of Michelangelo 96
5.5 Mean Sensitivity per Finger of the Michelangelo hand 97
5.6 Sensitivity values of the FR-H 4 Hand 98
5.7 Overview of the tested hands 101
5.8 Results of the Thumb base optimization for the SensorHand. 102
5.9 Results of the orientation optimization of the SensorHand thumb 104
5.10 Coverages of the 10 runs of the 2D human hand model 105
5.11 Visualization of the 10 optimizations of the 2D human hand 106
5.12 Four results of the linear hand model optimization 107
5.13 Results of the couplings parameter optimization of the Michelangelo hand . 109
5.14 Optimization results of the Michelangelo hand with human thumb 3D . . . 111

5.15 Best Result of the Michelangelo hand with human thumb 111
5.16 Overlap of the Michelangelo Hand with PIP and DIP joints coupled to the MCP joint 112
5.17 Hand models that assess the importance of an independent index finger . . 114
5.18 Michelangelo hand model with underactuation capabilities 116
5.19 Overlap O_{rel} as function of the maximal flexion value 116
5.20 Hand that combines the result of the underactuated fingers with a human thumb 117

List of Tables

2.1 Comparison of human hand models 22

3.1 Kapandji's grasp type classification 50
3.2 Taxonomy comparison sheet 52
3.3 Grasp list 54
3.4 Comprehensive Grasp Taxonomy 55

4.1 Scores of the latent space models 76

Bibliography

[1] L. Biagiotti, F. Lotti, C. Melchiorri, and G. Vassura, "How far is the human hand? a review on anthropomorphic end effectors," DIES Internal Report, University of Bologna, Tech. Rep., 2004.

[2] P. Parker, K. Englehart, and B. Hudgins, "Myoelectric signal processing for control of powered limb prostheses." *Journal of electromyography and kinesiology*, vol. 16, no. 6, pp. 541–548, Dec. 2006.

[3] W. Craelius, "The bionic man: Restoring mobility," *Science*, vol. 295, no. 5557, pp. 1018–1021, Feb. 2002.

[4] P. J. Kyberd, C. Wartenberg, L. Sandsjö, S. Jönsson, D. Gow, J. Frid, C. Almström, and L. Sperling, "Survey of upper extremity prosthesis users in sweden and the united kingdom," *JPO: Journal of Prosthetics and Orthotics*, vol. 19, no. 2, p. 55, 2007.

[5] C. Pylatiuk, S. Schulz, and L. Döderlein, "Results of an internet survey of myoelectric prosthetic hand users." *Prosthetics and orthotics international*, vol. 31, no. 4, pp. 362–370, Dec. 2007.

[6] E. N. Marieb and K. Hoehn, *Human Anatomy And Physiology*, 7th ed. Benjamin-Cummings Publishing Company, May 2006.

[7] J. M. Landsmeer, "The coordination of finger-joint motions." *The Journal of bone and joint surgery. American volume*, vol. 45, pp. 1654–1662, December 1963.

[8] H. Gray, *Anatomy of the human body.* Philadelphia: Lea & Febiger, 1918, bartleby.com, 2000. [Online]. Available: http://www.bartleby.com/107/

[9] I. A. Kapandji, *Funktionelle Anatomie der Gelenke. Schematisierte und kommentierte Zeichnungen zur menschlichen Biomechanik.* Thieme Georg Verlag, January 2006.

[10] Wikipedia, "Hand — wikipedia, the free encyclopedia," 2011, [accessed 15-September-2011]. [Online]. Available: http://en.wikipedia.org/w/index.php?title=Hand&oldid=450496853

[11] C. E. Lang and M. H. Schieber, "Human finger independence: limitations due to passive mechanical coupling versus active neuromuscular control." *Journal of neurophysiology*, vol. 92, no. 5, pp. 2802–2810, November 2004.

[12] C. H. Ross and M. H. Schieber, "Quantifying the independence of human finger movements: Comparisons of digits, hands, and movement frequencies," *The Journal of neuroscience : the official journal of the Society for Neuroscience*, vol. 20, no. 22, pp. 8542–8550, November 2000.

[13] J. Ingram, K. Körding, I. Howard, and D. Wolpert, "The statistics of natural hand movements," *Experimental Brain Research*, vol. 188, no. 2, pp. 223–236, June 2008.

[14] D. J. Giurintano, A. M. Hollister, W. L. Buford, D. E. Thompson, and L. M. Myers, "A virtual five-link model of the thumb." *Medical Engineering and Physics*, vol. 17, no. 4, pp. 297–303, June 1995.

[15] J. R. Napier, "The prehensile movements of the human hand." *The Journal of bone and joint surgery. British volume*, vol. 38-B, no. 4, pp. 902–913, November 1956.

[16] T. Iberall, G. Bingham, and M. A. Arbib, "Opposition space as a structuring concept for the analysis of skilled hand movements," *Experimental Brain Research Series*, vol. 15, pp. 158–173, 1986.

[17] T. Iberall, "Human prehension and dexterous robot hands," *The International Journal of Robotics Research*, vol. 16, no. 3, pp. 285–299, June 1997.

[18] C. L. Mackenzie and T. Iberall, *The Grasping Hand, Volume 104 (Advances in Psychology)*, 1st ed. North Holland, Feb. 1994.

[19] J. M. Landsmeer, "Power grip and precision handling." *Annals of the rheumatic diseases*, vol. 21, pp. 164–170, June 1962.

[20] N. Kamakura, M. Matsuo, H. Ishii, F. Mitsuboshi, and Y. Miura, "Patterns of static prehension in normal hands." *The American journal of occupational therapy.*

: official publication of the American Occupational Therapy Association, vol. 34, no. 7, pp. 437–445, July 1980.

[21] T. Iberall, "The nature of human prehension: Three dextrous hands in one," in *Robotics and Automation. Proceedings. 1987 IEEE International Conference on*, vol. 4, 1987, pp. 396–401.

[22] P. J. Kyberd, A. Clawson, and B. Jones, "The use of underactuation in prosthetic grasping," *Mechanical Sciences*, vol. 2, no. 1, pp. 27–32, 2011.

[23] Otto Bock. SensorHand Speed. [accessed 15-September-2011]. [Online]. Available: http://www.ottobock.com/cps/rde/xchg/ob_com_en/hs.xsl/3652.html

[24] A. Muzumdar, *Powered Upper Limb Prostheses: Control, Implementation and Clinical Application*, 1st ed. Springer, Feb. 2004.

[25] M. C. Carrozza, G. Cappiello, S. Micera, B. B. Edin, L. Beccai, and C. Cipriani, "Design of a cybernetic hand for perception and action," *Biological Cybernetics*, vol. 95, no. 6, pp. 629–644, Dec. 2006.

[26] Otto Bock. (2011) Otto Bock at the trade fair 2010 Leipzig. [accessed 15-September-2011]. [Online]. Available: http://leipzig.ottobock.de/index.php?id=161&no_cache=1&L=1

[27] Touch Bionics. Myoelectric Control. [accessed 28-September-2011]. [Online]. Available: http://www.touchbionics.com/media/2210/i-limb%20ultra%20data%20sheet%20lo-res.pdf

[28] ——. i-Limb ultra. [accessed 28-September-2011]. [Online]. Available: http://www.touchbionics.com/products/active-prostheses/i-limb-ultra/

[29] Shadow Robot Company. (accessed 15-September-2011) Shadow Hand range. [Online]. Available: http://www.shadowrobot.com/downloads/shadow_dextrous_hand_technical_specification_C6M.pdf

[30] ——. (accessed 28-September-2011, Aug.) Shadow Hand range. [Online]. Available: http://www.shadowrobot.com/hand/techspec.shtml

[31] I. Gaiser, S. Schulz, A. Kargov, H. Klosek, A. Bierbaum, C. Pylatiuk, R. Oberle, T. Werner, T. Asfour, G. Bretthauer, and R. Dillmann, "A new anthropomorphic robotic hand," Dec. 2008, pp. 418–422.

[32] A. Bicci, "Revisiting grasping basics," in *Robotics, Science and Systems Conference: Workshop Grasp Acquisition: How to Realize Good Grasps*, Jun. 2010.

[33] M. Mason, S. Srinivasa, and A. Vazquez, "Generality and simple hands," *Robotics Research*, pp. 345–361, 2011.

[34] A. Bicchi, "Hands for dexterous manipulation and robust grasping: a difficult road toward simplicity," *Robotics and Automation, IEEE Transactions on*, vol. 16, no. 6, pp. 652–662, 2000.

[35] M. T. Ciocarlie and P. K. Allen, "Hand posture subspaces for dexterous robotic grasping," *Int. J. Rob. Res.*, vol. 28, no. 7, pp. 851–867, July 2009.

[36] M. Ciocarlie and P. Allen, "Data-driven optimization for underactuated robotic hands," in *2010 IEEE International Conference on Robotics and Automation (ICRA 2010)*. IEEE, May 2010, pp. 1292–1299.

[37] D. Pratichizzo, M. Malvezzi, and A. Bicchi, "On motion and force controllability of grasping hands with postural synergies," in *Proceedings of Robotics: Science and Systems*, Zaragoza, Spain, June 2010.

[38] M. Malhotra and Y. Matsuoka, "The relationship between actuator reduction and controllability for a robotic hand," pp. 331–336, 2010.

[39] M. J. Farrugia and M. A. Saliba, "Optimisation of anthropomorphic robot hand design through human manual dexterity testing," *VDI BERICHTE*, vol. 1956, p. 147, 2006.

[40] R. S. Hartenberg and J. Denavit, *Kinematic Synthesis of Linkages (Mechanical Engineering Series)*, first edition ed. McGraw-Hill Inc.,US, 1964.

[41] J. Denavit and R. S. Hartenberg, "A kinematic notation for lower-pair mechanisms based on matrices." *Trans. of the ASME. Journal of Applied Mechanics*, vol. 22, pp. 215–221, 1955.

[42] M. W. Spong and M. Vidyasagar, *Robot Dynamics and Control*. Wiley, January 1989.

[43] K. N. An, E. Y. Chao, W. P. Cooney, and R. L. Linscheid, "Normative model of human hand for biomechanical analysis." *Journal of biomechanics*, vol. 12, no. 10, pp. 775–788, 1979.

[44] B. Buchholz, T. J. Armstrong, and S. A. Goldstein, "Anthropometric data for describing the kinematics of the human hand." *Ergonomics*, vol. 35, no. 3, pp. 261–273, March 1992.

[45] B. Buchholz and T. J. Armstrong, "A kinematic model of the human hand to evaluate its prehensile capabilities." *Journal of biomechanics*, vol. 25, no. 2, pp. 149–162, February 1992.

[46] J. L. Sancho Bru, A. P. González, M. Vergara, and D. J. Giurintano, "A 3d biomechanical model of the hand for power grip." *Journal of biomechanical engineering*, vol. 125, no. 1, pp. 78–83, February 2003.

[47] S. W. Lee and X. Zhang, "Development and evaluation of an optimization-based model for power-grip posture prediction." *Journal of biomechanics*, vol. 38, no. 8, pp. 1591–1597, August 2005.

[48] H. Rijpkema and M. Girard, "Computer animation of knowledge-based human grasping," *SIGGRAPH Comput. Graph.*, vol. 25, no. 4, pp. 339–348, 1991.

[49] Y. Yasumuro, "Three-dimensional modeling of the human hand with motion constraints," *Image and Vision Computing*, vol. 17, no. 2, pp. 149–156, February 1999.

[50] I. Albrecht, J. Haber, and H. P. Seidel, "Construction and animation of anatomically based human hand models," in *SCA '03: Proceedings of the 2003 ACM SIGGRAPH/Eurographics symposium on Computer animation.* Aire-la-Ville, Switzerland, Switzerland: Eurographics Association, 2003, pp. 98–109.

[51] H. Wan, Y. Luo, S. Gao, and Q. Peng, "Realistic virtual hand modeling with applications for virtual grasping," in *VRCAI '04: Proceedings of the 2004 ACM SIGGRAPH international conference on Virtual Reality continuum and its applications in industry.* New York, NY, USA: ACM, 2004, pp. 81–87.

[52] T. Kurihara and N. Miyata, "Modeling deformable human hands from medical images," in *SCA '04: Proceedings of the 2004 ACM SIGGRAPH/Eurographics symposium on Computer animation.* Aire-la-Ville, Switzerland, Switzerland: Eurographics Association, 2004, pp. 355–363.

[53] E. P. Pitarch, J. Yang, and K. A. Malek, "Santos hand: A 25-Degree-of-Freedom model," in *Proceedings of SAE Digital Human Modeling for Design and Engineering*, Iowa City, Iowa, USA, 2005.

[54] S. Cobos, M. Ferre, M. A. Sanchez Uran, J. Ortego, and C. Pena, "Efficient human hand kinematics for manipulation tasks," in *Intelligent Robots and Systems, 2008. IROS 2008. IEEE/RSJ International Conference on*, 2008, pp. 2246–2251.

[55] O. A. van Nierop, A. van der Helm, K. J. Overbeeke, and T. J. Djajadiningrat, "A natural human hand model," *The Visual Computer*, vol. 24, no. 1, pp. 31–44, January 2008.

[56] J. Lee and T. L. Kunii, "Model-based analysis of hand posture," *IEEE Comput. Graph. Appl.*, vol. 15, no. 5, pp. 77–86, 1995.

[57] J. Lin, Y. Wu, and T. S. Huang, "Modeling the constraints of human hand motion," in *Human Motion, 2000. Proceedings. Workshop on*, 2000, pp. 121–126.

[58] M. Veber and T. Bajd, "Assessment of human hand kinematics," in *Robotics and Automation, 2006. ICRA 2006. Proceedings 2006 IEEE International Conference on*, 2006, pp. 2966–2971.

[59] J. R. et al., "Hands in action, real-time 3d reconstruction of hands in interaction with objects," in *ICRA 09:00-09:15, Paper TuA12.3*, 2010.

[60] N. Rezzoug and P. Gorce, "Prediction of fingers posture using artificial neural networks," *Journal of Biomechanics*, vol. 41, no. 12, pp. 2743–2749, August 2008.

[61] J. Choi, "Developing a 3-dimensional kinematic model of the hand for ergonomic analyses of hand posture, hand space envelope, and tendon excursion," Ph.D. dissertation, The University of Michigan, 2008.

[62] C. Goldfeder, M. Ciocarlie, H. Dang, and P. K. Allen, "The columbia grasp database," in *2009 IEEE International Conference on Robotics and Automation*, May 2009.

[63] M. Ciocarlie, C. Goldfeder, and P. Allen, "Dimensionality reduction for hand-independent dexterous robotic grasping," in *Intelligent Robots and Systems, 2007. IROS 2007. IEEE/RSJ International Conference on*, 2007, pp. 3270–3275.

[64] X. Zhang, S. W. Lee, and P. Braido, "Determining finger segmental centers of rotation in flexion-extension based on surface marker measurement." *J Biomech*, vol. 36, no. 8, pp. 1097–1102, August 2003.

[65] L. A. Jones and S. J. Lederman, *Human Hand Function*, 1st ed. Oxford University Press, USA, April 2006.

[66] J. Romero, T. Feix, C.-H. Ek, H. Kjellström, and D. Kragic, "Extracting postural synergies for grasping," *Robotics and Automation, IEEE Transactions on*, submitted.

[67] I. T. Jolliffe, *Principal Component Analysis*, 2nd ed. Springer, October 2002.

[68] M. Santello, M. Flanders, and J. F. Soechting, "Postural hand synergies for tool use," *J. Neurosci.*, vol. 18, no. 23, pp. 10 105–10 115, December 1998.

[69] A. Cordero, O. Levin, Y. Li, and S. P. Swinnen, "Principal component analysis of complex multijoint coordinative movements." *Biological cybernetics*, vol. 93, no. 1, pp. 63–78, July 2005.

[70] E. Todorov and Z. Ghahramani, "Analysis of the synergies underlying complex hand manipulation," in *26th Annual International Conference of the IEEE Engineering in Medicine and Biology Society*, vol. 4. IEEE, 2004, pp. 4637–4640.

[71] P. Braido and X. Zhang, "Quantitative analysis of finger motion coordination in hand manipulative and gestic acts." *Human movement science*, vol. 22, no. 6, pp. 661–678, April 2004.

[72] H. Abdi and L. J. Williams, "Principal components analysis," *Wiley Interdisciplinary Reviews: Computational Statistics*, vol. 2, 2010.

[73] C. M. Bishop, *Pattern Recognition and Machine Learning (Information Science and Statistics)*, 1st ed. Springer, October 2007.

[74] J. B. Tenenbaum, V. Silva, and J. C. Langford, "A global geometric framework for nonlinear dimensionality reduction," *Science*, vol. 290, no. 5500, pp. 2319–2323, December 2000.

[75] P. H. Thakur, A. J. Bastian, and S. S. Hsiao, "Multidigit movement synergies of the human hand in an unconstrained haptic exploration task." *The Journal of neuroscience : the official journal of the Society for Neuroscience*, vol. 28, no. 6, pp. 1271–1281, February 2008.

[76] L. J. P. van der Maaten, E. O. Postma, and H. J. van den Herik, "Dimensionality reduction: A comparative review," MICC, Maastricht University, P.O. Box 616, 6200 MD Maastricht, Netherlands, Tech. Rep., February 2008.

[77] A. Tsoli and O. C. Jenkins, "Neighborhood denoising for learning high-dimensional grasping manifolds," in *2008 IEEE/RSJ International Conference on Intelligent Robots and Systems (IROS 2008)*. IEEE, Sep. 2008, pp. 3680–3685.

[78] S. T. Roweis and L. K. Saul, "Nonlinear dimensionality reduction by locally linear embedding," *Science*, vol. 290, no. 5500, pp. 2323–2326, December 2000.

[79] C. H. Ek, P. H. S. Torr, and N. D. Lawrence, *Gaussian Process Latent Variable Models for Human Pose Estimation.* Berlin, Heidelberg: Springer Berlin Heidelberg, 2008, vol. 4892, ch. 12, pp. 132–143.

[80] S. Hou, A. Galata, F. Caillette, N. Thacker, and P. Bromiley, "Real-time body tracking using a gaussian process latent variable model," *Computer Vision, IEEE International Conference on*, vol. 0, pp. 1–8, 2007.

[81] R. Urtasun, D. J. Fleet, and P. Fua, "3D people tracking with gaussian process dynamical models," in *CVPR '06: Proceedings of the 2006 IEEE Computer Society Conference on Computer Vision and Pattern Recognition.* Washington, DC, USA: IEEE Computer Society, 2006, pp. 238–245.

[82] J. M. Wang, D. J. Fleet, and A. Hertzmann, "Gaussian process dynamical models for human motion," *IEEE Transactions on Pattern Analysis and Machine Intelligence*, vol. 30, no. 2, pp. 283–298, Feb. 2008.

[83] R. Urtasun, D. J. Fleet, A. Geiger, J. Popović, T. J. Darrell, and N. D. Lawrence, "Topologically-constrained latent variable models," in *ICML '08: Proceedings of the 25th international conference on Machine learning*, ser. ACM International Conference Proceeding Series, vol. 307. New York, NY, USA: ACM, 2008, pp. 1080–1087.

[84] N. D. Lawrence, "The gaussian process latent variable model," The University of Sheffield, Department of Computer Science., Tech. Rep., 2006.

[85] N. D. Lawrence and J. Quiñonero Candela, "Local distance preservation in the GP-LVM through back constraints," in *the 23rd international conference*, ser. ICML '06. New York, New York, USA: ACM Press, 2006, pp. 513–520.

[86] N. Lawrence, "Probabilistic non-linear principal component analysis with gaussian process latent variable models," *Journal of Machine Learning Research*, vol. 6, pp. 1783–1816, 2005.

[87] T. Feix, R. Pawlik, H.-B. Schmiedmayer, J. Romero, and D. Kragic, "A comprehensive grasp taxonomy," in *Robotics, Science and Systems Conference: Workshop on Understanding the Human Hand for Advancing Robotic Manipulation, Poster Presentation*, June 2009. [Online]. Available: http://grasp.xief.net

[88] G. Schlesinger, *Der Mechanische Aufbau der Kunstlichen Glieder. Ersatzglieder und Arbeitshilfen, part II.* Berlin: Springer, 1919.

[89] C. L. Taylor and R. J. Schwarz, "The anatomy and mechanics of the human hand." *Artificial limbs*, vol. 2, no. 2, pp. 22–35, May 1955.

[90] D. B. Slocum and D. R. Pratt, "Disability evaluation of the hand," *J. Bone Joint Surg*, vol. 28, pp. 491–495, 1946.

[91] W. P. Cooney and E. Y. Chao, "Biomechanical analysis of static forces in the thumb during hand function," *J Bone Joint Surg Am*, vol. 59, no. 1, pp. 27–36, January 1977.

[92] G. Lister, *The hand: Diagnosis and surgical indications*. Churchill Livingstone, 1984.

[93] J. M. Elliott and K. J. Connolly, "A classification of manipulative hand movements." *Developmental medicine and child neurology*, vol. 26, no. 3, pp. 283–296, June 1984.

[94] D. Lyons, "A simple set of grasps for a dextrous hand," in *Robotics and Automation. Proceedings. 1985 IEEE International Conference on*, vol. 2, 1985, pp. 588–593.

[95] K. H. Kroemer, "Coupling the hand with the handle: an improved notation of touch, grip, and grasp." *Human factors*, vol. 28, no. 3, pp. 337–339, June 1986.

[96] M. Cutkosky and P. Wright, "Modeling manufacturing grips and correlations with the design of robotic hands," in *Robotics and Automation. Proceedings. 1986 IEEE International Conference on*, vol. 3, 1986, pp. 1533–1539.

[97] M. R. Cutkosky, "On grasp choice, grasp models, and the design of hands for manufacturing tasks," *Robotics and Automation, IEEE Transactions on*, vol. 5, no. 3, pp. 269–279, 1989.

[98] J. Z. Zheng, S. De La Rosa, and A. M. Dollar, "An investigation of grasp type and frequency in daily household and machine shop tasks," in *proceedings of the 2011 IEEE International Conference on Robotics and Automation (ICRA)*, May 2011.

[99] S. B. Kang and K. Ikeuchi, "A framework for recognizing grasps," Robotics Institute, Carnegie Mellon University, Pittsburgh, Pennsylvania 15213, Tech. Rep., 1991.

[100] ——, "Grasp recognition using the contact web," in *Intelligent Robots and Systems, 1992., Proceedings of the 1992 lEEE/RSJ International Conference on*, vol. 1, 1992, pp. 194–201.

[101] C. M. Light, P. H. Chappell, and P. J. Kyberd, "Establishing a standardized clinical assessment tool of pathologic and prosthetic hand function: normative data, reliability, and validity." *Archives of physical medicine and rehabilitation*, vol. 83, no. 6, pp. 776–783, June 2002.

[102] C. M. Light, P. H. Chappell, P. J. Kyberd, and B. S. Ellis, "Critical review of functionality assessment of natural and prosthetic hands," *British journal of occupational therapy*, vol. 62, pp. 7–12, 1999.

[103] C. E. Exner, "Development of hand skills," in *Occupational therapy for children*, C. J. Smith, Ed., 2001, pp. 289–328.

[104] S. J. Edwards, D. J. Buckland, and Jenna, *Developmental and Functional Hand Grasps*, 1st ed. Slack Incorporated, October 2002.

[105] T. Feix. (2011, Aug.) Human Grasping Database. [Online]. Available: http://grasp.xief.net

[106] T. Feix, J. Romero, C.-H. Ek, H.-B. Schmiedmayer, and D. Kragic, "Visualization of anthropomorphic hand performance," *Robotics and Automation, IEEE Transactions on*, submitted.

[107] J. W. Garrett, "Anthropometry of the hands of male air force flight personnel," Aerospace Medical Research Laboratory, Aerospace Medical Division, Air Force Systems Command,, Wright-Patterson Air Force Base, OH, USA, Tech. Rep., 1970.

[108] R. M. Murray, S. S. Sastry, and L. Zexiang, *A Mathematical Introduction to Robotic Manipulation*, 1st ed. Boca Raton, FL, USA: CRC Press, Inc., 1994.

[109] P. E. Nikravesh, *Computer-Aided Analysis of Mechanical Systems*. Prentice Hall, 1988, vol. 186.

[110] S. Calinon, *Robot Programming by Demonstration: A Probabilistic Approach*. EPFL/CRC Press, 2009.

[111] S. Calinon, F. Guenter, and A. Billard, "On learning, representing and generalizing a task in a humanoid robot," *IEEE Transactions on Systems, Man and Cybernetics, Part B*, vol. 37, pp. 286–298, 2007.

[112] J. Romero, T. Feix, H. Kjellström, and D. Kragic, "Spatio-Temporal modeling of grasping actions," in *IEEE/RSJ International Conference on Intelligent Robots and Systems (IROS)*, 2010.

[113] P. Corke, "A robotics toolbox for MATLAB," *IEEE Robotics and Automation Magazine*, vol. 3, no. 1, pp. 24–32, Mar. 1996.

[114] S. Kirkpatrick, C. D. Gelatt, and M. P. Vecchi, "Optimization by simulated annealing," *Science*, vol. 220, no. 4598, pp. 671–680, May 1983.

Curriculum Vitae

Personal Information

Name	Thomas Feix
Address	Stadtplatz 9 3400 Klosterneuburg
E-Mail	thomasfeix [at] yahoo.com
Date of Birth	October 6, 1983
Place of Birth	Vienna, Austria
Nationality	Austria

Education

07/2008 –	PhD in Mechanical Engineering under supervision of Heinz-Bodo Schmiedmayer (TU Wien) and Danica Kragic (KTH Stockholm). PhD Thesis: "Anthropomorphic Hand Optimization based on a Latent Space Analysis"
10/2004 –	Diploma study of Physics at the University of Vienna
10/2003 – 06/2007	Graduation (with distinction) as Dipl.Ing(FH) of Sports Equipment Technology at the University of Applied Science Technikum Wien, Vienna

Publications

2009	T. Feix, R. Pawlik, H.-B. Schmiedmayer, J. Romero, and D. Kragic, "A comprehensive grasp taxonomy," in *Robotics, Science and Systems Conference: Workshop on Understanding the Human Hand for Advancing Robotic Manipulation, Poster Presentation*, Jun. 2009.
2010	J. Romero, T. Feix, H. Kjellström, and D. Kragic, "Spatio-Temporal

modeling of grasping actions," in *IEEE/RSJ 2010 International Conference on Intelligent Robots and Systems (IROS 2010)*, 2010.

2010 T. Feix, J.Romero, H.Kjellström, D.Kragic, "GP-LVMs for studying human grasping actions", in *Robotics, Science and Systems Conference: Workshop on Representations for object grasping and manipulation in single and dual arm tasks, Oral Presentation*, Jun. 2010.

2011 T. Feix, J. Romero, C.-H. Ek, H.-B. Schmiedmayer, and D. Kragic, "Visualization of anthropomorphic hand performance," in *IEEE Transactions on Robotics and Automation*, submitted.

2011 J. Romero, T. Feix, C.-H. Ek, H. Kjellström, and D. Kragic, "Extracting postural synergies for grasping," in *IEEE Transactions on Robotics and Automation*, submitted.

2008 – 2011 T. Feix, Human Grasping Database, [online]. Available: http://grasp.xief.net

Vienna, October 27, 2011